FATIGUE PERFORMANCE OF ENGINEERED CEMENTITIOUS COMPOSITES

A THESIS SUBMITTED TO
THE GRADUATE SCHOOL OF NATURAL AND APPLIED SCIENCES
OF
MIDDLE EAST TECHNICAL UNIVERSITY

BY

BURHAN ALEESSA ALAM

IN PARTIAL FULFILLMENT OF THE REQUIREMENTS
FOR
THE DEGREE OF DOCTOR OF PHILOSOPHY
IN
CIVIL ENGINEERING

MARCH 2016

Approval of the thesis:

FATIGUE PERFORMANCE OF ENGINEERED CEMENTITIOUS COMPOSITES

submitted by **BURHAN ALEESSA ALAM** in partial fulfillment of the requirements for the degree of **Doctor of Philosophy in Civil Engineering Department, Middle East Technical University** by,

Prof. Dr. Gülbin Dural Ünver _____
Dean, Graduate School of **Natural and Applied Sciences**

Prof. Dr. İsmail Özgür Yaman _____
Head of Department, **Civil Engineering**

Prof. Dr. İsmail Özgür Yaman _____
Supervisor, **Civil Engineering Dept., METU**

Examining Committee Members:

Prof. Dr. Mustafa Tokyay _____
Civil Engineering Dept., METU

Prof. Dr. İsmail Özgür Yaman _____
Civil Engineering Dept., METU

Prof. Dr. Murat Güler _____
Civil Engineering Dept., METU

Assoc. Prof. Dr. Mustafa Şahmaran _____
Civil Engineering Dept., Gazi University

Assoc. Prof. Dr. Recep Birgül _____
Civil Engineering Dept., Muğla Sıtkı Koçman University

Date: 29/03/2016

I hereby declare that all information in this document has been obtained and presented in accordance with academic rules and ethical conduct. I also declare that, as required by these rules and conduct, I have fully cited and referenced all material and results that are not original to this work.

Name, Surname: BURHAN ALEESSA ALAM

Signature :

ABSTRACT

FATIGUE PERFORMANCE OF ENGINEERED CEMENTITIOUS COMPOSITES

Aleessa Alam, Burhan
PhD., Department of Civil Engineering
Supervisor: Prof. Dr. İsmail Özgür Yaman

March 2016, 100 pages

The maintenance and rehabilitation of a pavement during its service life is as much important as the construction works of this pavement. In this scope, applying the correct and efficient repair method is highly critical for economic and technical reasons. Depending on the damage level of the pavement, there are many different methods that can be used to repair the pavement. The use of an overlay is one of the most common methods, where a new layer can be applied directly over or replace the top part of an existing pavement. This overlay can be made from asphalt or concrete as well. Concrete overlays are gaining importance recently, especially with the increasing use of concrete pavements. All of these can be related to the long service life of concrete pavements compared to asphalt. However, because of the rigid nature of concrete the thickness of this overlay is higher.

In this work, ECC type of concrete was suggested to be used as an overlay because with a less thickness it has the ability to reduce the reflection of the cracks from the old pavement and the overlay. To testify this property, the performance of two ECC mixtures as a concrete pavement overlay was investigated under fatigue loading. Along with that, the fatigue performance of ECC mixtures of different compositions was examined. Moreover, using Weibull distribution the failure probability of these

mixtures under fatigue was determined. In addition to this, to reduce the time of the fatigue examination two new fatigue life prediction methods were suggested.

Keywords: Engineered Cementitious Composites (ECC), overlays, fatigue testing, Weibull distribution, fatigue life prediction

ÖZ

TASARLANMIŞ ÇİMENTO BAĞLAYICILI KOMPOZİTLERİN YORULMA PERFORMANSI

Aleessa Alam, Burhan
Doktora, İnşaat Mühendisliği Bölümü
Tez yöneticisi: Prof. Dr. İsmail Özgür Yaman

Mart 2016, 100 sayfa

Bir yolun kullanım süresi boyunca gerçekleştirilen onarım ve takviye işlemleri o yolun yapım işleri kadar önemlidir. Bu kapsamda, doğru ve verimli tamir yöntemi uygulamak ekonomik ve teknik nedenlerden dolayı son derece önemlidir. Yolda oluşan hasar seviyesine bağlı olarak bu hasarı onarmak için kullanılabilecek pek çok farklı yöntem vardır. Bu yöntemlerin arasında yer alan ve doğrudan yol üzerine ya da yolun üst tabakasının bir kısmıyla değiştirilen takviye yöntemi en yaygın yöntemlerinden biridir. Bu takviye yöntemi asfalt veya beton üzerine uygulanabilir. Beton takviyeler özellikle beton yolların artan kullanımı ile beraber son zamanlarda büyük bir önem kazanmaktadır. Bunların hepsi asfalt ile karşılaştırıldığında beton yolun uzun ömürlü özeliğiyle ilişkilendirilebilir. Ancak, betonun rijit doğası yüzünden bu kaplamanın kalınlığı daha yüksektir.

Bu çalışmada, daha az kalınlıkta kullanıldığında yol ve kaplama arasındaki çatlakların aktarılmasını azaltma kabiliyeti olan şekil değiştirme sertleşmesi gösteren yüksek performanslı lif donatılı çimento bağlayıcılı kompozitlerin kullanılması önerilmektedir. Bu özelliği test etmek için beton yol üzerine uygulanacak şekilde iki ECC karışımının yorulma altındaki performansları incelenmiştir. Bununla beraber, farklı bileşenler içeren ECC karışımlarının yorulma performansı incelenmiştir. Ayrıca, Weibull dağılımı kullanarak yorulma altında bu karışımın başarısızlık olasılığı tespit

edilmiştir. Buna ek olarak, yorulma deneyinin süresini azaltmak için iki yeni yorulma dayanımı tahmin eden yöntemler önerilmiştir.

Anahtar kelimeler: Tasarlanmış çimento bağlayıcılı kompozitler (ECC), kaplama, yorulma deneyi, Weibull dağılımı, yorulma dayanımı tahmini

To my brother Dignar,
may your soul rest in peace

ACKNOWLEDGEMENT

In my PhD journey I had the honor to work with a professor whom I believe that no one can better teach me the real meaning of doctorate degree better than him. No matter how good I am or I will be, I can only thank him for everything he has done to me. My deepest appreciations are for Prof. Dr. İsmail Özgür YAMAN.

I want also to thank Prof. Dr. Mustafa TOKYAY, Prof Dr. Murat GÜLER, Assoc. Prof. Dr. Mustafa Şahmaran, Assoc. Prof. Dr. Sinan Turhan ERDOĞAN and Assoc. Prof. Dr. Serdar GÖKTEPE for all their help and valuable advices and recommendations

Certainly, I would thank my parents Hasan and Siham, and my brothers Aslan and Hani for their endless support, and being my motivation to work.

I also want to thank the people who were always with me in my all ups and downs, my new family, my friends who I can sort them only in alphabetic order Deniz KOÇAK, Derya ÖVER, Emre AKIN, Emre KAMAN, Görkem BAYRAMTAN, Gözde ÖZERKAN, Işın MERİÇ, Mehmet Kıvanç KASAPGİL, Melis YILDIZ, Meltem ERDİL, Meltem TANGÜLER, Merve ZORLU, Negar MADANİ, Sema Melek YILMAZTÜRK, Süleyman Bahadır KESKİN, Tümay ÇELİKKOL KOÇAK, Umut SILAY, Yaprak ONAT and Yaprak SERVİ.

My special thanks go to my colleagues at the METU Materials of Construction Laboratory Kemal ARDOĞA, Mahdi MAHYAR, Murat ŞAHİN and Hasan ESER.

I want to thank the Turkish Cement Manufacturer Association for all its supports.

Last but not least, I want to thank the staff of METU Materials of Construction Laboratory; Cuma Yıldırım, İsmail Tekin and Ali Sünbüle for their physical support during my experiments

TABLE OF CONTENTS

APPENDICES

LIST OF FIGURES

FIGURES

LIST OF TABLES

TABLES

CHAPTER 1

INTRODUCTION

1.1. General

Being one of the most interactively used infrastructure in Turkey, pavements have seen lot of attention in the last decades. Along with this, the growing sector of cement and concrete production is also trying to take its place in the pavement sector. The application of concrete pavements is not restricted to newly constructed roads, but can also be applied to existing asphalt or concrete pavements as an overlay. In this work, Engineered Cementitious Composites (ECC) was suggested as an overlay material for pavements since it has the ability to prevent the reflection of cracks upwards into the new pavement layer. This suggestion is based on the good ductile performance of ECC, which will allow it to have a better fatigue strength compared to traditional concrete. However, determining this strength is not an easy job, and might be really time and effort consuming. For this a good test planning is needed to determine the proper design parameters of ECC mixtures. This will also be very helpful when there is a need for a repair work. The previously determined behavior and parameters of different ECC mixtures can help in the design stage to choose the correct material to be applied and hence the required thickness of this application to be able to handle the traffic loads.

1.2. Objective and scope

This work has three main objectives. Firstly, the use of two ECC mixtures as a pavement overlay was investigated through experimental fatigue testing. The second objective is investigating the effects of mineral admixtures and aggregate size on the

fatigue performance of ECC. To testify this, three different ECC mixtures were prepared and tested under monotonic and fatigue loading. The failure probabilities of these mixtures under fatigue were calculated using statistical Weibull analysis. Finally, since fatigue testing involves a tedious testing program, two new methods related to fatigue life prediction (based on the relation of the specimen under the monotonic and cyclic loadings) were developed as a third objective.

This thesis contains six chapters including this one. In the second chapter, a brief background about concrete pavements and overlays, fatigue tests and previous works related to ECC are explained. In the third chapter, the materials and the devices used in this work along with and the test procedures and the analysis methods are explained. Chapter four contains the test results and the discussion made about them. The fifth chapter explains the steps and procedures used to develop the new fatigue prediction methods. At the last chapter the conclusions along with the recommendations of this work are presented.

CHAPTER 2

LITERATURE REVIEW

The greatest unknown soldier behind the modern civilization is probably the infrastructure developed by humans. Roads for example have been acting as the main veins between populations since centuries. However, making a road does not end by just building it, but that is just the beginning. The service life of a road is expected to be over several decades, and that can be reached only through proper repair and maintenance methods. Pavement overlays are one of these methods where there is no need to build the subgrade of the road again. These overlays can be made by using the latest developed materials and technologies to withstand any severe conditions. Still, no matter how good an overlay can do against weather, its first problem will be the mechanical stresses developed by the repeated passage of vehicles. This fatigue problem can lead to inevitable failure where even repair is not a solution. Although that the source of this problem looks simple and easy to be understood, testing it in a way that represents the real conditions (randomly passage of vehicles with different loads at various time) and service life duration (which might extend to years or billions passage of vehicles) is closer to impossible than hard. For that, researchers keep developing new materials to perform better under fatigue. Along with this search, they are also looking for best fatigue testing methods that suit the investigated elements, and trying to invent new materials when the boundaries of the tested ones are not enough.

This thesis is investigating the fatigue performance of a relatively new material that can be used as an overlay for both asphalt and concrete pavements. It is also suggesting new methods to predict fatigue life based on monotonic test results.

2.1. Concrete pavements

Like many other infrastructure types, concrete is used as a pavement in various places such as roads, parking lots and airport runways. The high durability and low maintenance costs through decades of concrete pavements' service life are the main properties that outcome the low initial costs of asphalt pavements. However, these properties can be reached only through a proper design, selection and use of the concrete ingredients and application techniques. This is mainly because of the fact that pavements can be exposed to severe environmental conditions not to mention the dynamic loadings of vehicles from different sizes and speeds. For that, a low performance concrete or a one with many flaws will not survive too much as a pavement (Al-Qadi, Scarpas, & Loizos, 2008; Delatte, 2014).

With a great success, the first use of concrete in pavement dates back to 1891 in Ohio. Following that in the early of the 20th century many streets in USA were paved using concrete like Front Street in Chicago, which lasted for 60 years after it was built in 1905. At the end of that century some states used concrete pavements in excess of 90% of their new roads (Delatte, 2014). However, this widely use in USA and many advanced countries was not reflected in Turkey in contrary to its cement production capacity. While most of the concrete pavements in Turkey were in airports and parking lots, a shy but promising application of few kilometers long roads has started in this century.

Beside concrete pavements, concrete overlays are also widely used when the roads are maintained or upgraded using the original pavement as a base layer. With this method, it is also possible to get the traffic back on track more rapidly. This kind of concrete overlays, compared to the asphalt ones, has the advantages of extending service life, increasing structural capacity, reducing maintenance requirements and lower life cycle costs. Concrete overlays are divided into three categories: bonded, partially bonded and unbonded concrete overlays (Bissonnette, Courard, Fowler, & Granju, 2011). In Table 2.1 a comparison between these three types is presented. If the concrete overlay is to be applied on an asphalt pavement, there are two more types used for this case, whitetopping and ultra-thin whitetopping. It is also possible to use hot mixture asphalt

as an overlay over concrete pavements. All of these overlays have their advantages and disadvantages. The selection of an overlay type is done mainly based on the evaluation of existing pavement condition and traffic capacity (ACI Committee 325, 2006).

Table 2.1 Summary of concrete overlays of existing concrete pavements (ACI Committee 325, 2006)

	Bonded	Partially bonded	Unbonded
Typical thickness	75 to 100 mm	150 to 200 mm	150 to 300 mm
How bonding condition is achieved	- Cleaning and preparing surface (such as shotblasting) - Possible application of bonding agent	No special surface preparation other than sweeping	Placement of a layer to separate overlay from existing pavement
Condition of existing pavement	- Relatively good condition - No materials-related distress	Fair to moderate condition	Fair to poor condition
Preoverlay repair	All deteriorated cracks, joints, and punchouts	Most deteriorated cracks, joints, and punchouts	Limited repair
Special design and construction considerations	- Achieving bond between two concrete layers - Matching joints of overlay with those in existing pavement	Matching joints of overlay with those in existing pavement	- Achieving separation between two concrete layer - Mismatching joints of overlay with those in existing pavement

The quality of concrete overlay is measured by different tests and aspects. These tests are related to the type of the concrete used in the pavement. Besides the strength proerties, unit weight, air-voids characteristics, durability and permeability are the commonly controlled properties. But to measure the effect of the repeated transportation loads fatigue properties must be determined.

2.2. Fatigue testing

An application of a load below the ultimate strength of a material mostly will not lead to failure. However, if this load application is repeated continuously the nucleated small cracks of flaws occurred in the production of the material will be followed by crack growth and then a sudden fatigue failure. The number of the repetitions is related to many factors like the scale of the applied load, the type of the material and the frequency of the load application. All of these make the fatigue incident a hard one to investigate, but yet an important one because of the catastrophic damage that might occur without any warning. Once the fatigue cracks are initiated the failure will happen when a combination of the following basic loading patterns occur (Schijve, 2001).

1. The repetition of the load must have a pattern of a low and high peak values in tension, compression or both combined, Figure 2.1.
2. The level of the peaks and the difference between them must be both high enough to allow the initiation of the cracks.
3. The loading pattern should be repeated at a sufficient number to make the cracks grow and reach the failure point. This number is related to nature and the level of the peaks.

In addition to these three patterns, there are some secondary ones like the shape and the condition of the element subjected to the fatigue loading and the frequency and the continuity of load pattern application. All of these factors make each material or specimen a unique one under fatigue tests. In general, there are two main methods used to investigate the fatigue behavior of a material, the stress-life method and the strain-life method. The first one, based on stress levels only, is the most commonly and traditionally used method despite of being the least accurate approach, especially for low-cycle applications. However, the application of this method is much easier for a wide range of design applications, and it represents high-cycle applications accurately, therefore it has been used by many researchers, hence it has a big database. On the other hand, the plastic deformation at localized regions are more detailed analyzed through the strain life methods where the stresses and strains are considered for life estimates, which makes this method more adequate for low-cycle fatigue applications.

However, some idealizations should be compounded, and so some uncertainties will exist in the results (Campbell, 2012; Lee, Pan, Hathaway, & Barkey, 2011; Pokluda, 2010).

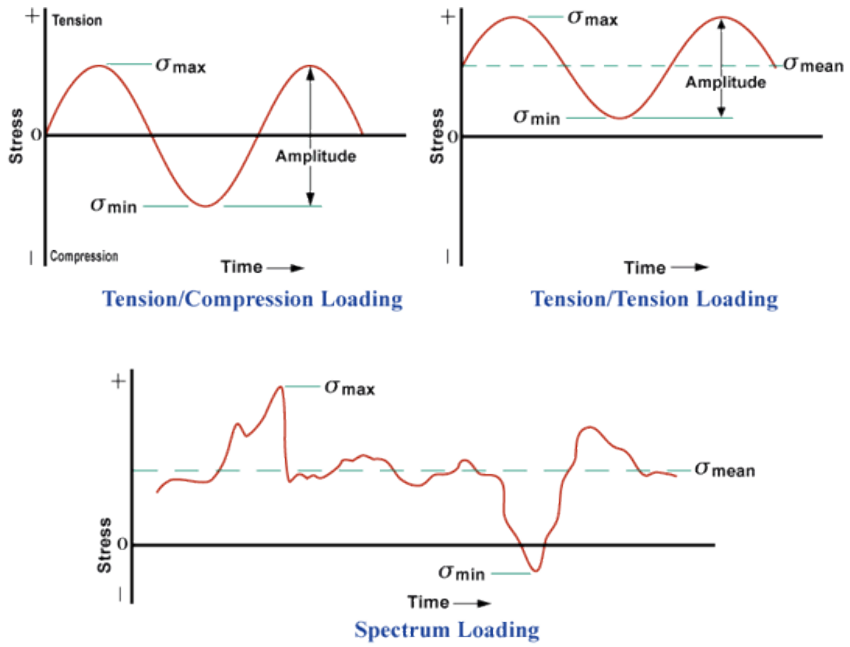

Figure 2.1 Different fatigue loading patterns

2.2.1. The stress-life method

In this method a repeated or varying forces of specified magnitudes are applied on the specimens until failure occurs or the counted number of cycles reach a specific limit. The final number of the cycles represents the fatigue life of the material under the fatigue loading. This strength can only be obtained after performing a quite number of tests because of the scattered nature of fatigue. The first set of the fatigue test is made at a stress level close to (like 90%) the ultimate strength of the material. The second set of tests is made at a stress level that is less than the first one, and this continues until enough test results are obtained to plot the S-N curve (Figure 2.2). This diagram might be the most commonly used output of a fatigue test, which is Stress-Number of cycles to failure curve, or as it is usually called S-N curve. To obtain this curve

different loading patterns based on one of the following rules can be applied on the test specimens (Shigley, 2011):

1. Keep the minimum stress level constant and change the maximum stress level.
2. Keep the average stress level constant and change the minimum and maximum stress levels.
3. Keep the stress level ratio constant and change the value of the maximum and minimum stress level.

At high stress levels the number of cycles to failure is low, and vice versa. One thousand is the number that separate low cycles fatigue from high cycles fatigue (Figure 2.2). The failure mechanism in this two types of fatigue is the same:

1. a crack is initiated in the weakest region or the stress concentration area
2. the crack propagates with repeated loading
3. when the crack size reaches a critical size a final rapid crack propagation occurs and the specimen fails

The last stage of the failure mechanism might occur in one cycle or even less than that. For this, the sum of the cycles of the first two stages represents the fatigue life N_f

$$N_f = N_i + N_p \qquad \textit{Equation 2.1}$$

Where N_i is the number of cycles for crack initiation and N_p is the number of cycles for crack propagation. In high cycle fatigue N_i is relatively high. With increasing stress level, N_i decreases and N_p dominates

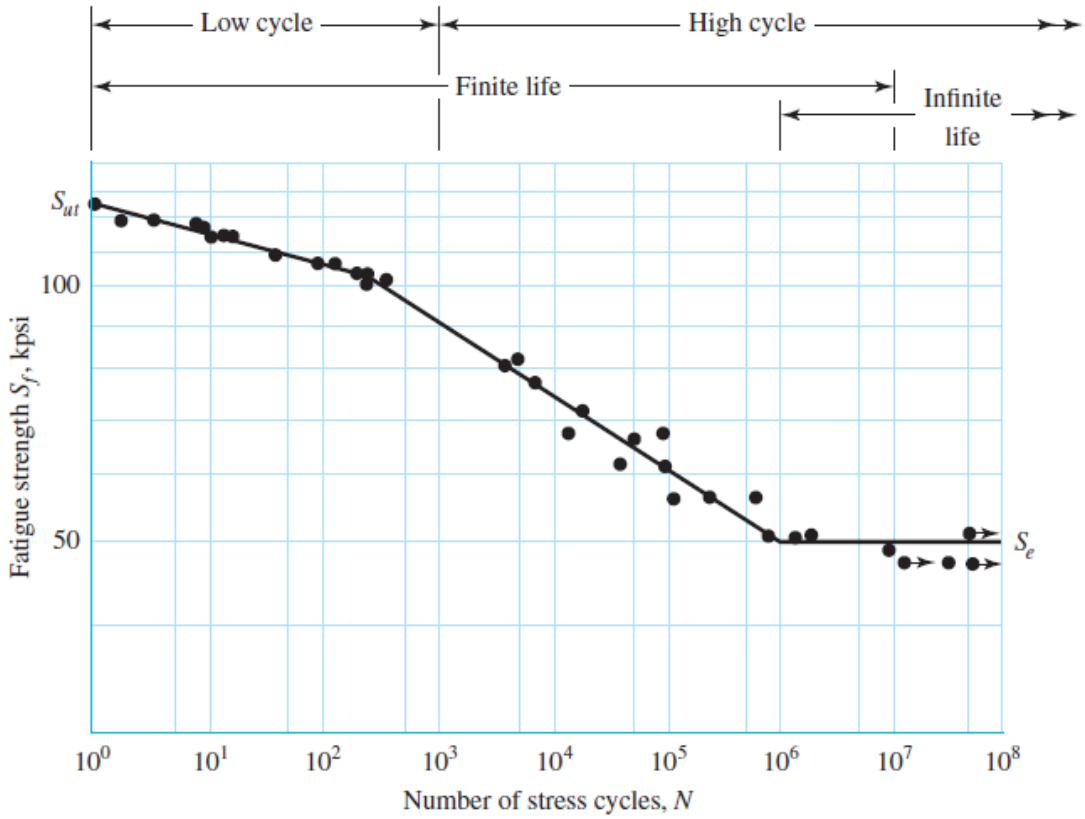

Figure 2.2 An S-N diagram shows the low and high cycles regions (Shigley, 2011)

2.2.2. The strain-life method

Notch, crack, or other area of stress concentration that form a local discontinuity in the material are generally the main place where the fatigue failure begins. At this discontinuity, a plastic strains occurs when the stress exceeds the elastic limit. When the plastic strains are repeated in a cyclic way the fatigue fracture comes into place. Because of this, the behavior of the materials under cyclic deformations should be investigated. In this case the fatigue limits are defined by low and high strain levels, and the changes occur in the stress amounts corresponding to those levels. For example, the elastic limits of annealed steels are likely to increase when subjected to cycles of stress reversals, while cold-drawn steels exhibit a decreasing elastic limit. In other words, under strain life method some materials show stress hardening and some materials show stress softening (Figure 2.3). For concrete structures the stress life

method is usually the one used because in real life the cyclic loadings are done through the variations of the loads applied (Shigley, 2011).

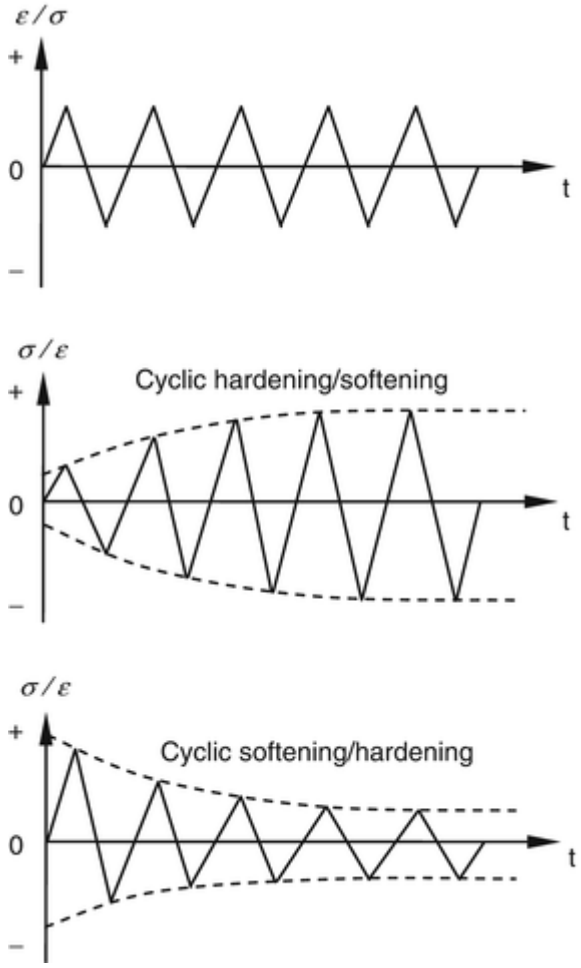

Figure 2.3 Definition of cyclic hardening/softening, hardening in the middle graph and softening in the one at the bottom (Z. Zhang, 2013)

2.2.3. Fatigue of concrete

Fatigue failures are usually seen in machine parts since they are more subjected to vibration and dynamic loads. This let the focus on metal fatigue bigger compared to the rest of the materials, hence most of the laws and equations are about metal specimens. Yet, for concrete specimens, it is found that the Paris law, for example, which states that the crack length increment per cycle is a power function of the stress intensity factor amplitude, is valid only for one specimen size (the law parameters

being adjusted for that size) or asymptotically for very large specimens (Bazant & Xu, 1991). This for example helps to understand the fatigue occurred under the effect of creep. Under static loading, the creep deflections grow in an approximately logarithmically way while for the cyclic loading case they grow linearly. This can be considered as an outcome of the Paris law. As a result of that, the fact that cyclic creep is not that important for ten years of service, this might not be true for longer periods. (Bazant & Hubler, 2014). For plain concrete the stress level of failure under high fatigue cycles (more than one million cycles) is low (around 60% of ultimate stress). This is naturally because plain concrete does not have any mechanism that allow it to handle the loads after the occurrence of the first crack (ACI Committee 215, 1992).

For that, concrete is not used under dynamic loads unless it contains some type of reinforcement. In this scope fibers seem to be a promising solution for many applications where ordinary reinforcement rebars are hard to be used. It is well known that the contribution of fibers to compressive strength is not significant generally, but they can increase the tensile strength tremendously in the whole part of the concrete homogenously (Balaguru & Shah, 1992; Gopalaratnam & Shah, 1987; Song & Hwang, 2004; Yao, Li, & Wu, 2003; Zollo, 1997). However, this improvement depends on a good combination between the fiber type and the matrix of the concrete, which can be only done through a wise selection of fibers, binding materials, aggregate and mix design (Collins, Mitchell, & MacGregor, 1993; Ferrara, Park, & Shah, 2007; Walraven, 2009). All of these actually provide a wide variety of fiber reinforced concrete that can be used under dynamic loads.

2.3.Engineered Cementitious Concrete (ECC)

The use of fiber with a moderate fraction of 1 to 2% per volume makes the concrete an adaptable material that can serve many different structural needs and functions while preserving the ability to be cast and produced like an ordinary concrete. The main advantages of this kind of fiber reinforced concrete are improving the modulus of rupture, increase the resistance against impact and fatigue loads, fracture toughness, crack resistance, etc. There are many types of fibers that can be used in this application, like steel, glass fibers and polypropylene. With the optimized use of these fibers they

can control the crack width and even act as secondary reinforcement (Li, Banthia, Bentur, & Mufti, 1997; Li, 2002).

Engineered Cementitious Composites (ECC) is a special type of fiber reinforced concrete that uses PVA fibers and mortar as the main components (Li & Kanda, 1998a). The main advantage of ECC is its high strain capacity compared to normal concrete, which allows it to absorb more energy and hence perform much better under dynamic loads (Boshoff & van Zijl, 2007; Habel & Gauvreau, 2008; Maalej, Quek, & Zhang, 2005). Besides being ductile, ECC is also known to be a strong and durable material. The durability of ECC has been studied by many researchers. For example, Şahmaran and Li had examined the durability of ECC in highly alkaline environment (Şahmaran & Li, 2008). In their work, pre-deformed specimens were immersed in alkaline solution for three months at a constant temperature of 38 ºC. When the specimens were tested again it was found that self-healing ability of ECC is effective based on the occurrence of a slight drop only on the ductility of the pre-deformed specimens. Also in that work it was reported that no expansion occurred on the lengths of the bar specimens after 30 days of curing at a temperature of 80 ºC in alkali solution.

In another study, it was found out that when ECC is used in a pavement it showed good wear resistance under traffic loads (Li & Lepech, 2004). Moreover, the freezing-thawing resistance of ECC was reported to be five times better than that of traditional concrete after 300 cycles, where the ECC preserved its strain capacity (Li et al., 2003). In addition to all of the above, reinforced ECC also shows a good corrosion resistivity. Researches on this topic reported that ECC showed almost no damage due to the corrosion compared to normal concrete, which makes the service life of reinforced ECC much higher when compared to concrete (Kanda, Saito, Sakata, & Hiraishi, 2003; Miyazato & Hiraishi, 2005).

Nevertheless, this enhancement is obtained for a high cost unfortunately, the thing that makes a perfect design and a correct use of ECC inevitable to compensate that cost. The use of such a material in the connection joints of steel-concrete hybrid structures for example can be effective against the high stress concentrations. Not to mention that this type of material has an enhanced ductile performance which can improve the

behavior of the structure under seismic and dynamic loads (Li & Kanda, 1998b). This is due to the ability of fibers to control and reduce crack nucleation and hence enhance the performance of the structural elements under impact and fatigue loadings (Mindess, Young, & Darwin, 2003).

The origin of ECC goes back to the University of Michigan where a research about high performance fiber reinforced composite material resulted in a product patented as Engineered Cementitious Composites. The main advantage of ECC is that it has a tensile strain capacity of about 300-500 times higher than normal concrete. The working mechanism of ECC at micro scale allows it to exhibit strain hardening after the initiation of the first crack. The well working bridging incident of the fiber in ECC ensure that a new crack occurs after the previous one reach an average opening of about 60 μm. That is how ECC is able to show multiple cracking in a way of more numbers of the cracks with small sizes (Figure 2.4) (Li & Kanda, 1998a; Li et al., 1994, 1997).

All of these are possible because of the engineered design of the ECC matrix. The high performance in this type of materials is obtained through the good interface interaction between the fibers and the bonding part. In ECC the matrix is formed from cement, water, sand, chemical admixtures and sometimes mineral additives. The absence of coarse aggregate allows the matrix to be more homogenous (Li & Kanda, 1998a). ECC matrix is designed in a way that lowers the toughness, the bridging stress and the chemical bond of the fiber matrix interface, while at the same time allows enough friction between the fibers and bonding material to form multiple cracks. The volume percentage of the fibers in ECC is about 2% and the fiber type preferred is PVA. This type of fibers is easier to be produced with a diameter less than 50 μm, which allows a strain hardening of the matrix for that volume percentage (Li et al., 1997; Li, Mishra, & Wu, 1995; Li, Wu, Wang, Ogawa, & Saito, 2002; Wang & Li, 2007).

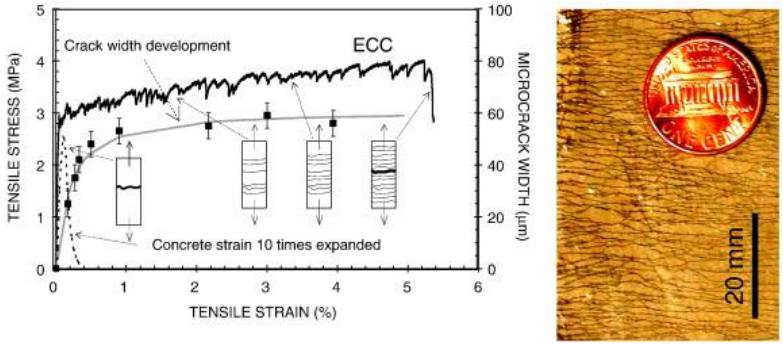

Figure 2.4 Typical tensile stress–strain curve and crack width development of ECC (Şahmaran & Li, 2009)

There is a limited amount of research on the fatigue performance of ECC, and the existing work on ECC under fatigue loads were more concerned on its use as a repair layer over normal concrete. In 2002, Zhang and Li have conducted an experimental study and theoretical analyses on the monotonic and fatigue performance in bending of a PVA-ECC overlay system. An old concrete substrate was covered by a layer of ECC with equal thickness to form a beam specimen. The bottom layer of the beams formed of two halves where isolating tapes were applied on the face and the upper corner of the joint sides of the two parts to form a totally un-bounded crack zone, Figure 2.5. Three combinations were used for the tests. The first one was a concrete overlay with a smooth interface with the bottom layer. The other two were formed of an ECC overlay with one smooth and one rough interfaces. The test results showed that ECC overlay has better performance under both monotonic and cycling loadings when compared to normal concrete. In addition to this, the interface condition between the two layers had almost no effect on the fatigue life but the deformations for specimen with smooth interfaces were larger (J. Zhang & Li, 2002).

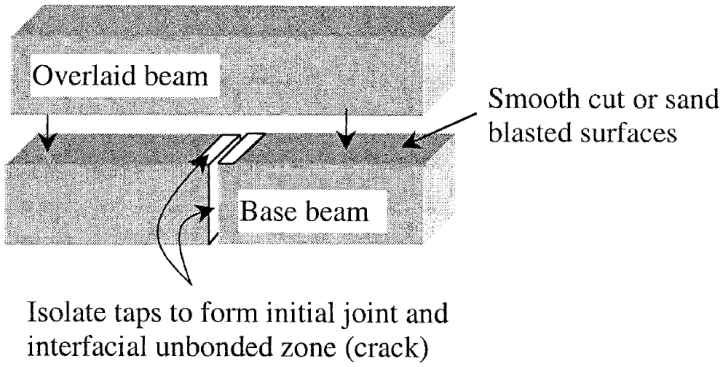

Figure 2.5 Test specimen preparation

A similar work was done by Leung et al. in 2007, but in this one there was no crack or isolated interfaces between the layers. The dimensions of the specimens were kept constant as 100×100×500 mm^3. Three types of specimens were prepared, where the thicknesses of ECC top layer were 0, 25 and 50 mm. The test results showed that with the increase of ECC thickness the flexural strength and the deflection of the beams were increased compared to normal concrete with ratios of 18% and 42% for flexural strength and 64% and 200% for deflection for 25 mm and 50 mm thicknesses respectively. Along with that, the fatigue life time was also improved with magnitudes of 2 and 3 times for thicknesses of 25 and 50 mm respectively. The deflection capacity without failure under fatigue loading was also increased with the increment of ECC thicknesses. All of these are because of high ductility and multiple cracking capability of ECC (Leung, Cheung, & Zhang, 2007).

In 2011 Kakuma et al. have performed an analysis of an ECC-Steel composite deck under fatigue loading of wheel trucking. This was done by applying a fiber bridging degradation model to finite element analysis. The analysis results showed that even after 1.2 million cycles the maximum crack width did not exceed 0.04 mm, which means that ECC overlay over the steel deck will improve its long term durability. Moreover, for a loading pattern of 2400 vehicle/day/lane the fatigue assessment showed that for the above number of cycles the service life of the deck will be about 400 years (Kakuma, Matsumoto, Hayashikawa, & He, 2011).

While the above mentioned works have investigated ECC under fatigue as a part of a composite structure, Qian et al. in 2013 have published a research where ECC was tested alone under fatigue. In that work, the authors integrated the finite element analysis method with fatigue test results of concrete and ECC specimens to obtain a design chart for service life of overlay thickness (Figure 2.6). The test results showed that compared to unbonded concrete or hot mixture asphalt overlays ECC has a significant advantage because of its reduced thickness, extended service life and/or less frequent repair events. In addition to these, the total costs of ECC when compared to unbonded concrete and hot mixture asphalt were less by 39.2% and 55.7% respectively (Qian, Li, Zhang, & Keoleian, 2013).

However, investigating the ECC itself under fatigue loading would provide better understanding of how it works, since the fatigue properties are highly influenced by the ingredients and the composition, and in the literature there was no published test results showing the fatigue performance of ECC up to the date where this thesis work has started.

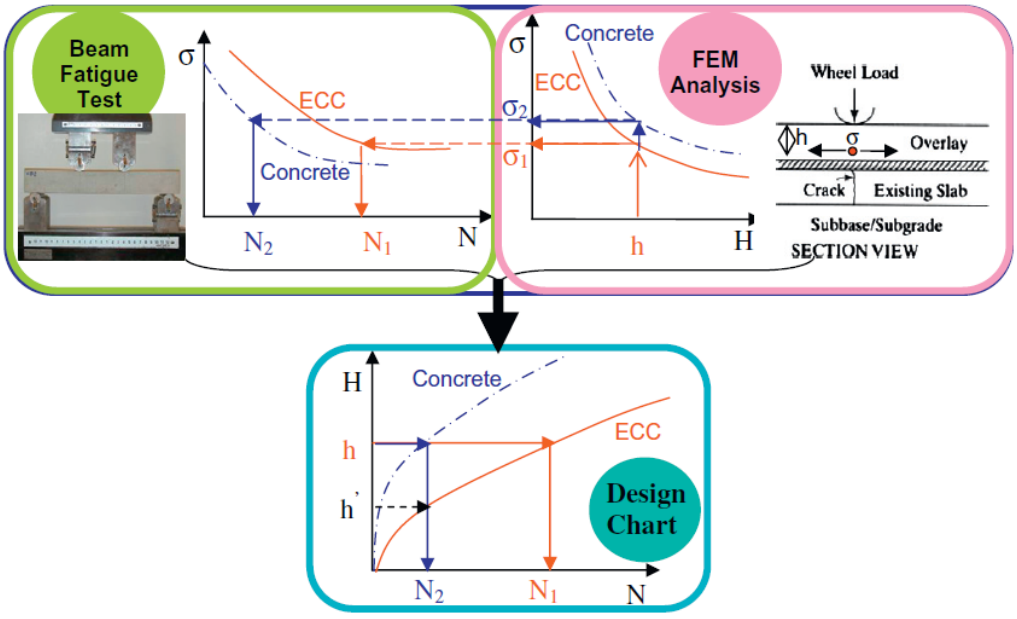

Figure 2.6 Integration of FEM analysis and fatigue test results into a design chart (Qian et al., 2013)

2.4. Fatigue life analysis

Considering the inevitable scatter in the fatigue life, to evaluate the results of fatigue tests in a proper way a statistical approach is needed where a new relationship between probability of failure, stress level and number of fatigue life cycles (P-S-N) is defined. This relationship can be presented through different S-N curves, each for a given probability of fatigue, P. A simple and easily applied probability density function, the two-parameter Weibull distribution, is widely used in this case, presented in Equation 2.2 (Liu, Meng, Ning, & Li, 2015; Sakin & Ay, 2008; Weibull, 1961; Wormsen & Haerkegaard, 2015).

$$f(x) = \frac{\beta}{\alpha}\left(\frac{x}{\alpha}\right)^{\beta-1} e^{-\left(\frac{x}{\alpha}\right)^{\beta}} \quad \alpha \geq 0, \beta \geq 0 \qquad \textit{Equation 2.2}$$

Where α and β are the scale and shape parameters. By taking the integral of this equation a cumulative density function is obtained, as shown below.

$$F_f(x) = 1 - e^{-\left(\frac{x}{\alpha}\right)^{\beta}} \qquad \textit{Equation 2.3}$$

The last equation can be rewritten as:

$$e^{-\left(\frac{x}{\alpha}\right)^{\beta}} = 1 - F_f(x) \qquad \textit{Equation 2.4}$$

Considering that $R_x = e^{-\left(\frac{x}{\alpha}\right)^{\beta}}$ is the probability of survival (or reliability), and $P_x = F_f(x)$ is the probability of failure, Equation 2.4 can be rewritten as:

$$R_x = 1 - P_x \qquad \textit{Equation 2.5}$$

In Equation 2.5, if $x = \alpha$ then $F_f(\alpha) = 1 - e^{-(1)^\beta} = 1 - 0.368$ which means the probability of failure at α number of cycles is $F_f(\alpha) = P_\alpha = 63.2\%$.

From this, it can be seen that the aim of using Weibull distribution in fatigue test is to find the S-N curves that correspond to different failure probabilities like P=[0.1, 1, 10, 50, 90, 99, 99.9], or the corresponding reliability of R=[99.9, 99, 90, 50, 10, 1, 0.1].

Since $R_x = e^{-\left(\frac{x}{\alpha}\right)^\beta}$, when $x = N_{R_x}$the number of cycle indicating a survival probability ratio of R_x, the following equation can be written.

$$N_{R_x} = -\alpha(ln(R_x))^{1/\beta} = 1 - N_{P_x} \qquad \textit{Equation 2.6}$$

Where N_{P_x} is the number of cycle indicating a failure probability ratio of P_x.

By taking the double natural logarithm of Equation 2.4 the following equation is obtained.

$$ln\left(ln\left(\frac{1}{1 - F_f(x)}\right)\right) = \beta\, ln(x) - \beta\, ln(\alpha) \qquad \textit{Equation 2.7}$$

This equation can be written in linear form as:

$$Y = jX - k \qquad \textit{Equation 2.8}$$

Where $Y = \ln\left(\ln\left(\frac{1}{1-F_f(x)}\right)\right)$, $j = \beta$, $X = \ln(x)$ and $k = -\beta\ln(\alpha)$

By using Equation 2.8, the set of fatigue test results can be verified whether it complies to the two parameter Weibull distribution or not. This can be done by performing a regression analysis on the linear relationship between Y and X, and see how good it is.

During the calculation steps, the probability of failure $F_f(x)$ are determined using Equation 2.9.

$$F_f(x) = P_x = \frac{i}{h+1} \qquad \textit{Equation 2.9}$$

Where i is the number of the test specimen in ascending order of failure cycles and h is the total number of test specimens.

To evaluate a fatigue test using Weibull distribution the following steps can be applied.

1. For each stress level, the values of failure cycles are sorted ascendingly, and the number i for each specimen is given according to this sorting.
2. The failure probability for each specimen is calculated using Equation 2.9.
3. Using the results from the previous step and the number of failure cycle (x), the values of Y and X from Equation 2.8 can be calculated.
4. After all the values of Y and X for a stress level are determined, a linear regression can be applied to these points to determine the parameters j and k from Equation 2.8, and hence α and β.

Using α and β the number of cycle indicating a survival probability R_x can be calculated using Equation 2.6 for each stress level, and by using these numbers new S-N curves for the desired survival probabilities can be drawn.

The slope of the Weibull plot, beta (β), indicates the class of the failure and also determines which member of the family of Weibull failure distributions best fits or describes the data. (Abernethy, 2006). In Figure 2.7 the effect of this slope on Weibull function is presented.

- β < 1.0 is an indication of infant mortality
- β = 1.0 shows that random failures occur (independent of age)
- β > 1.0 is an indication of wear out failures

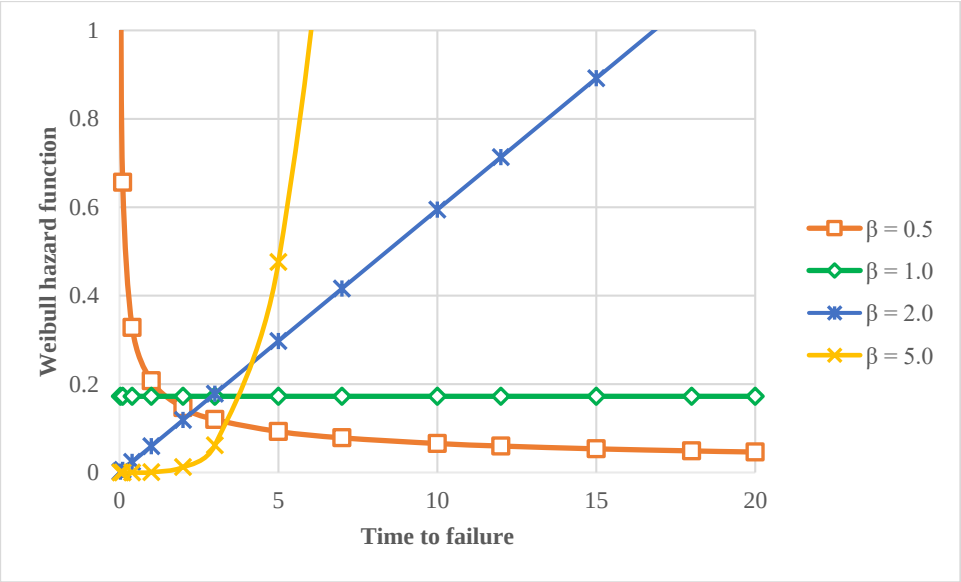

Figure 2.7 Effect of β on the Weibull function

CHAPTER 3

EXPERIMENTAL PROGRAM

3.1. General

The main experimental work in this study was divided into two parts. The first one is investigating the fatigue performance of a normal concrete base coated with ECC overlays. The second one is determining the fatigue performance of ECC mixtures made with different mineral admixtures. The tests carried out in both cases were fatigue tests on beam specimens under third point bending. While the aim of the first part was to evaluate the performance of the different overlays, the second part was aimed to evaluate the fatigue performance of ECC mixtures and determine their design parameters.

3.2. Materials

3.2.1. Cementitious material

The main binder material used in this study was an ordinary portland cement CEM I 42.5R produced according to TS EN 197-1. Along with the cement three different types of mineral additives, class F Fly ash (FA) from Sugözü Thermal Power Plant, Ground Granulated Blast Furnace Slag (GGBFS) from İsdemir Iron and Steel Plant and Micro Silica (MS) were used in the production of the different mixtures.

3.2.2. PVA Fibers

The type of fibers used in this study is oil coated Polyvinyl alcohol (PVA). This fiber type can provide the ECC mixtures with the required interface properties. Oil coating helps to prevent the chemical bonding between the fiber and the matrix and ensure the

ductility needed. The PVA fiber used in this study is commercially obtained, which is stated to be coated with 1.2% hydrophobic oiling agent and have a diameter of about 39µm, a length of 8 mm, an elongation of 6%, a tensile strength of 1600 MPa, an elastic modulus of 42.8 GPa and a density of 1300 kg/m^3.

3.2.3. Aggregate

Two types of aggregates were used in this study, silica sand for ECC mixtures, and a mix of river sand and crushed limestone for base concrete and Micro Silica mixtures. The silica sand aggregates were divided into three sizes 0-400 µm, 300-700 µm and 600-1200 µm. The sizes of river sand and the crushed limestone were 0.1-5 mm and 0- 15 mm respectively.

3.2.4. Chemical admixture

To compensate the workability loss due to the low water/binder ratio, Glenium 51 trademark polycarboxylic ether (PCE) based, high range superplasticising admixture (SP) was used in all the mixtures. Also, an air entraining agent (AEA) was used in the production of the base concrete and micro silica mixtures to simulate the real conditions, where these types of concretes are designed to be durable against freezing and thawing.

3.3. The production of the mixtures and the specimens

Preparing ECC mixtures was performed by first mixing the cement and the mineral admixtures (FA or GGBFS) together. Later the water and SP are added and the mixture is continuously mixed for 2 minutes before adding the sand and mix for another 2 minutes. Finally, the fibers were added and the mixing was continued until a homogenous mixture was obtained. As for the base concrete and concrete with micro silica mixtures, the aggregates were mixed together for one minute. After that the binder materials were added to mixer and mixed for another minute. At the end the water and the chemical admixture were introduced and mixing was continued until a homogenous mixture was obtained.

3.3.1. Fatigue performance of ECC as an overlay

The base concrete mixtures (SUBC) were cast into steel molds with dimensions of 400×75×75 mm^3. These specimens were cured for three months to form an old concrete for the base layer, and after that they have been cut into two parts with a height of 30 mm. The overlays were cast over these parts with three different thicknesses of 25, 35 and 50 mm. The overlays were formed of three mixtures, F-ECC1 (ECC with fly ash), S-ECC (ECC with slag) and MSC (concrete with micro-silica). The mixture properties are presented in Table 3.1.

Table 3.1 Mixture properties of overlay test specimens

	F-ECC1	S-ECC	SUBC	MSC
OPC	1	1	1.0	1.0
FA	1.2	-	-	-
GGBFS	-	1.2	-	-
MS	-	-	-	0.1
Water	0.59	0.59	0.5	0.3
SP	0.01	0.01	0.005	0.012
AEA	-	-	0.001	0.001
Silica sand 0-0.4 mm	0.77	0.77	-	-
Silica sand 0.3-0.7 mm	-	-	-	-
Silica sand 0.6-1.2 mm	-	-	-	-
Fine aggregate	-	-	2.3	1.5
Coarse aggregate	-	-	2.3	2.4
PVA fiber	0.05	0.04	-	-
Density (kg/m^3)	1990	2149	2402	2422

To increase the homogeneity in the production procedure of ECC overlay and reduce the variability in the fatigue test results, the new overlay specimens were casted into plate molds with plane section of 600×600 mm^2. The base concrete was cast first with a height of 30 mm. After that, ECC mixtures were cast at the desired thickness. The specimens for the fatigue tests were cut out of these plates according to the pattern shown in Figure 3.1.

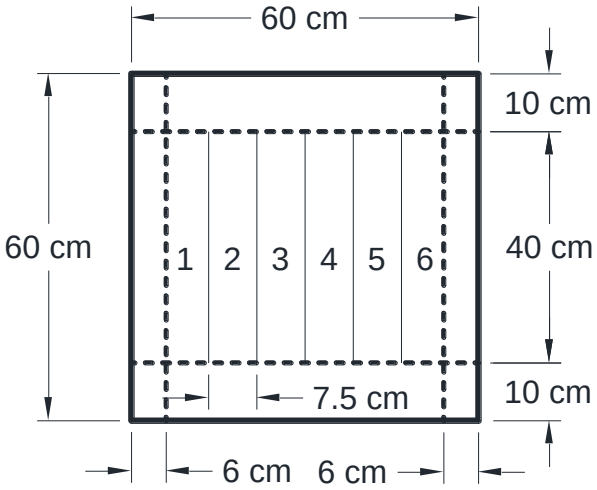

Figure 3.1 Plate cutting plan to obtain overlay beams

3.3.2. Bonding and shrinkage testing of ECC as an overlay

Casting ECC overlay specimens as plates showed a bonding problem between ECC and base concrete after a period of time. To investigate the cause of this problem two methods were used. The first one was used to examine the bonding strength between ECC and concrete base through the slant shear test (Figure 3.2). First the base concrete mixture was cast into cylindrical molds with 45º inclined position. On the next day different ECC mixtures were cast on top of the base concrete after the position of the molds was returned to normal. The specimens after that were tested under compression at 7 and 28 days.

The second method was used to determine the shrinkage behavior of ECC mixtures and base concrete. For that, beam specimens with dimensions of 320×75×75 mm^3 were prepared from the base concrete and one selected ECC mixture. On three sides of each beam specimens two pins were glued with an approximate distance of 250 mm. The exact distances between the pins after they were mounted were measured (Figure 3.3). At the desired time periods the change in the distance was determined.

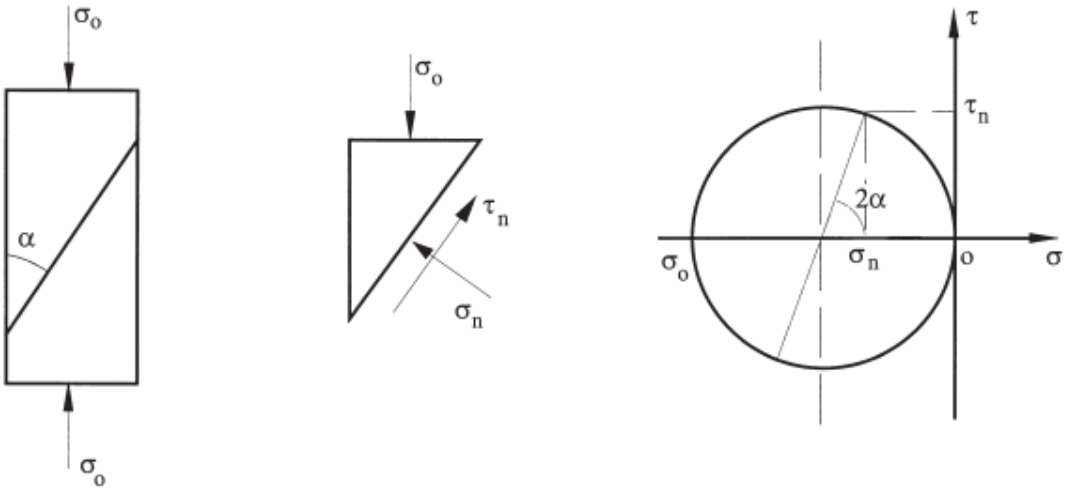

Figure 3.2 Slant shear test

Figure 3.3 Shrinkage measurement with a 0.001 mm precision DEMEC gage

3.3.3. Effect of mix design parameters on the fatigue performance of ECC

The concrete was filled into prismatic steel molds with dimensions of 320×75×75 mm^3. The specimens were removed from the molds and cured in water at temperature

of 22°C for 28 days. The ECC mixtures used in these molds were labeled as F-ECC1, F-ECC2 and S-ECC. The mixture properties are presented in Table 3.2.

Table 3.2 Mixture properties of ECC test specimens

	F-ECC1	F-ECC2	S-ECC
OPC	1	1	1
FA	1.2	1.2	-
GGBFS	-	-	1.2
Water	0.59	0.59	0.59
SP	0.01	0.01	0.01
Silica sand 0-0.4 mm	0.77	0.39	0.77
Silica sand 0.3-0.7 mm	-	0.19	-
Silica sand 0.6-1.2 mm	-	0.19	-
PVA fiber	0.05	0.05	0.04
Density (kg/m^3)	1990	1990	2149

3.4. Testing procedure

In this work a servohydraulic universal testing machine, MTS trademark, with a 250 kN load and a 200 mm stroke capacity was used. This machine has the ability to conduct both load- and deformation-controlled experiments under static and dynamic conditions. All the tests were applied through third point bending test setup (Figure 3.4). During the tests applied load data were obtained using a load cell mounted on the upper part of the bending fixture. Displacement data were gathered using a frame mounted on the specimen to measure the mid-span deflection through two LVDT devices. The data were recorded on a computer using a data acquisition device with a sampling rate of 100 Hz.

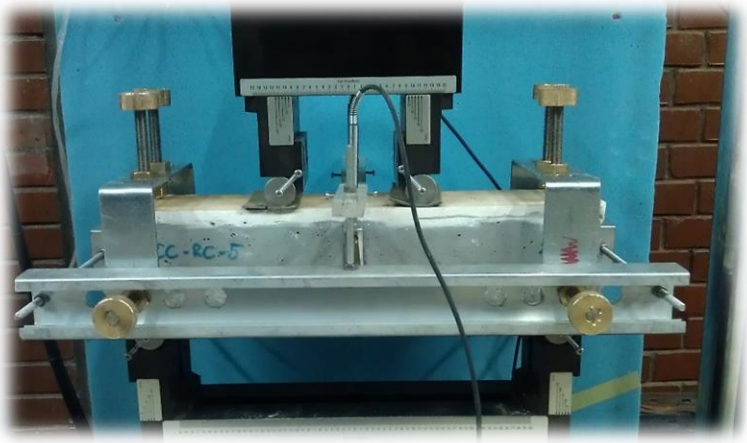

Figure 3.4 Loading setup

In this work before the fatigue tests, the monotonic bending tests were conducted in displacement control mode with a displacement increment rate of 1 mm/minute. An example of bending test results is presented on Figure 3.5.

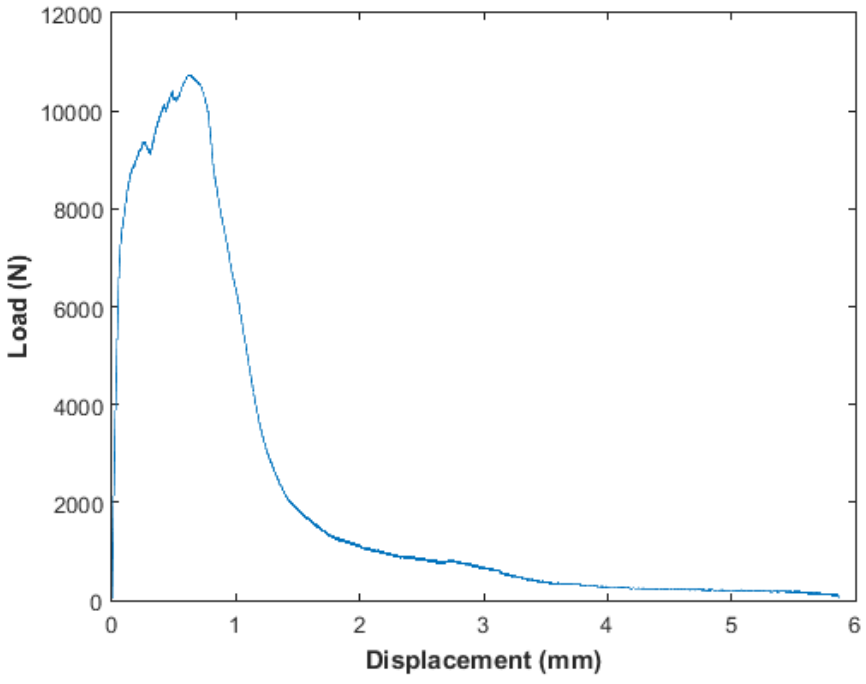

Figure 3.5 Load displacement curve of a monotonic bending test

The fatigue tests were conducted under load controlled mode only. Overlay specimens were tested under two positions named as “Normal” and “Reflective” (Figure 3.6). In the first position the overlay is placed at the bottom. The aim of this test, besides testing the performance of the overlay, is to test the bonding between the overlay and the subgrade. The first one represents the normal condition of an overlay where it is on top and a crack is introduced in the subgrade. The aim of this test is to represent a cracked and deteriorated subgrade. During the fatigue tests, a frequency of 10 Hz was used along with a constant minimum stress (20%) and maximum stress of 80% for overlay mixtures. The tests were kept running until a failure has occurred, or one million cycles were reached.

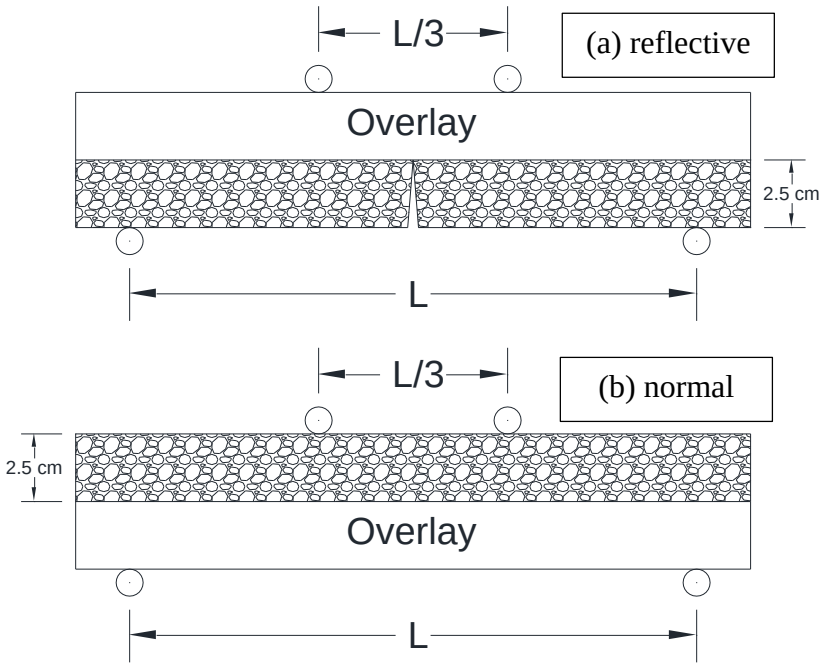

Figure 3.6 Test patterns of overlay specimens, Reflective at the top and Normal at the bottom

For testing the fatigue performance of ECC alone, the same a frequency of 10 Hz was used along with a constant minimum stress (20%). However, different maximum stresses (70, 80 and 90%) were used to obtain the S-N curves. For this case, an example

of fatigue test results is presented on Figure 3.7. The tests were kept running until a failure has occurred.

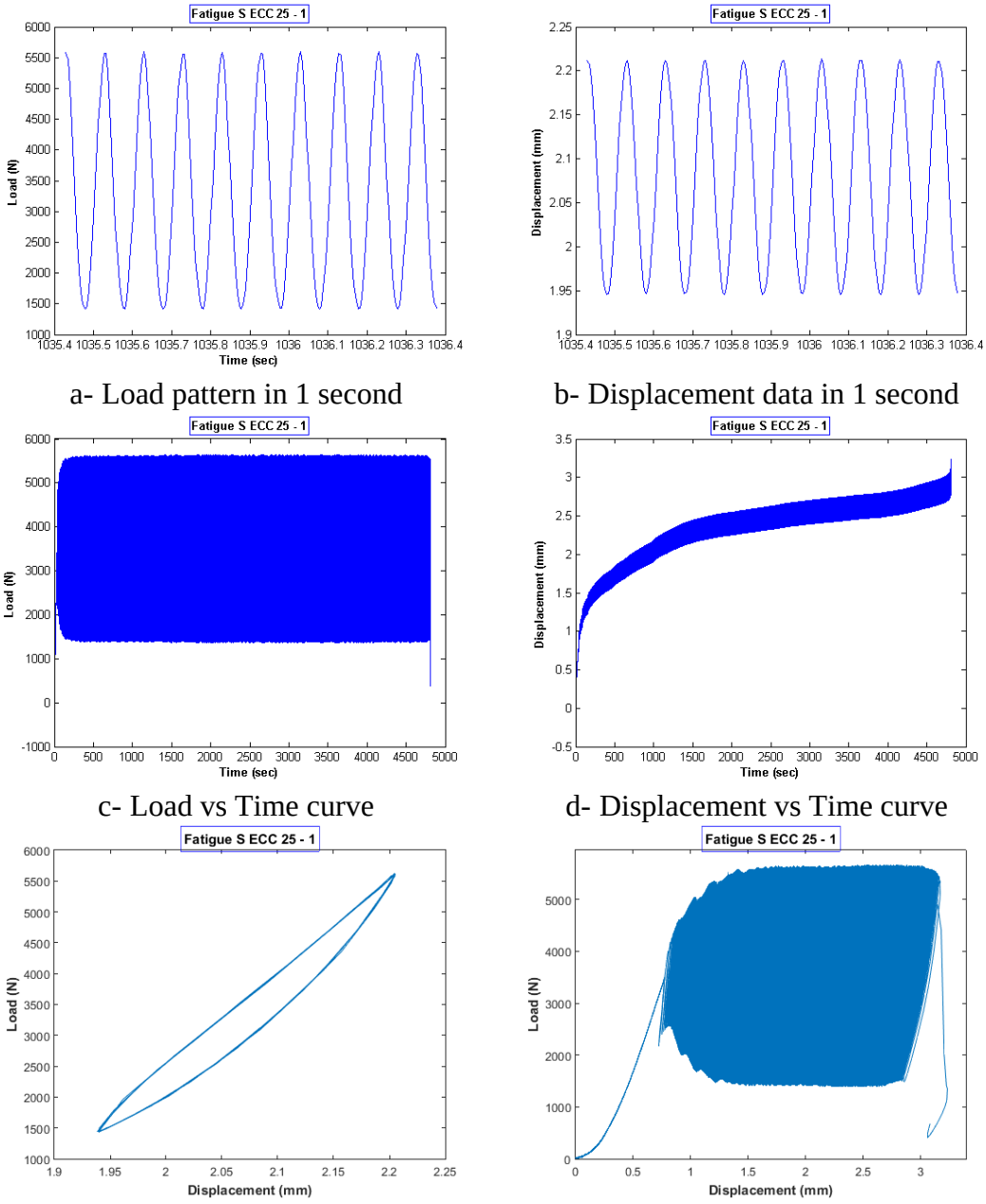

a- Load pattern in 1 second

b- Displacement data in 1 second

c- Load vs Time curve

d- Displacement vs Time curve

e- 10 cycles Load Displacement curve

f- Total load Displacement curve

Figure 3.7 Test results of a fatigue test

3.5. Statistical analysis by Weibull analysis

This analysis was performed on ECC specimens. The failure cycle values (N) of five specimens from each mix at stress levels of S=70%, 80% and 90% of ultimate are first determined. The average and the Coefficient of Variation (COV) of the results are also calculated. When the test data of each mix are evaluated as S-log(N) graph the fatigue equation of each mix can be obtained using a linear regression in the form of $Y = mX + n$. By using Equation 2.7 for each stress level the points corresponding to the number of cycles against the probability of failure are plotted. The lines that pass through the points of each stress level, called the Weibull lines, are plotted. From these lines the parameters of Weibull equation for each mix at every stress level are determined. By using these parameters, the failure probabilities of every ECC mix can be plotted. The results of these analyses are presented in Chapter 4.

CHAPTER 4

EXPERIMENTAL TEST RESULTS AND DISCUSSION

4.1. Fatigue performance of ECC as an overlay

The results of flexural tests for three Reflective and Normal overlay specimens for each combination are shown in Table 4.1 and Table 4.2 respectively. As it can be seen from the results, the effect of the introduced crack found in the reflective is clear from the reduction of the flexural load, along with the help of the ECC in increasing that strength for normal specimens because of the fibers. Because of the reduced flexural loads in the reflective case, applying the fatigue loading pattern with an average minimum stress level of about 290 N made it very difficult for a 250 000 N testing machine to apply that test in an appropriate way.

Table 4.1 Flexural and applied fatigue loads of Reflective overlay specimens

Thickness (mm)	Mix ID	28 Days Flexural Load (N)			Fatigue Load (N)	
		Minimum	Maximum	Mean	$0.2\times P_{average}$	$0.8\times P_{average}$
25	F-ECC1	1300	1508	1404	280	1125
	S-ECC	1735	2050	1893	380	1515
	MSC	1200	1300	1250	250	1000
35	F-ECC1	2529	3150	2840	570	2270
	S -ECC	3291	3931	3611	720	2890
	MSC	2068	2137	2103	420	1680
50	F-ECC1	4729	6231	5480	1095	4385
	S-ECC	6496	6950	6723	1345	5380
	MSC	3282	3438	3360	670	2690

Table 4.2 Flexural and applied fatigue loads of Normal overlay specimens

Thickness (mm)	Mix ID	28 Days Flexural Load (N)			Fatigue Load (N)	
		Minimum	Maximum	Mean	$0.2\times P_{average}$	$0.8\times P_{average}$
25	F-ECC1	5658	6609	6134	1225	4905
	S-ECC	6515	7553	7034	1405	5625
	MSC	3557	4112	3835	765	3070
35	F-ECC1	8507	9665	9086	1815	7270
	S -ECC	9946	9992	9969	1995	7975
	MSC	5598	6219	5909	1180	4725
50	F-ECC1	13087	15787	14437	2885	11550
	S-ECC	14408	17087	15748	3150	12600
	MSC	8462	8954	8708	1740	6965

The fatigue test results of the Reflective and Normal overlay specimens are presented in Table 4.3 and Table 4.4 respectively. For the Reflective test specimens, the fatigue test on overlays with 25 mm in thickness were not be able to be performed due to the machine sensitivity. For the specimens with 35 mm and 50 mm in thicknesses, the ones with fly ash had better performance than the ones with slag, and most of the MSC specimens were damaged before conducting the test while the ones that were tested showed lower performance. However, in all the Reflective tests, the variabilities were very high. In a similar way, for the Normal test specimens with a thickness of 25 mm fly ash specimens showed the best performance then the slag ones while the MSC ones had the least performance. As for the specimens with 35 mm in thickness, fly ash and MSC specimens showed a close performance that was better than the one with slag. However, for the specimens with 50 mm in thickness, the performance was improved starting from fly ash then slag and at the end MSC mixtures.

It can be seen that for F-ECC1 and S-ECC mixtures the fatigue performance (represented by the Number of Cycles to Failure) is not enhanced with the increase of overlay thickness. The increase of the thickness while keeping the distance between the supports in bending tests will actually makes the specimens that are made from the same material act more brittle. The thing that can change the slope of the S-N curve for specimens of the same material with different thicknesses and makes the

performance at low cycles higher for less thicknesses. In addition to that, it should be also considered that these fatigue tests are performed with a constant stress level (0.8), not the same stresses or loads. The application of fatigue tests on specimens with different dimensions under various ranges of the same load or stresses will give the curves needed for the design purposes. In this work, since that the main aim is to compare different materials, the stress level is the one that kept constant. Moreover, the difference in the thickness might results somehow in an alignment in the fiber direction for small thicknesses, making them parallel to the horizontal plane during the casting of ECC overlay into the molds. The thing that will increase the flexural performance of these specimens. On another side, when the flexural strength is compared to the fatigue performance, it is clearly seen that this performance is not directly related to the strength. While the S-ECC specimens have the highest strength, their fatigue performance still lower than both F-ECC1 and MSC. This support the fact that the behavior under fatigue test is related to the complete performance of the material under bending test, not only its ultimate strength.

Table 4.3 Number of cycles to failure after fatigue test of Reflective overlay

Specimen Type	Specimen ID	Overlay thickness (mm)		
		25	35	50
F-ECC1	1	22689	110902	316592
	2	NA	366546	25313
	3	NA	1000000	3075
	4	NA	Damaged	1437
S-ECC	1	NA	2613	12244
	2	NA	200087	695
	3	NA	11302	104380
	4	NA	9490	286
MSC	1	Damaged	13341	4788
	2	Damaged	Damaged	6602
	3	Damaged	Damaged	Damaged
	4	Damaged	Damaged	Damaged

* Damaged before performing the test
* NA: the loads required to be applied are smaller than the machine sensitivity for cyclic loading test

Table 4.4 Number of cycles to failure after fatigue test of Normal overlay

Specimen Type	Specimen ID	Overlay thickness (mm) 25	35	50
F ECC1	1	25187	5264	18202
	2	215125	626072	186
	3	52698	186136	432
	4	Damaged*	12039	13144
S ECC	1	47715	39331	787
	2	84965	53511	19566
	3	3805	17660	24787
	4	55686	59901	2187
MSC	1	1408	619137	218625
	2	1368	160168	322652
	3	2278	95214	461
	4	Damaged*	Damaged*	1000000+

* Damaged before performing the test

4.2. Bonding and shrinkage test results

The decision to cast the overlay specimens as plates came after the high variability in the fatigue test results presented above. However, the debonding of the ECC layer from the base concrete required further tests to investigate this incident, (Figure 4.1). The first test performed on cylindrical specimens tested under slant shear showed that at the age of 7 days the bonding between ECC and base concrete is strong enough and the crack occurred during the compressive test transformed vertically from the top part to bottom part (Figure 4.2.a). However, at 28 days when the load was applied on the specimen a complete separation between the two parts of the specimen occurred without any crack transformation (Figure 4.2.b).

Figure 4.1 Debonding of ECC layer from base concrete layer

a- 7 days b-28 days

Figure 4.2 Slant shear test results

These results can be also supported by the results of shrinkage tests (Figure 4.3). As it can be seen from that figure, ECC shrinks about 5 times higher than the base concrete after 12 days only.

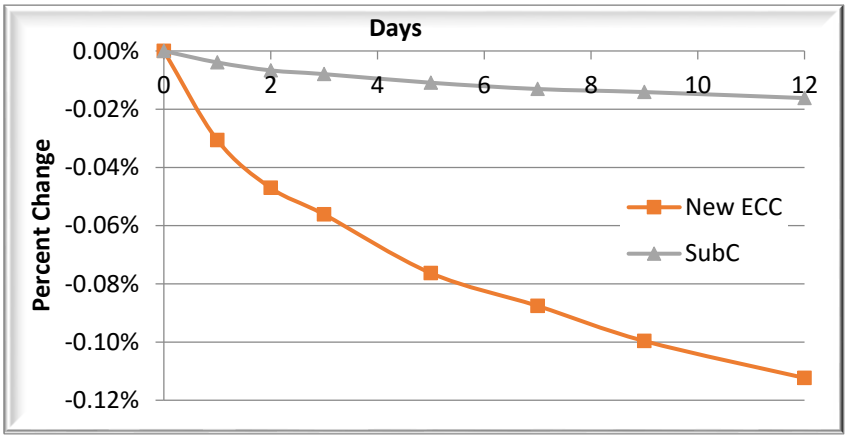

Figure 4.3 Shrinkage test results

4.3.Effects of ECC ingredients on its fatigue behavior

The fatigue test results are processed and presented in a group of four figures as shown in Figure 4.4. In the first three figures, the x-axis is the number of cycles of the test, while the y-axis is maximum and minimum displacement, maximum and minimum load and the stiffness (which is the load of the load displacement curve) respectively. The last figure shows the change in the dissipated energy (which is the area under the load displacement curve) during the change in the displacement. In this figure the Displacement, Load and Stiffness changes through the fatigue test are plotted. In addition to that the Energy absorption is also plotted against the Displacement. On the Load-N plot in this figure, the upper line represents the applied load of the maximum stress level and the lower line represents the applied load of the minimum stress level. Although these loads are supposed to be applied constantly on the specimen, the difference at the first few hundred cycles is due to the inability of the hydraulic pump to adjust itself to maintain the required load at a frequency of 10 Hz. This is also the reason why the Energy-Displacement curve is not completely linear. Moreover, it can be seen from the Displacement-N curve that the displacement increase rate is kind of constant. This is also applied to the crack propagation rate since the relation between it and the displacement values is almost linear. The similar results of the rest of the specimens are presented in Appendix A.

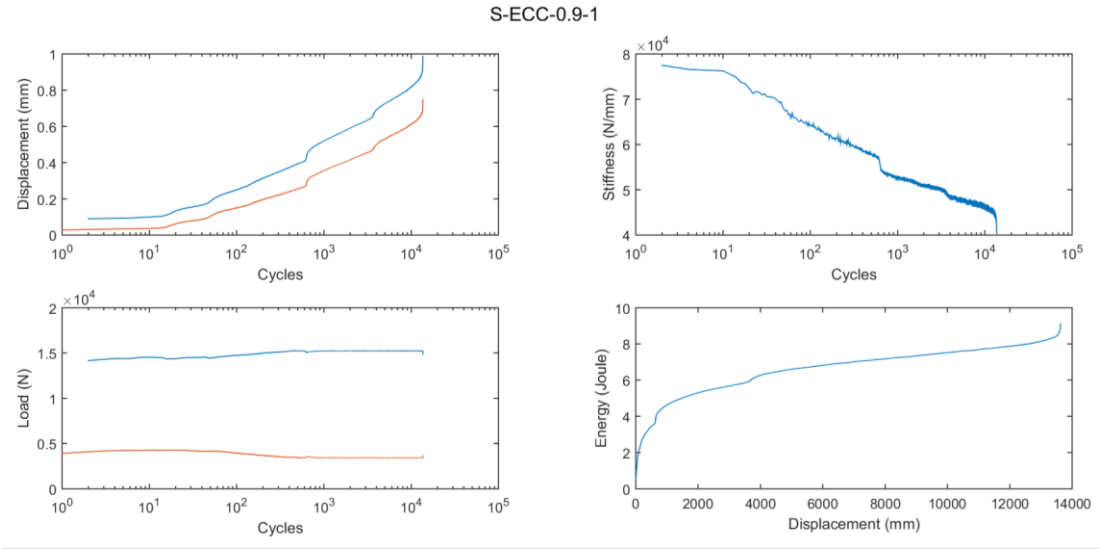

Figure 4.4 An example of fatigue test results

The Number of Cycles to Failure (N) of five specimens from each mix at stress levels of S=70%, 80% and 90% of ultimate can be seen in Table 4.5. The average and the Coefficient of Variation (COV) of the results are also calculated and presented in Table 4.6. When the test data of each mix are evaluated as S-log(N) graph, Figure 4.5, the fatigue equation of each mix can be obtained using a linear regression in the form of $Y = mX + n$. The parameters of the fatigue equations of the mixtures are presented in Table 4.7.

The fatigue test results show that mixtures incorporating fly ash have better performance than the one with GGBFS. On the other hand, the use of larger aggregate size decreased the fatigue performance of ECC. All of these might be due to the fact that GGBFS and larger aggregate grains reduce the ductility of ECC mixtures (Şahmaran, Yücel, Demirhan, & Li, 2012).

Table 4.5 Failure cycles values

Stress Level	Number of cycles (N)		
	F-ECC1	F-ECC2	S-ECC
70%	880761	308766	78403
	1000000+	592843	157378
	1052566	820319	217493
	1237743	964009	293012
	1312782	1185518	325093
80%	153471	42893	26436
	217039	45877	46401
	222861	78025	80734
	243292	212048	87319
	414718	274577	112719
90%	32475	9446	6818
	38330	14597	10124
	72238	15209	12504
	82667	18817	13599
	112504	31791	16696

Table 4.6 The average and COV of the test results

Stress Level		F-ECC1	F-ECC2	S-ECC
70%	Average	1096770	774291	214276
	COV (%)	14.4%	39.0%	41.8%
80%	Average	250276	130684	70722
	COV (%)	35.0%	72.6%	43.3%
90%	Average	67643	17972	11948
	COV (%)	43.6%	41.9%	27.8%

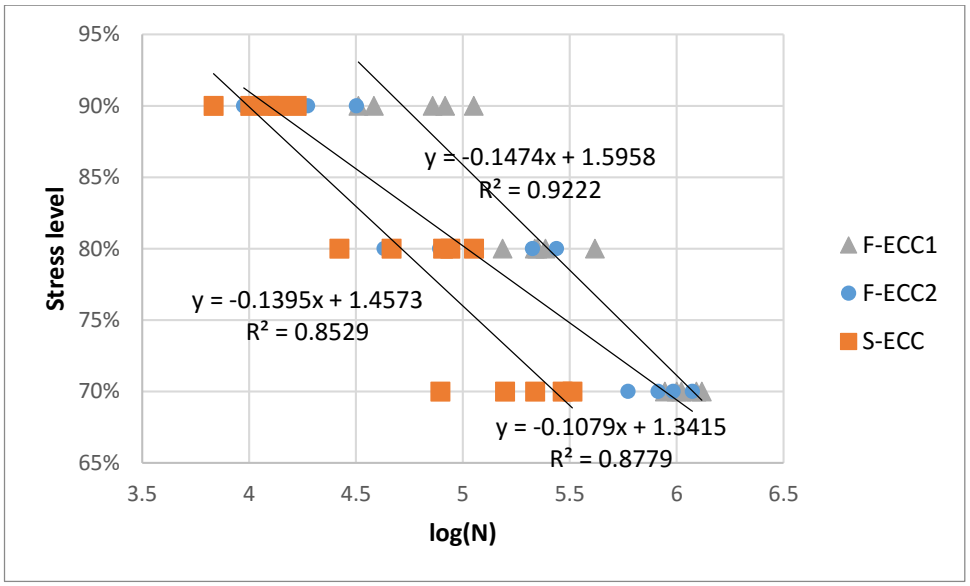

Figure 4.5 S-log(N) curves

Table 4.7 The parameters of the fatigue equations

Mixture	*m*	*n*	R^2
F-ECC1	-0.1474	1.5958	0.9222
F-ECC2	-0.1079	1.3415	0.8779
S-ECC	-0.1395	1.4573	0.8529

4.4. Statistical analysis and interpreting the fatigue test results

By using Equation 2.7 the Weibull lines are plotted in Figure 4.6. From these lines the parameters of Weibull equation for each mix at every stress level are determined as shown in Table 4.8.

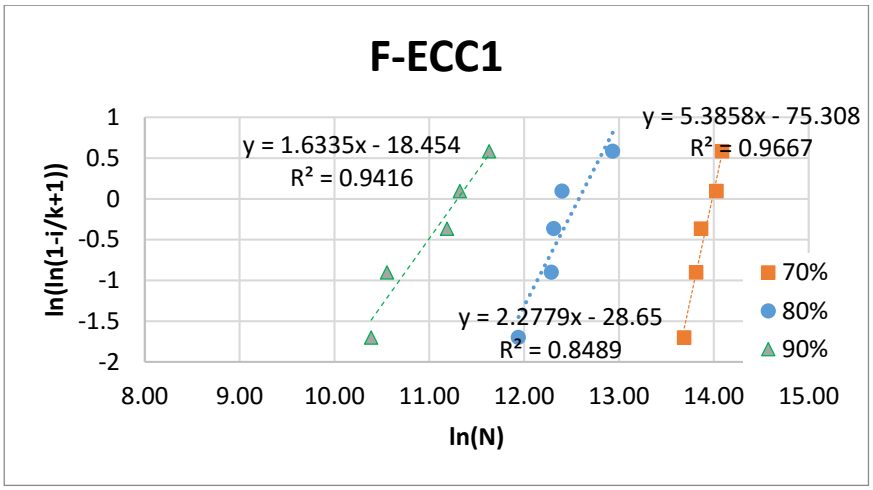

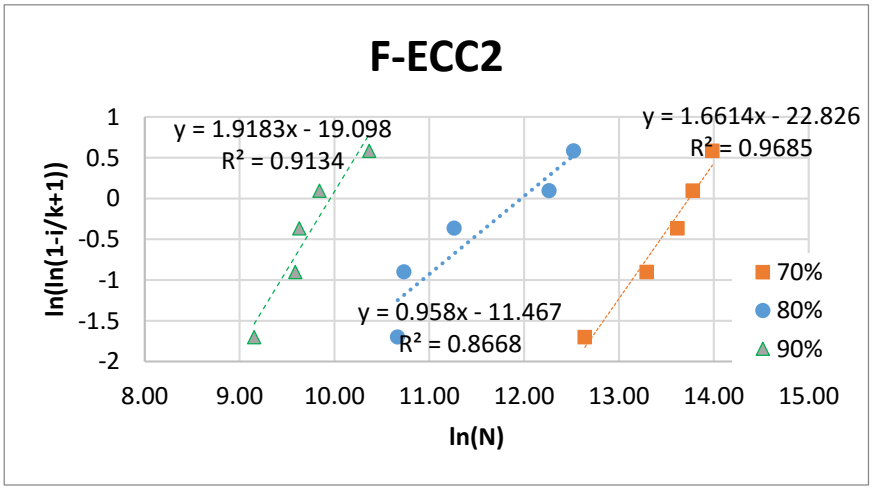

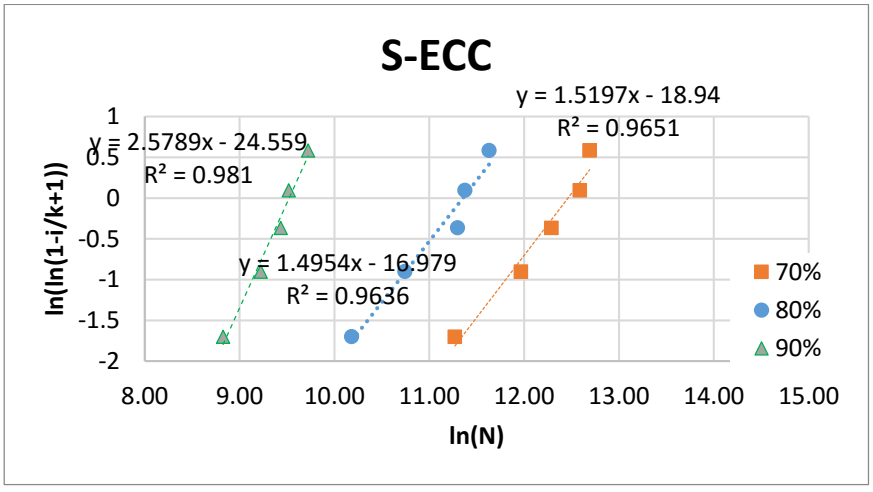

Figure 4.6 Weibull lines for each mix at different stress levels

Table 4.8 The parameters of Weibull equation

Mix	S	β	k	α	R^2
F-ECC1	70%	5.39	75.31	1181972.53	0.97
	80%	2.28	28.65	289923.94	0.85
	90%	1.63	18.45	80596.83	0.94
F-ECC2	70%	1.66	22.83	926357.30	0.97
	80%	0.96	11.47	157901.80	0.87
	90%	1.92	19.10	21071.78	0.91
S-ECC	70%	1.52	18.94	258586.65	0.97
	80%	1.50	16.98	85319.02	0.96
	90%	2.58	24.56	13671.28	0.98

By using these parameters the failure probabilities (5, 15, 30, 50, 75 and 95%) of every mix are plotted in Figure 4.7 to Figure 4.9.

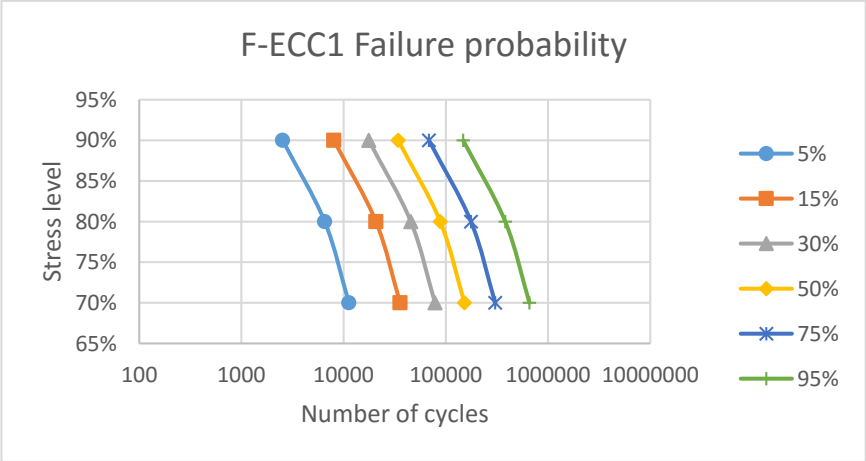

Figure 4.7 Failure probability curves for F-ECC1

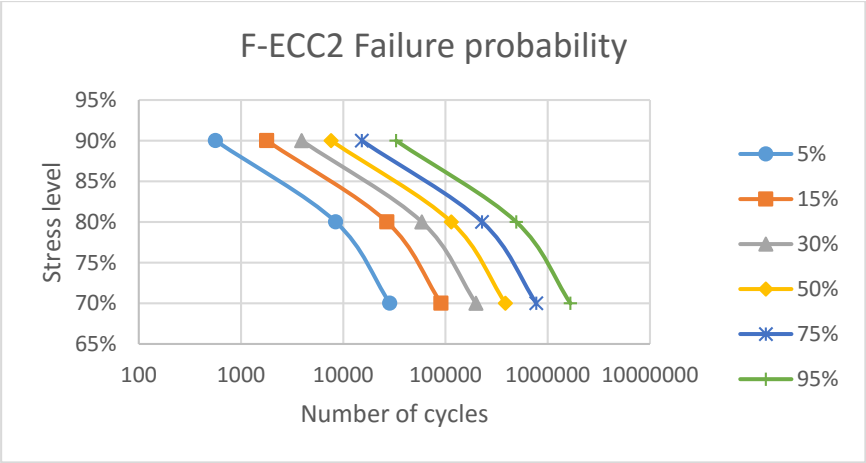

Figure 4.8 Failure probability curves for F-ECC2

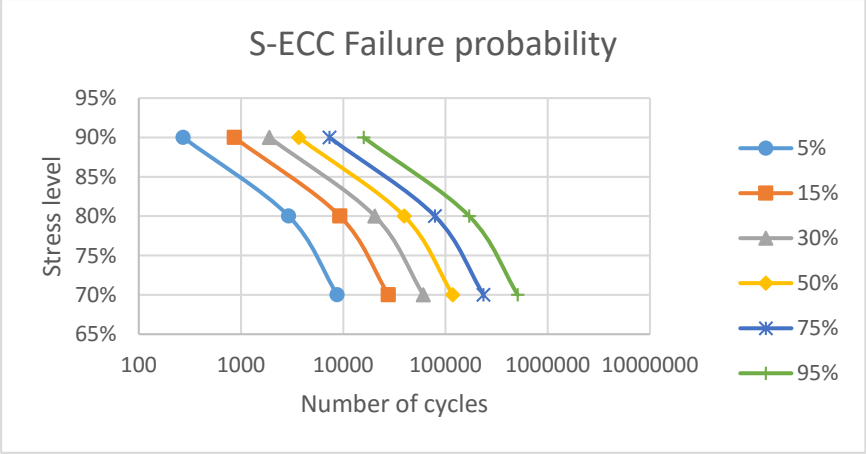

Figure 4.9 Failure probability curves for S-ECC

This data can be interpreted by plotting the ECC mixtures for a specific probability like 95%. As shown in Figure 4.10 the mineral admixture slag reduced the fatigue life when compared to fly ash. Moreover, the incorporation of larger aggregate size also reduced the fatigue life. The reason behind these reduction is the change in ductility when slag is used instead of fly ash and when coarser aggregates are found in the mixture. The fly ash to cement ratio used in the ECC mixtures was 1.2, and for this high amount of fly ash inside there is no enough cement hydration product (calcium hydroxide) to react with all the fly ash. Hence, the toughness of the matrix for fly ash mixtures is less than the slag mixture and their ductility is better. On the other hand,

when larger aggregate size is used more fibers will be forced to take place in smaller region, and for that the dispersion of the fibers within the matrix will be less homogenous, which will also reduce the ductility (Şahmaran et al., 2012).

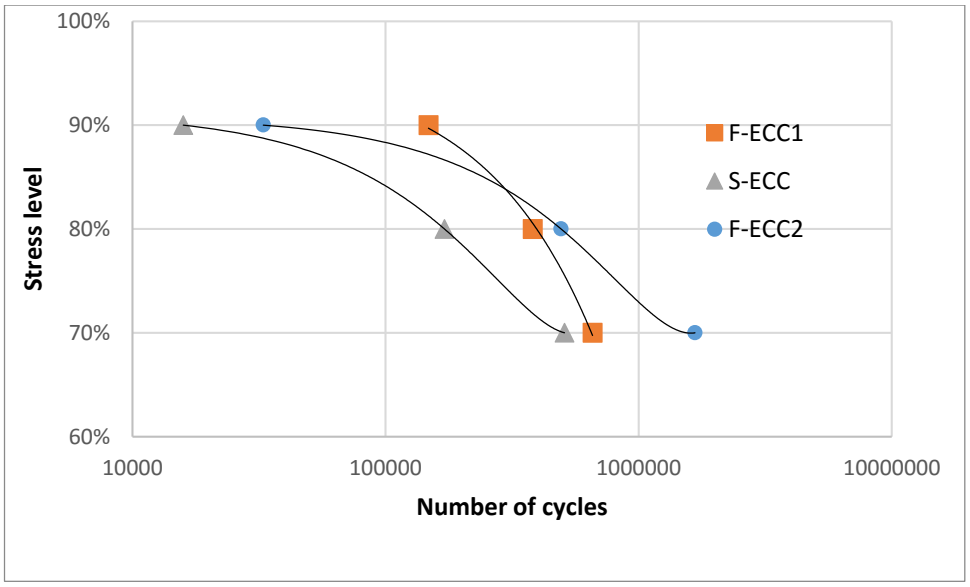

Figure 4.10 S-N curves of ECC mixtures at 95% Failure probability

CHAPTER 5

FATIGUE LIFE PREDICTION

5.1. The relationship between static and monotonic test results

The monotonic test results define the limits of the tested specimens under a specific loading pattern. In fatigue tests, since the loading setup is the same and the loading levels do not exceed the strength of the specimens, the specimens will respond only under the limits defined by the monotonic tests. In other words, the fatigue performance of a specimen is somehow related to its static bending response. In Figure 5.1, the resemblance between the behavior of two specimens of the same ECC batch under monotonic and fatigue tests can be seen. All of this pointed out that a relationship can be drawn between the monotonic and fatigue behavior of a material. It should also be noticed that each ECC specimen will give a unique result under either of these tests, which is the reason behind the big scatter between the test results.

The energy absorption of a specimen under monotonic bending test is calculated as the area under the load-displacement curve. When this energy is plotted against the stress levels (which can be obtained by dividing the load values on the maximum load for the same test) the resulting figure will be obtained (Figure 5.2).

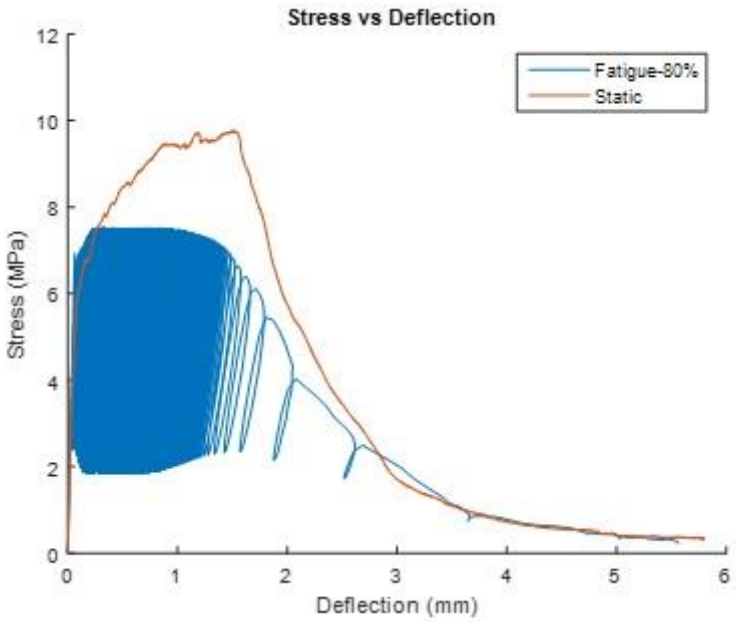

Figure 5.1 An example of monotonic static test and fatigue test of two specimens from the same material

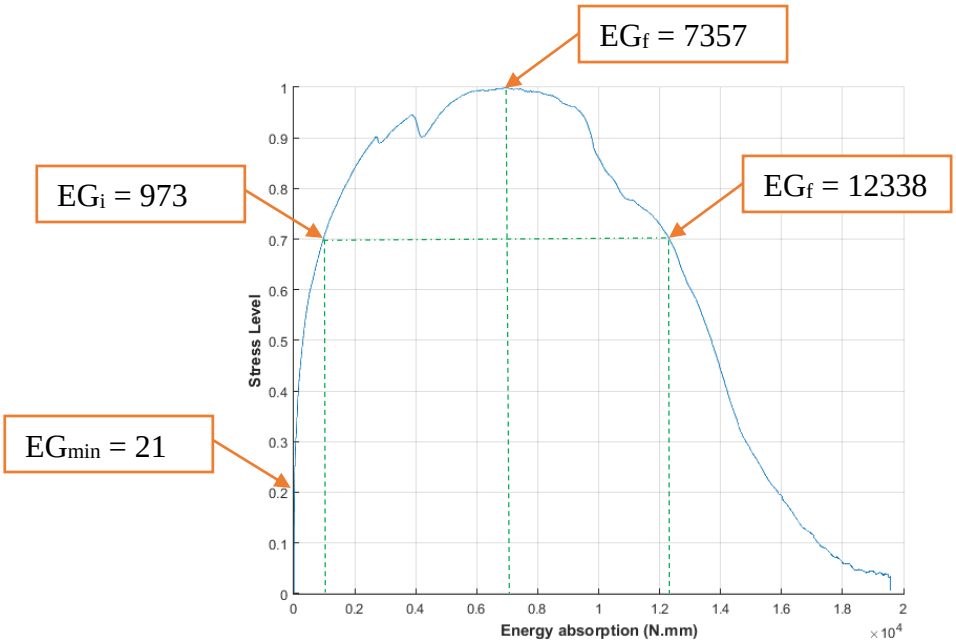

Figure 5.2 Stress Level-Energy Absorption curve

From the data of this curve it can be seen that at the ultimate stress level (S=1) the energy absorption capacity equals to 7357 N.mm. This means if that amount of energy is applied the specimen will reach its maximum load bearing capacity, and further application the same stress will lead to a direct failure. In a similar way, it can be seen from the data that for a fatigue load of 70% of the ultimate load, i.e. S=0.7, the Initial Absorbed Energy equals to 973 N.mm, which means that a direct application of this amount of energy would not lead to a direct failure. Moreover, if this energy application continues the total failure will need naturally a period of time to occur. This period can be explained as the time needed to absorb extra energy until the total absorbed one equals to 12338 N.mm, which is the Final Absorbed Energy that correspond to the same stress level. In other words, each stress level has two particular energy absorption values, a first one that is found on the increasing stress level part of the curve shown in Figure 5.2, and a last one that is found on the decreasing part. In addition to this, the period needed for the specimen to fail under that stress level is related to the difference between these two energy absorption values and the repeated number of cycles that load is applied.

Using this energy absorption curve the Predicted Number of Cycles to Failure (N_p)can be calculated as:

$$N_p = \frac{EG_d}{CPR} \qquad \textit{Equation 5.1}$$

where: N_p is the Predicted Number of Cycles to Failure,

EG_d is the difference between EG_f (the Final Energy Absorption) and EG_i (the Initial Energy Absorption),

CPR is the Crack Propagation Rate

The Crack Propagation Rate can be estimated from two methods as explained below.

5.1.1. Crack propagation rate determined from actual fatigue tests

For fatigue tests, the energy absorption for each cycle is calculated as the area under the load-displacement curve of the loading part of that cycle. Then, the total energy absorption is calculated as the cumulative energy for all the cycles. In Figure 5.3 the change in the energy values during fatigue test at three different maximum stress level for three specimens of the same mixture are presented. From this figure it can be seen that during the stabilized phase of the test (the phase between the cracks are initiated at the beginning of the test and the cracks start being unstable at the end of the test) the energy is increasing almost linearly. The slope of this increase represents the amount of energy absorbed in each cycle under that specific stress level. This amount can accepted to be constant for the same stress level of the same test conditions on specimens of the same material. The slopes of the curves shown in this figure are determined to be 0.0168, 0.0435 and 0.1317 for the stress levels of 0.7, 0.8 and 0.9.

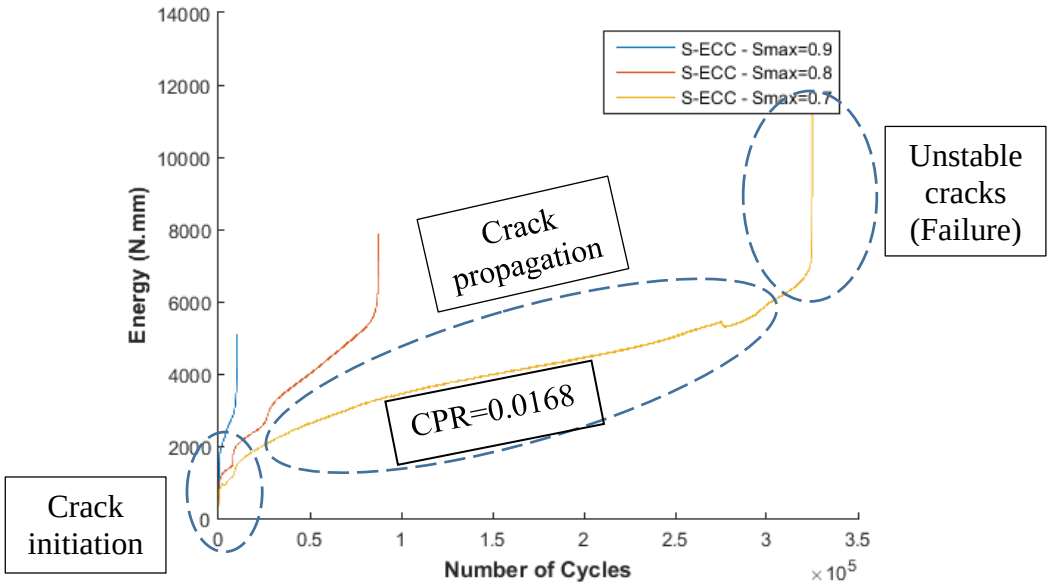

Figure 5.3 Example of energy vs number of cycles during a fatigue test

In Table 5.1 the energy absorption values (obtained from Figure 5.2) for three different stress levels are presented along with the rate of crack propagation during the fatigue

loading. The Predicted Number of Cycles to Failure can be calculated as shown in this table.

Table 5.1 An example of fatigue prediction values

Stress Level	Energy Absorption (N.mm)			Crack Propagation Rate	Predicted Number of Cycles to Failure
	Initial	Final	Difference		
0.7	973	12338	11365	0.0168	676488

5.1.2. Crack propagation rate determined from monotonic loading tests

By using the following equation the Crack Propagation Rate can be determined.

$$CCPR = \frac{EG_i}{EG_f} \times \frac{EG_m}{EG_i - EG_{min}} \times (S_{max} - S_{min}) \qquad \textit{Equation 5.2}$$

where: $CCPR$ is the Calculated Crack Propagation Rate,

EG_f the Final Energy Absorption,

EG_i the Initial Energy Absorption,

EG_{min} the Energy Absorption corresponding to S_{min},

EG_m the average of EG_i and EG_{min},

S_{min} and S_{max} are the minimum and maximum applied stress level respectively.

In the above equation, the first part "$\frac{EG_i}{EG_f}$" represents the amount of energy needed to be absorbed. The higher the difference between the initial and final energies, the lower is CPR. The second part "$\frac{EG_m}{EG_i - EG_{min}}$" represents the effect of the average stress level. This average might be considered as the real effective stress level. The last part of the

equation "$(S_{max} - S_{min})$" represents the speed of the CPR related to the applied stress levels. For lower stress levels, or stress levels with small differences, CPR will be high. If the maximum and minimum stress levels are equal, CPR will be zero, and this will be the case of creep.

5.2. Applying the prediction methods on the monotonic test results

For each ECC mixture, three monotonic test results were analyzed to obtain the Stress Level-Energy Absorption curves presented in Figure 5.4 to Figure 5.6. Then, the Energy Absorption values mentioned in section 5.1 for the stress levels of 0.7, 0.8 and 0.9 are all determined to be used in calculating the Predicted Numbers of Cycles to Failure, Np_1 and Np_2, according to the first and the second methods suggested in this work. The determination of the crack propagation rates is explained in Appendix B. The average values for each stress level of every ECC mixture are obtained. In Table 5.2 to Table 5.4 the Predicted Number of Cycles to Failure according to the first suggested method are presented.

In a similar way, after determining the Energy Absorption values mentioned in section 5.1.1, the Calculated Crack Propagation Rates are found using Equation 5.2. In Table 5.5 to Table 5.7 the Predicted Number of Cycles to Failure according to the first suggested method are presented.

The predicted and measured numbers are compared to each other in Table 5.8 and Figure 5.7 to Figure 5.9. From this comparison it can be seen that a good correlation is found between the predicted and the measured values. The sources of the variations between the results are firstly the high scatter of the bending test results under both monotonic and fatigue tests, and secondly the prediction methods use a constant Crack Propagation Rate, while this rate in actual test changes because of many factors, like the not applying the fatigue loading by its defined limits at the beginning of the test due to the machine capacity, and also when the cracks start to be unstable before the failure.

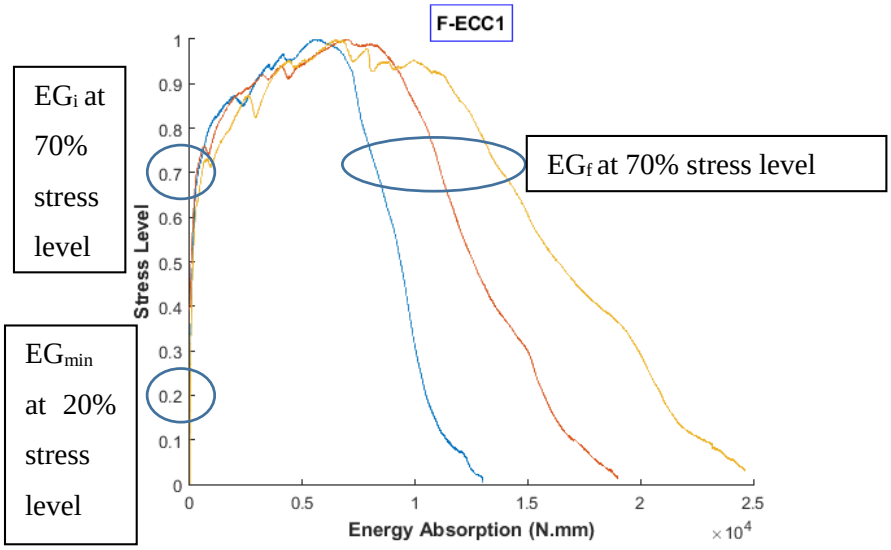

Figure 5.4 Stress Level-Energy Absorption curves of F-ECC1 mixtures

Table 5.2 Fatigue life prediction of F-ECC1 mixture using prediction method 1

Stress Level	EG_i	EG_f	$EG_d = EG_f - EG_i$	***CPR***	N_{p1}
0.9	2848.7	7299.7	4450.9	0.1048	42469
	2831.9	9525.2	6693.3		63864
	3521.0	11506.2	7985.2		76191
Average	3067.2	9443.7	6376.5		**60841**
0.8	864.8	7711.4	6846.6	0.0448	152888
	1175.2	10524.5	9349.3		208775
	1788.6	12784.8	10996.2		245550
Average	1276.2	10340.3	9064.1		**202405**
0.7	361.4	8331.4	7969.9	0.0087	912457
	303.0	11132.4	10829.4		1239827
	540.7	13873.4	13332.8		1526431
Average	401.7	11112.4	10710.7		**1226238**

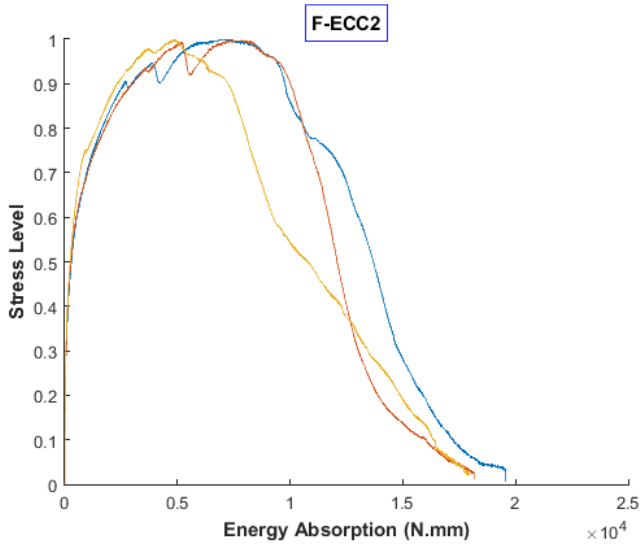

Figure 5.5 Stress Level-Energy Absorption curves of F-ECC2 mixtures

Table 5.3 Fatigue life prediction of F-ECC2 mixture using prediction method 1

Stress Level	EG_i	EG_f	$EG_d = EG_f - EG_i$	CPR	N_{p1}
0.9	2631.3	9746.6	7115.3	0.1671	42582
	3033.7	9999.7	6966.0		41688
	2315.1	7240.3	4925.2		29475
Average	2660.0	8995.5	6335.5		**37915**
0.8	1648.1	10634.3	8986.3	0.0563	159725
	1781.3	10601.3	8820.0		156770
	1403.1	7973.2	6570.0		116777
Average	1610.8	9736.3	8125.4		**144424**
0.7	972.9	12338.2	11365.3	0.0154	738968
	1020.0	11221.2	10201.2		663280
	668.7	8573.1	7904.3		513935
Average	887.2	10710.8	9823.6		**638728**

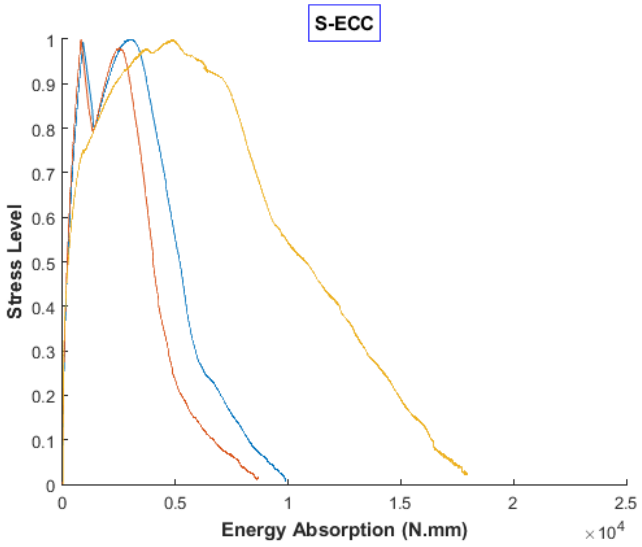

Figure 5.6 Stress Level-Energy Absorption curves of S-ECC mixtures

Table 5.4 Fatigue life prediction of S-ECC mixture using prediction method 1

Stress Level	EG_i	EG_f	$EG_d = EG_f - EG_i$	CPR	N_{p1}
0.9	726.9	3713.2	2986.3	0.2163	13805
	644.4	2966.3	2321.9		10734
	2315.1	7240.3	4925.2		22768
Average	1228.8	4640.0	3411.1		**15769**
0.8	566.2	4080.0	3513.8	0.0531	66226
	503.6	3285.8	2782.2		52438
	1403.1	7973.2	6570.0		123828
Average	824.3	5113.0	4288.7		**80831**
0.7	427.2	4474.4	4047.2	0.0304	133056
	381.6	3556.1	3174.5		104365
	668.7	8573.1	7904.3		259863
Average	492.5	5534.5	5042.0		**165761**

Table 5.5 Fatigue life prediction of F-ECC1 mixture using prediction method 2

Stress Level	EG_{min}	$EG_d = EG_f - EG_i$	*CCPR*	N_{p2}
0.9	15.4	4450.9	0.1381	32236
	13.8	6693.3	0.1051	63700
	19.8	7985.2	0.1083	73723
Average	16.3	6376.5	0.1149	**55499**
0.8	15.4	6846.6	0.0349	196383
	13.8	9349.3	0.0343	272626
	19.8	10996.2	0.0429	256262
Average	16.3	9064.1	0.0380	**238616**
0.7	15.4	7969.9	0.0118	674804
	13.8	10829.4	0.0075	1452753
	19.8	13332.8	0.0105	1271754
Average	16.3	10710.7	0.0098	**1092539**

Table 5.6 Fatigue life prediction of F-ECC2 mixture using prediction method 2

Stress Level	EG_{min}	$EG_d = EG_f - EG_i$	*CCPR*	N_{p2}
0.9	20.9	7115.3	0.0960	74116
	19.7	6966.0	0.1076	64758
	17.9	4925.2	0.1137	43334
Average	19.5	6335.5	0.1050	**60324**
0.8	20.9	8986.3	0.0477	188446
	19.7	8820.0	0.0515	171152
	17.9	6570.0	0.0542	121310
Average	19.5	8125.4	0.0508	**159794**
0.7	20.9	11365.3	0.0206	552297
	19.7	10201.2	0.0236	431936
	17.9	7904.3	0.0206	384203
Average	19.5	9823.6	0.0216	**454001**

Table 5.7 Fatigue life prediction of S-ECC mixture using prediction method 2

Stress Level	EG_{min}	$EG_d = EG_f - EG_i$	***CCPR***	N_{p2}
0.9	34.6	2986.3	0.0754	39627
	30.3	2321.9	0.0835	27792
	17.9	4925.2	0.1137	43334
Average	27.6	3411.1	0.0970	**35184**
0.8	34.6	3513.8	0.0470	74692
	30.3	2782.2	0.0519	53635
	17.9	6570.0	0.0542	121310
Average	27.6	4288.7	0.0517	**82928**
0.7	34.6	4047.2	0.0281	144173
	30.3	3174.5	0.0315	100897
	17.9	7904.3	0.0206	384203
Average	27.6	5042.0	0.0249	**202580**

Table 5.8 Comparison between the measured and predicted fatigue life values

Mixture ID	Stress Level	N_{p1}	N_{p2}	Measured N	N/N_{p1}-1	N/N_{p2} -1
F-ECC1	0.9	60841	55499	67643	11%	22%
	0.8	202405	238616	250276	24%	5%
	0.7	1226238	1092539	1096770	-11%	0%
F-ECC2	0.9	37915	60324	17972	-53%	-70%
	0.8	144424	159794	130684	-10%	-18%
	0.7	638728	454001	774291	21%	71%
S-ECC	0.9	15769	35184	11948	-24%	-66%
	0.8	80831	82928	70722	-13%	-15%
	0.7	165761	202580	214276	29%	6%

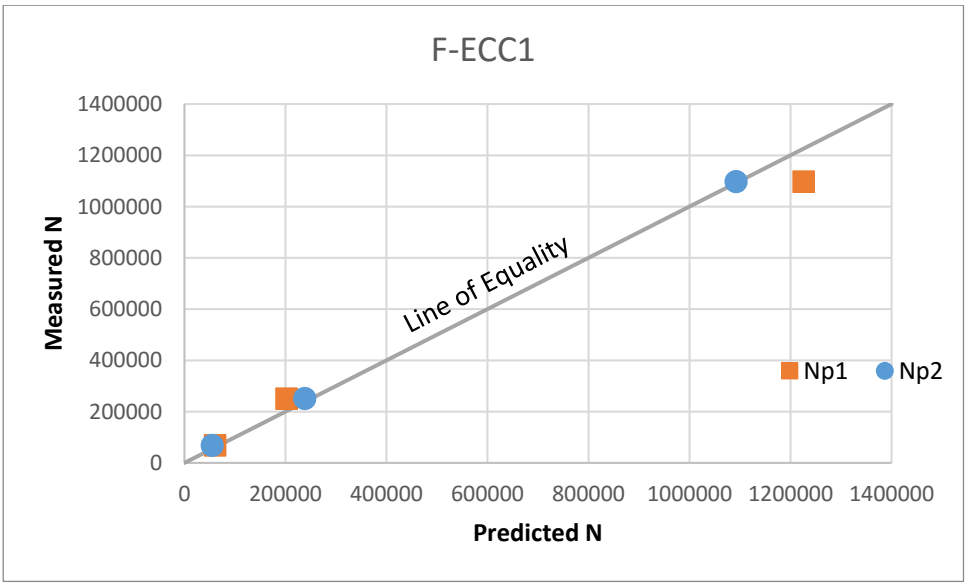

Figure 5.7 The measured vs. predicted fatigue life values of F-ECC1

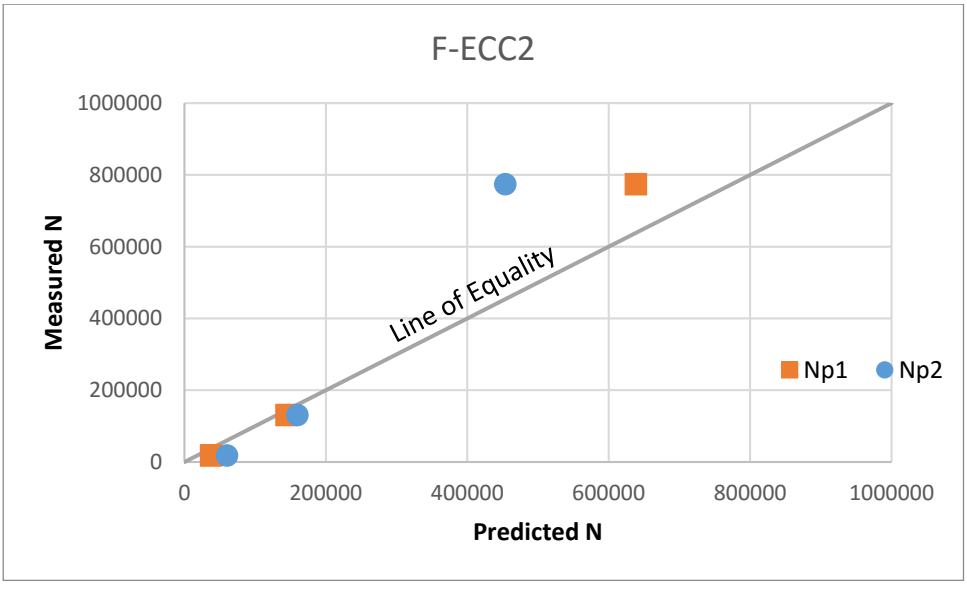

Figure 5.8 The measured vs. predicted fatigue life values of F-ECC2

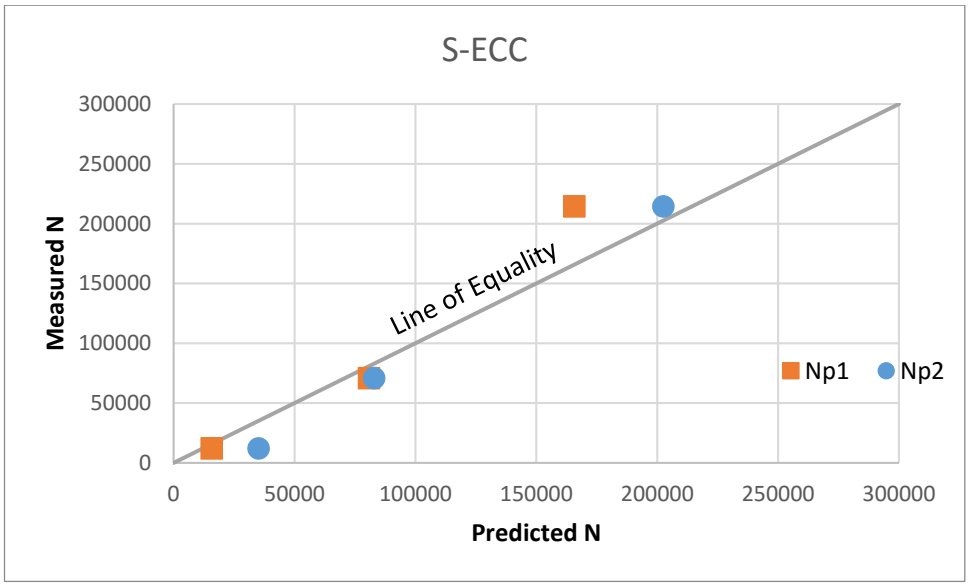

Figure 5.9 The measured vs. predicted fatigue life values of S-ECC

CHAPTER 6

SUMMARY, CONCLUSIONS AND RECOMMENDATIONS

6.1. Summary

Considering the importance and the benefits of concrete overlays in Turkey, this thesis was done to evaluate the performance of ECC material as an overlay repair. To fulfill this aim, an application of two different ECC mixtures of different thicknesses over a concrete subgrade was performed to simulate the overlay behavior. These overlay test specimens were examined under fatigue loading. After that, the flexural behavior and fatigue performance of ECC mixtures under cyclic loading was examined. In this scope, the effects of mineral admixtures and aggregate size on the fatigue performance were also investigated. Then, the probabilities of failure under fatigue for these mixtures were determined. Finally, to correlate the flexural behavior and the fatigue performance, two methods were suggested to predict the number of cycles to failure based on the monotonic test results.

6.2. Conclusions

Based on the test results, the following conclusions can be drawn:

- The test results showed that fly ash incorporation will lead to a better performance under fatigue compared to the addition of slag.
- Because of the presence of fibers and the special matrix design of ECC, this special type of concrete has a better performance under fatigue loading than

the traditional concrete. The main reason behind that is the high ductility of ECC compared to normal concrete.

- Although the use of slag leads to a higher strength, the fatigue performance of ECC mixtures containing fly ash is much better. This is because the improved ductility obtained when the fly ash is used. The reason behind this is the self-cementitious property that slag has, allows it to react and make the matrix stronger and tougher. On the other hand, the use of high amount of mineral admixture makes a considerable amount of unhydrated fly ash take place in the matrix, and because of that this type of ECC shows a higher ductility. In addition to that, when slag is used a chemical bonding between the matrix and the fibers occurs which affects the smoothness of the fibers surfaces and prevent them from slipping under tension.
- Increasing the aggregate size has also a negative effect on the fatigue performance. This is also because the ductility reduction that occur because of the larger aggregate size. This large parts decrease the amount of fibers that can be mixed homogenously with the matrix to form a continuous ductile material.
- Under fatigue tests, especially the high cycle ones, there are three main phases. The first one occurs at the beginning where the cracks initiate. In the second one the cracks propagate during the test, and in the third one the cracks start to be unstable and the failure occur. While the first and the last phases are considerably short, the second is the dominant phase. In this phase the crack propagation rate dominates the fatigue life. Considering that the crack propagation rate represents the energy absorbed at each cycle, the number of cycles to failure can be predicted by dividing the amount of the remaining energy that corresponds to the applied stress level, on the crack propagation rate.
- While the crack propagation rate for a specific stress level can be calculated from the fatigue test curves for the same stress level, in this thesis an equation was suggested to calculate this rate based on the stress-energy curve obtained from the monotonic test.

- When the results obtained by the two suggested number of cycles prediction methods are compared to the number of cycles obtained from the actual fatigue tests, it can be seen that there is a good fit between them. The first method that uses the crack propagation rate from the fatigue test is better. Yet the amount of difference that exists can be related to the high scatter of the fatigue test.

6.3.Recommendations

For future works and further researches, the following are recommended:

- The strain life based fatigue tests can be performed to understand the behavior of ECC specimens under this type of fatigue.
- An accelerated fatigue test procedure can be developed by starting from lower to higher stress levels and perform an enough number of cycle for each stress level to obtain the corresponding crack propagation rate.

REFERENCES

Abernethy, R. B. (2006). *The new Weibull handbook*. Dr. Robert B. Abernethy.

ACI Committee 215, A. C. (1992). *Considerations for Design of Concrete Structures Subjected to Fatigue Loading*. American Concrete Institute.

ACI Committee 325. (2006). 325.13R-06: Concrete Overlays for Pavement Rehabilitation. *Manual of Concrete Practice*, 1–39.

Al-Qadi, I. L., Scarpas, T., & Loizos, A. (2008). *Pavement Cracking: Mechanisms, Modeling, Detection, Testing and Case Histories*. CRC Press.

Balaguru, P. N., & Shah, S. P. (1992). *Fiber-reinforced cement composites* (Iillustrat). McGraw-Hill.

Bazant, Z. P., & Hubler, M. H. (2014). Theory of cyclic creep of concrete based on Paris law for fatigue growth of subcritical microcracks. *Journal of the Mechanics and Physics of Solids*, *63*, 187–200.

Bazant, Z. P., & Xu, K. (1991). Size effect in fatigue fracture of concrete. *ACI Materials Journal*, *88*(4), 390–399.

Bissonnette, B., Courard, L., Fowler, D. W., & Granju, J. L. (2011). *Bonded Cement-Based Material Overlays for the Repair, the Lining or the Strengthening of Slabs or Pavements: State-of-the-Art Report of the RILEM Technical Committee 193-RLS*. Springer Netherlands.

Boshoff, W. P., & van Zijl, G. (2007). Time-dependent response of ECC: Characterisation of creep and rate dependence. *Cement and Concrete Research*, *37*(5), 725–734. http://doi.org/10.1016/j.cemconres.2007.02.001

Campbell, F. C. (2012). *Fatigue and fracture: understanding the basics*. ASM

International.

Collins, M. P., Mitchell, D., & MacGregor, J. G. (1993). Structural design considerations for high-strength concrete. *Concrete International*, *15*(5).

Delatte, N. J. (2014). *Concrete pavement design, construction, and performance*. CRC Press.

Ferrara, L., Park, Y.-D., & Shah, S. P. (2007). A method for mix-design of fiber-reinforced self-compacting concrete. *Cement and Concrete Research*, *37*(6), 957–971. http://doi.org/10.1016/j.cemconres.2007.03.014

Gopalaratnam, V., & Shah, S. (1987). Tensile Failure of Steel Fiber Reinforced Mortar. *Journal of Engineering Mechanics*, *113*(5), 635–652. http://doi.org/10.1061/(ASCE)0733-9399(1987)113:5(635)

Habel, K., & Gauvreau, P. (2008). Response of ultra-high performance fiber reinforced concrete (UHPFRC) to impact and static loading. *Cement and Concrete Composites*, *30*(10), 938–946. http://doi.org/10.1016/j.cemconcomp.2008.09.001

Kakuma, K., Matsumoto, T., Hayashikawa, T., & He, X. (2011). Fatigue Analysis of ECC-Steel Composite Deck under Wheel Trucking Load. *Procedia Engineering*, *14*, 1838–1844. http://doi.org/10.1016/j.proeng.2011.07.231

Kanda, T., Saito, T., Sakata, N., & Hiraishi, M. (2003). Tensile and anti-spalling properties of direct sprayed ECC. *Journal of Advanced Concrete Technology*, *1*(3), 269–282.

Lee, Y. L., Pan, J., Hathaway, R., & Barkey, M. (2011). *Fatigue Testing and Analysis: Theory and Practice*. Elsevier Science.

Leung, C. K. Y., Cheung, Y. N., & Zhang, J. (2007). Fatigue enhancement of concrete beam with ECC layer. *Cement and Concrete Research*, *37*(5), 743–750. http://doi.org/10.1016/j.cemconres.2007.01.015

Li, V. C. (2002). Advances in ECC research. *ACI Special Publications*, *206*, 373–400.

Li, V. C., Banthia, N., Bentur, A., & Mufti, A. (1997). Engineered Cementitious Composites—Tailored Composites Through Micromechanical Modeling, to appear in Fiber Reinforced Concrete: Present and the Future, Eds: N. *Banthia et Al, CSCE*.

Li, V. C., Fischer, G., Kim, Y., Lepech, M. D., Qian, S., Weimann, M., & Wang, S. (2003). *Durable link slabs for jointless bridge decks based on strain-hardening cementitious composites*.

Li, V. C., & Kanda, T. (1998a). Engineered Cementitious Composites for structural applications. *Journal of Materials in Civil Engineering*, *10*(2), 66–69. http://doi.org/10.1061/(ASCE)0899-1561(1998)10:2(66)

Li, V. C., & Kanda, T. (1998b). Innovations Forum: Engineered cementitious composites for structural applications. *Journal of Materials in Civil Engineering*, *10*(2), 66–69.

Li, V. C., & Lepech, M. (2004). Crack resistant concrete material for transportation construction. In *Transportation Research Board 83rd Annual Meeting, Washington, DC, Compendium of Papers CD ROM, Paper* (pp. 4–4680). Citeseer.

Li, V. C., Mishra, D. K., Naaman, A. E., Wight, J. K., LaFave, J. M., Wu, H.-C., & Inada, Y. (1994). On the shear behavior of engineered cementitious composites. *Advanced Cement Based Materials*, *1*(3), 142–149.

Li, V. C., Mishra, D. K., & Wu, H.-C. (1995). Matrix design for pseudo-strain-hardening fibre reinforced cementitious composites. *Materials and Structures*, *28*(10), 586–595.

Li, V. C., Wu, C., Wang, S., Ogawa, A., & Saito, T. (2002). Interface tailoring for strain-hardening polyvinyl alcohol-engineered cementitious composite (PVA-ECC). *ACI Materials Journal-American Concrete Institute*, *99*(5), 463–472.

Liu, F., Meng, L., Ning, G.-F., & Li, L.-J. (2015). Fatigue performance of rubber-modified recycled aggregate concrete (RRAC) for pavement. *Construction and Building Materials*, *95*, 207–217. http://doi.org/10.1016/j.conbuildmat.2015.07.042

Maalej, M., Quek, S., & Zhang, J. (2005). Behavior of Hybrid-Fiber Engineered Cementitious Composites Subjected to Dynamic Tensile Loading and Projectile Impact. *Journal of Materials in Civil Engineering*, *17*(2), 143–152. http://doi.org/10.1061/(ASCE)0899-1561(2005)17:2(143)

Mindess, S., Young, J. F., & Darwin, D. (2003). *Concrete*. Prentice Hall PTR. Retrieved from http://books.google.com.tr/books?id=38VoQgAACAAJ

Miyazato, S., & Hiraishi, Y. (2005). Transport properties and steel corrosion in ductile fiber reinforced cement composites. In *Proceedings of the Eleventh International Conference on Fracture* (pp. 20–25).

Pokluda, J. (2010). *Micromechanisms of Fracture and Fatigue: In a Multi-Scale Context*. Springer Science & Business Media.

Qian, S. Z., Li, V. C., Zhang, H., & Keoleian, G. A. (2013). Life cycle analysis of pavement overlays made with Engineered Cementitious Composites. *Cement and Concrete Composites*, *35*(1), 78–88. http://doi.org/10.1016/j.cemconcomp.2012.08.012

Şahmaran, M., & Li, V. C. (2008). Durability of mechanically loaded engineered cementitious composites under highly alkaline environments. *Cement and Concrete Composites*, *30*(2), 72–81.

Şahmaran, M., & Li, V. C. (2009). Durability properties of micro-cracked ECC containing high volumes fly ash. *Cement and Concrete Research*, *39*(11), 1033–1043. http://doi.org/10.1016/j.cemconres.2009.07.009

Şahmaran, M., Yücel, H. E., Demirhan, S., & Li, V. C. (2012). Combined Effect of Aggregate and Mineral Admixtures on Tensile Ductility of Engineered

Cementitious Composites. *ACI Materials Journal*, *109*(6).

Sakin, R., & Ay, İ. (2008). Statistical analysis of bending fatigue life data using Weibull distribution in glass-fiber reinforced polyester composites. *Materials & Design*, *29*(6), 1170–1181. http://doi.org/10.1016/j.matdes.2007.05.005

Schijve, J. (2001). *Fatigue of structures and materials*. Springer.

Shigley, J. E. (2011). *Shigley's mechanical engineering design*. Tata McGraw-Hill Education.

Song, P. S., & Hwang, S. (2004). Mechanical properties of high-strength steel fiber-reinforced concrete. *Construction and Building Materials*, *18*(9), 669–673. http://doi.org/10.1016/j.conbuildmat.2004.04.027

Walraven, J. (2009). High performance fiber reinforced concrete: progress in knowledge and design codes. *Materials and Structures*, *42*(9), 1247–1260. http://doi.org/10.1617/s11527-009-9538-3

Wang, S., & Li, V. C. (2007). Engineered cementitious composites with high-volume fly ash. *ACI Materials Journal-American Concrete Institute*, *104*(3), 233–241.

Weibull, W. (1961). *Fatigue Testing and Analysis of Results*. *Fatigue Testing and Analysis of Results*. Elsevier. http://doi.org/10.1016/B978-0-08-009397-0.50001-1

Wormsen, A., & Haerkegaard, G. (2015). A statistical investigation of fatigue behaviour according to Weibullś weakest link theory. In *ESIS -ECF 15 Sweden*.

Yao, W., Li, J., & Wu, K. (2003). Mechanical properties of hybrid fiber-reinforced concrete at low fiber volume fraction. *Cement and Concrete Research*, *33*(1), 27–30. http://doi.org/10.1016/S0008-8846(02)00913-4

Zhang, J., & Li, V. C. (2002). Monotonic and fatigue performance in bending of fiber-reinforced engineered cementitious composite in overlay system. *Cement and Concrete Research*, *32*(3), 415–423. http://doi.org/10.1016/S0008-

8846(01)00695-0

Zhang, Z. (2013). Encyclopedia of Tribology. In Q. J. Wang & Y.-W. Chung (Eds.), (pp. 687–691). Boston, MA: Springer US. http://doi.org/10.1007/978-0-387-92897-5_245

Zollo, R. F. (1997). Fiber-reinforced concrete: an overview after 30 years of development. *Cement and Concrete Composites*, *19*(2), 107–122. http://doi.org/10.1016/S0958-9465(96)00046-7

APPENDIX A

ANALYSIS OF FATIGUE TEST RESULTS

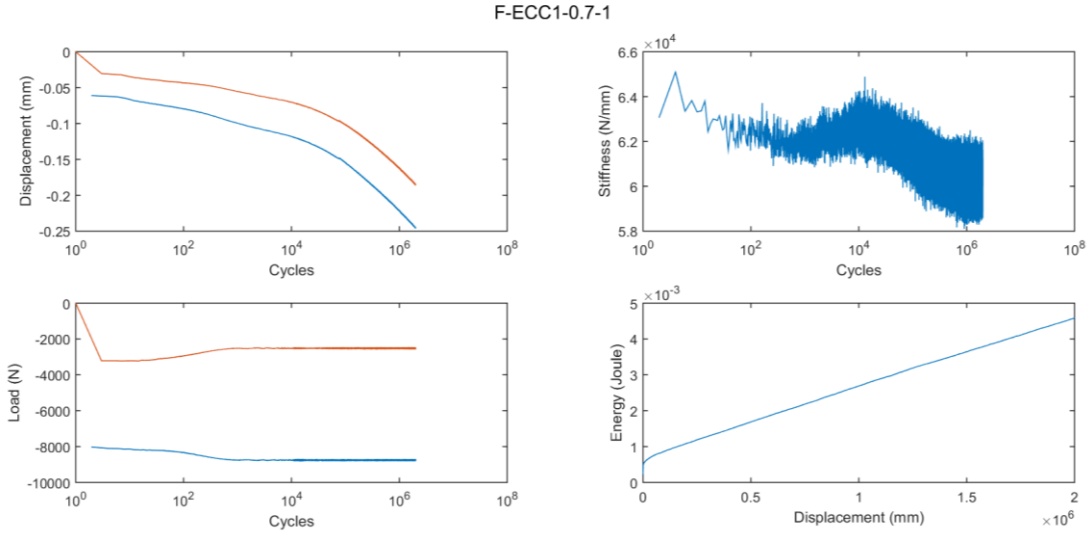

a) F-ECC1 - %70 -1

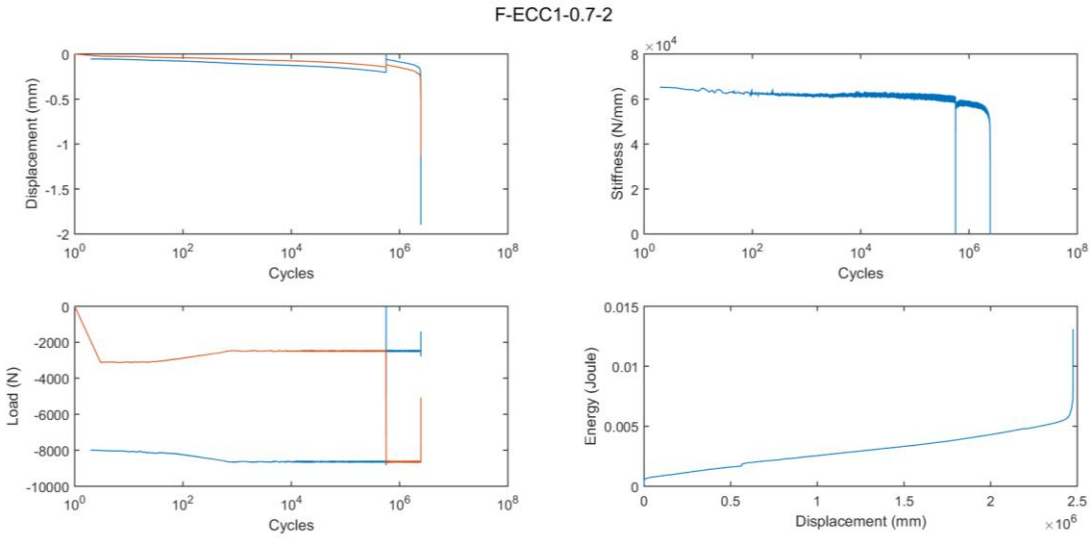

b) F-ECC1 - %70 -2

Figure A.1 Fatigue test results of F-ECC1 specimens at 70% of σ_{max}

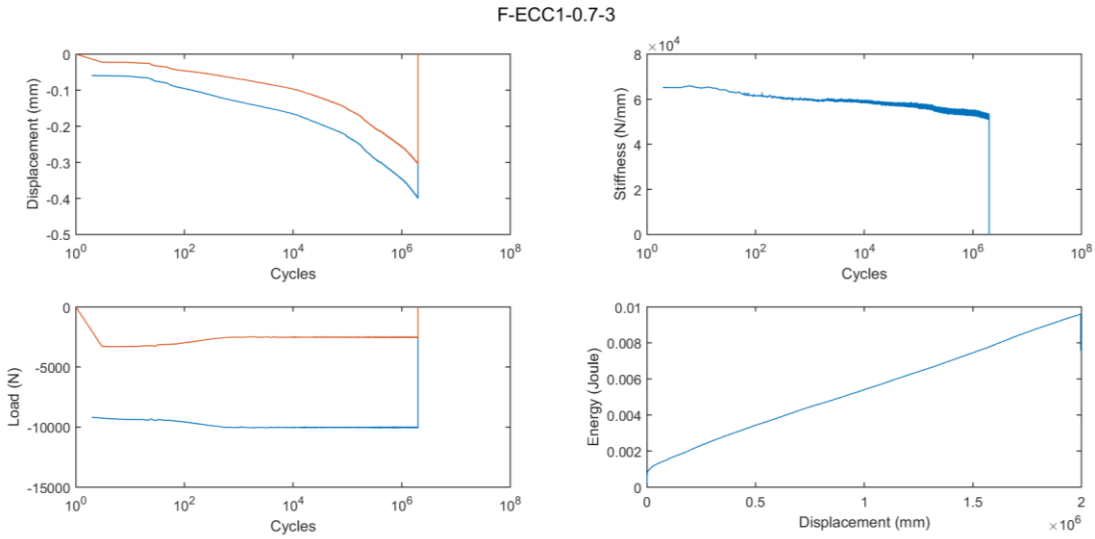

c) F-ECC1 - %70 -3

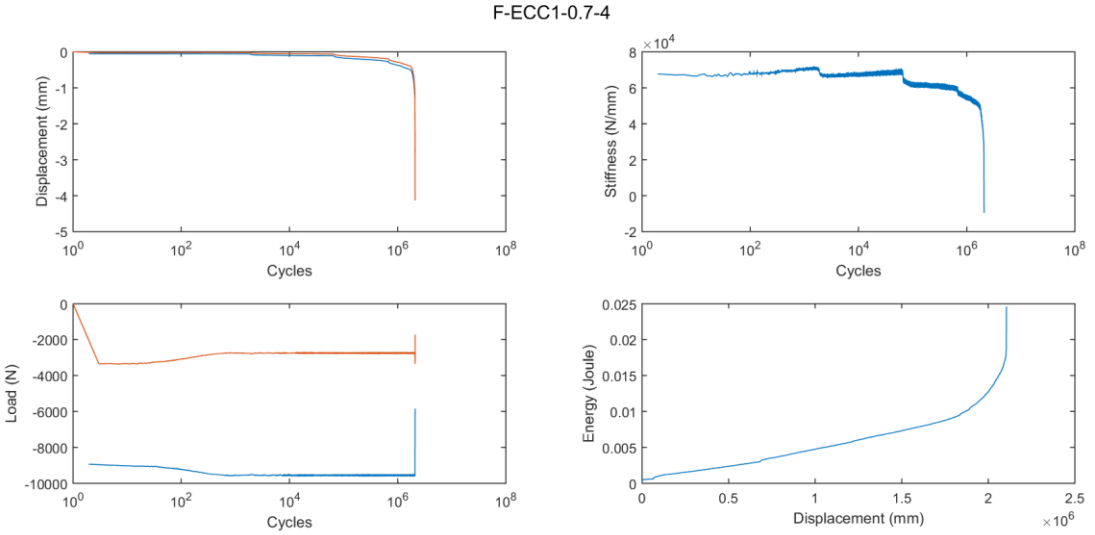

d) F-ECC1 - %70 -4

Figure A.1 (continued)

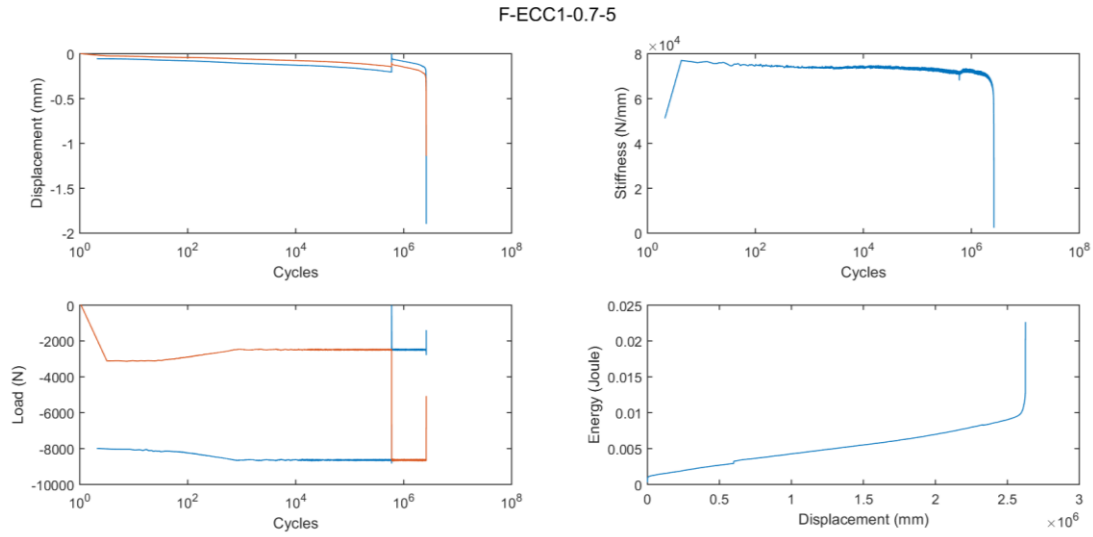

e) F-ECC1 - %70 -5

Figure A.1 (continued)

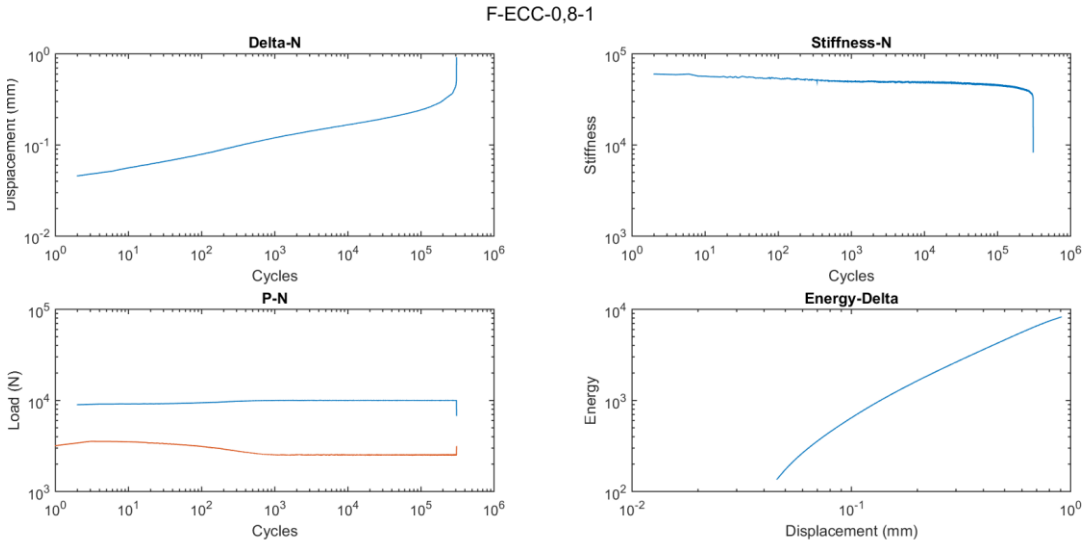

a) F-ECC1 - %80 -1

Figure A.2 Fatigue test results of F-ECC1 specimens at 80% of σ_{max}

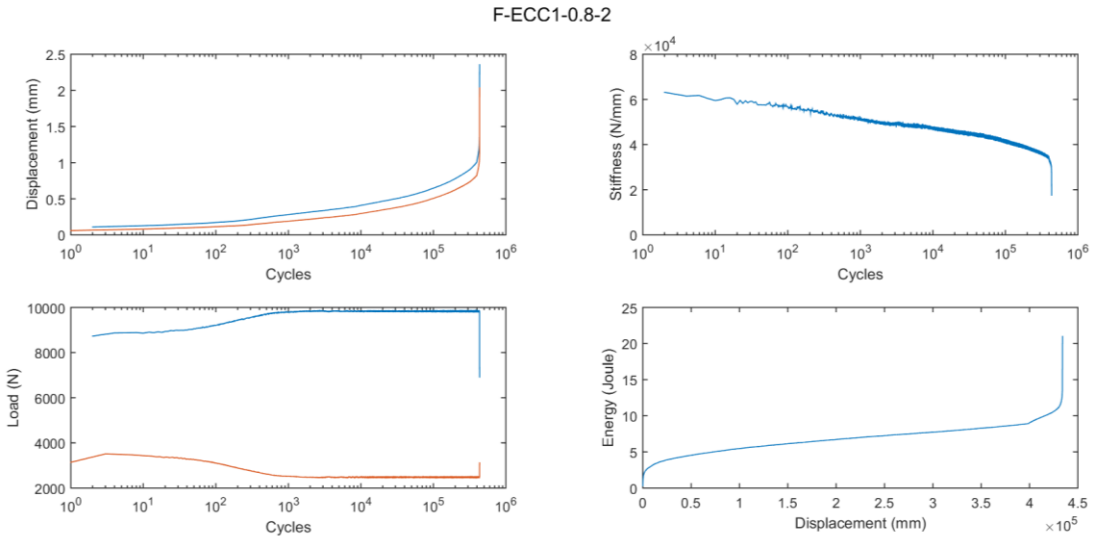

b) F-ECC1 - %80 -2

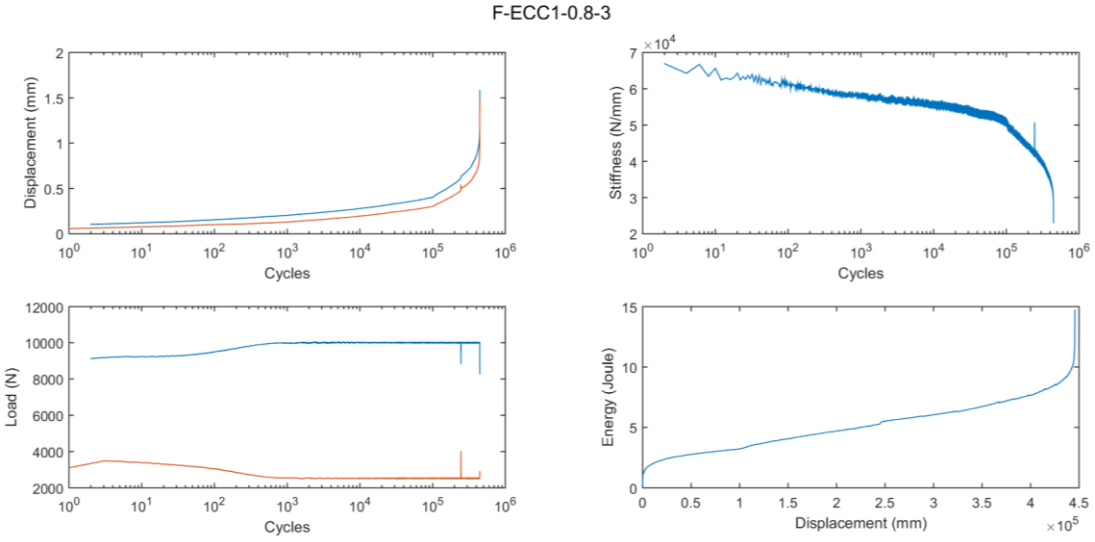

c) F-ECC1 - %80 -3

Figure A.2 (continued)

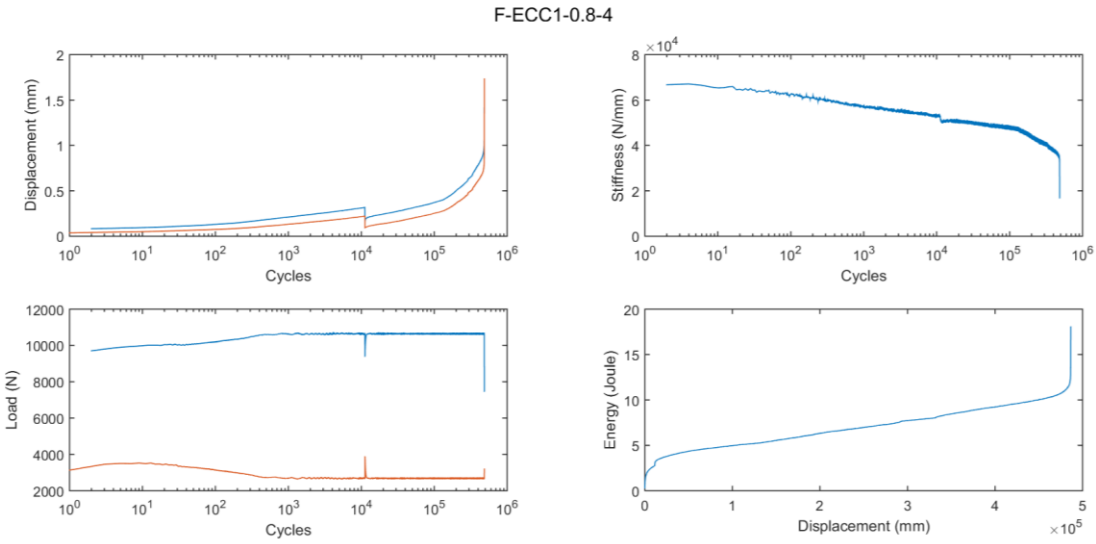

d) F-ECC1 - %80 -4

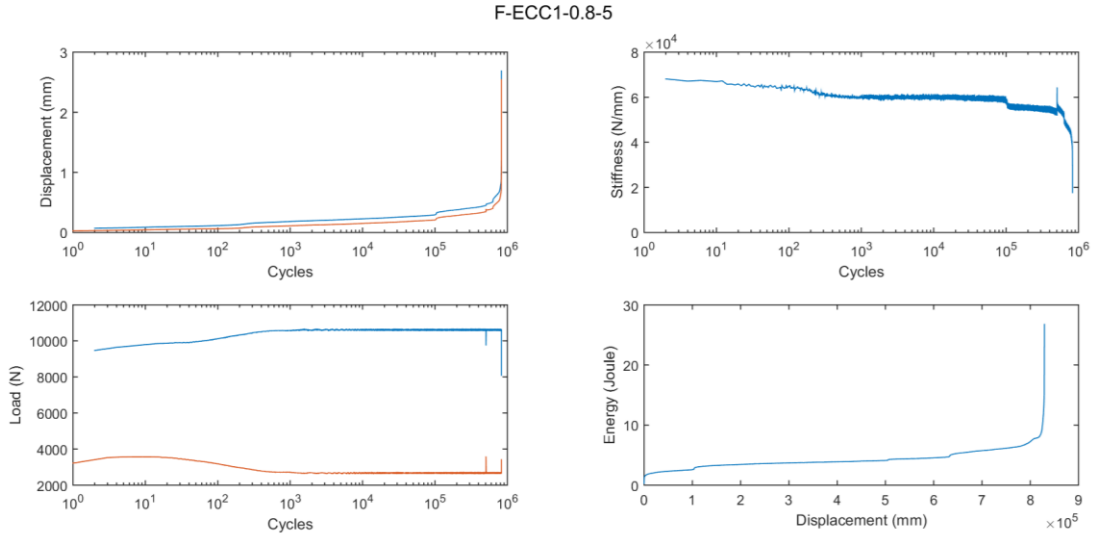

e) F-ECC1 - %80 -5

Figure A.2 (continued)

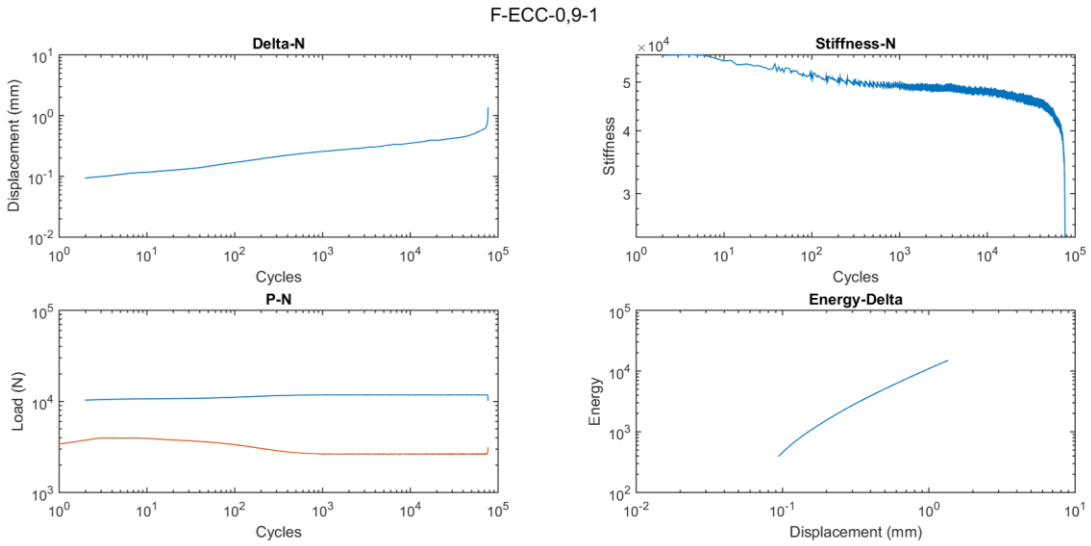

a) F-ECC1 - %90 -1

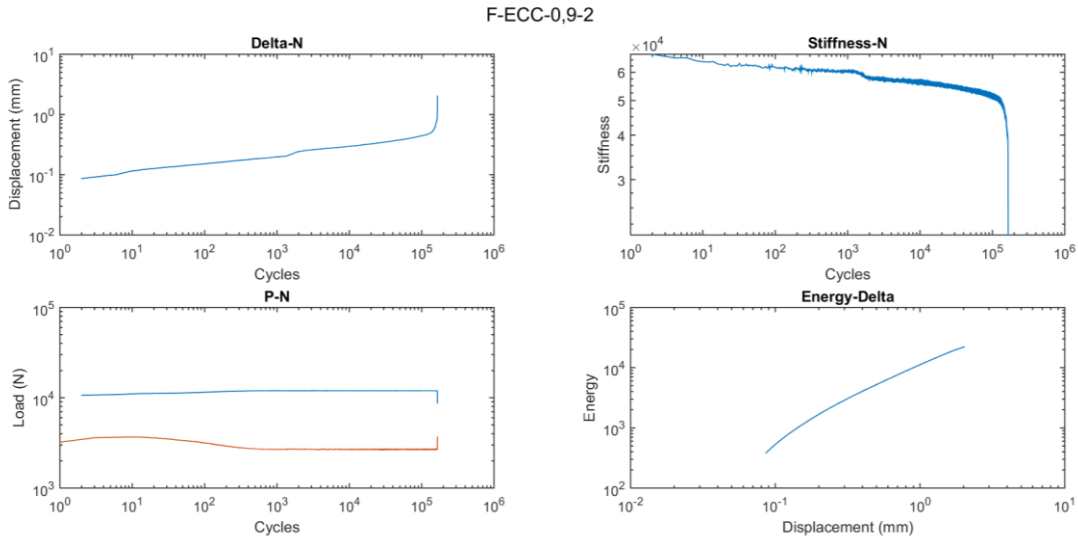

b) F-ECC1 - %90 -2

Figure A.3 Fatigue test results of F-ECC1 specimens at 90% of σ_{max}

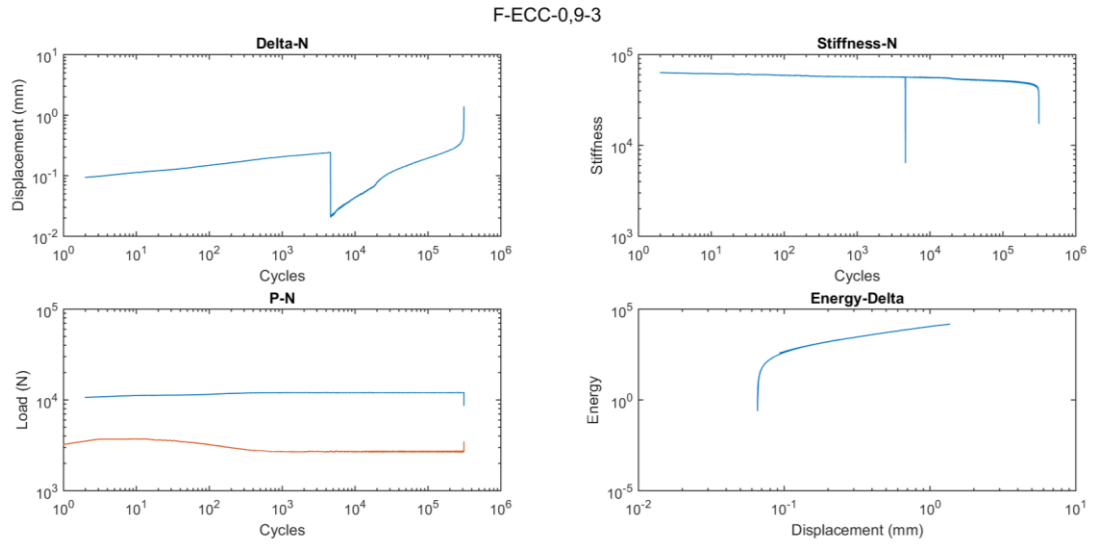

c) F-ECC1 - %90 -3

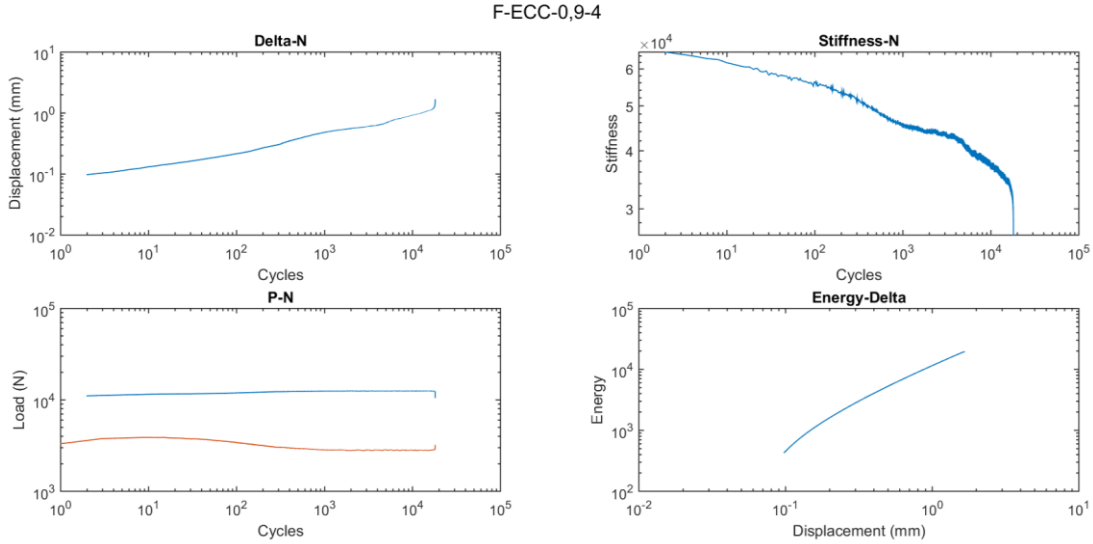

d) F-ECC1 - %90 -4

Figure A.3 (continued)

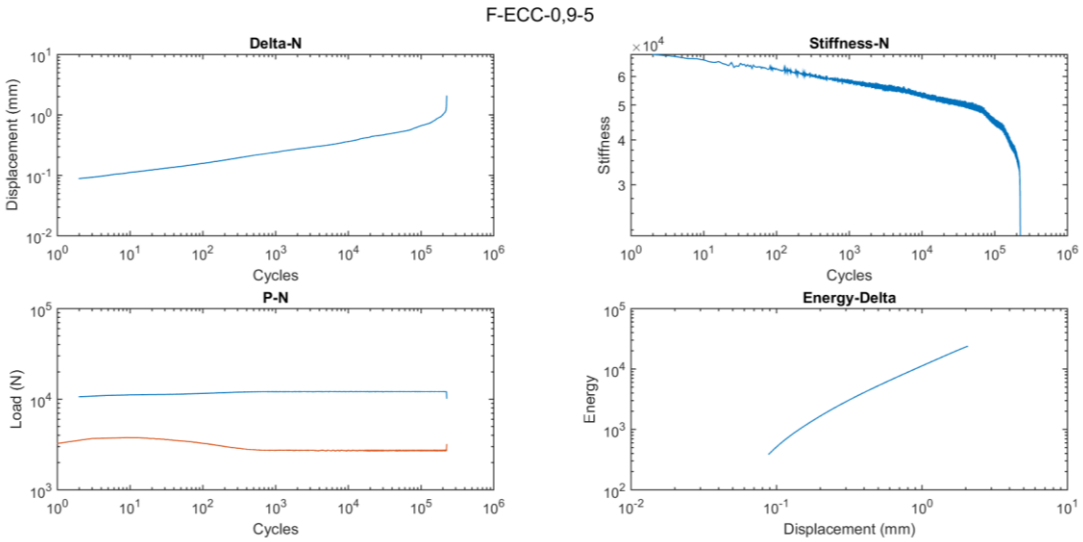

e) F-ECC1 - %90 -5

Figure A.3 (continued)

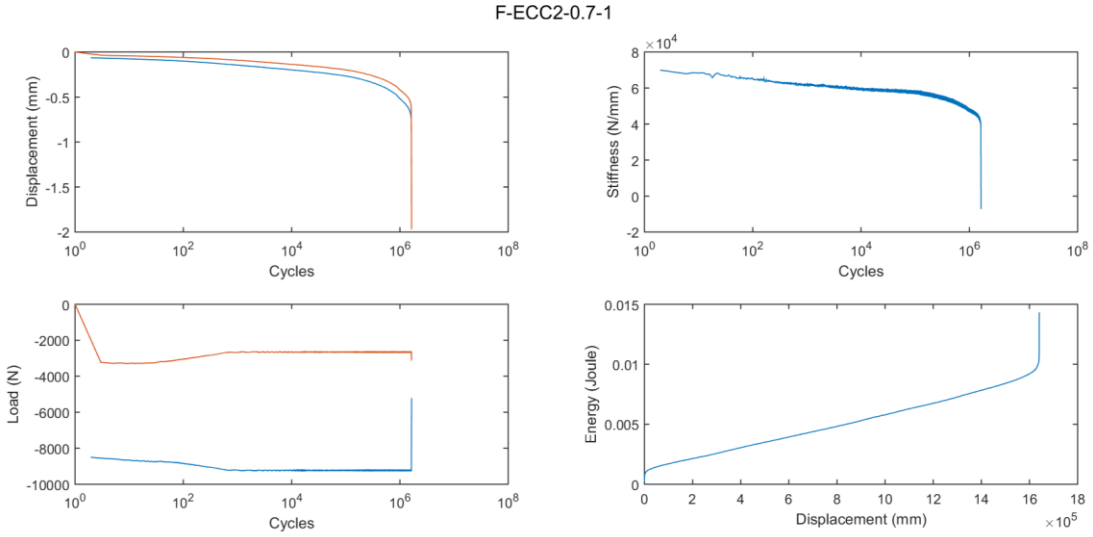

a) F-ECC2 - %70 -1

Figure A.4 Fatigue test results of F-ECC2 specimens at 70% of σ_{max}

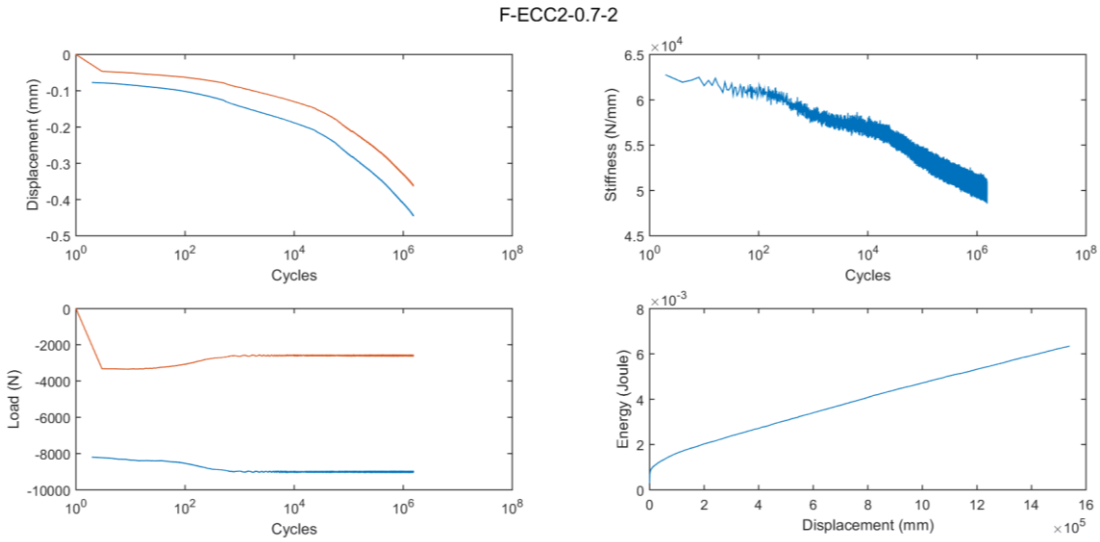

b) F-ECC2 - %70 -2

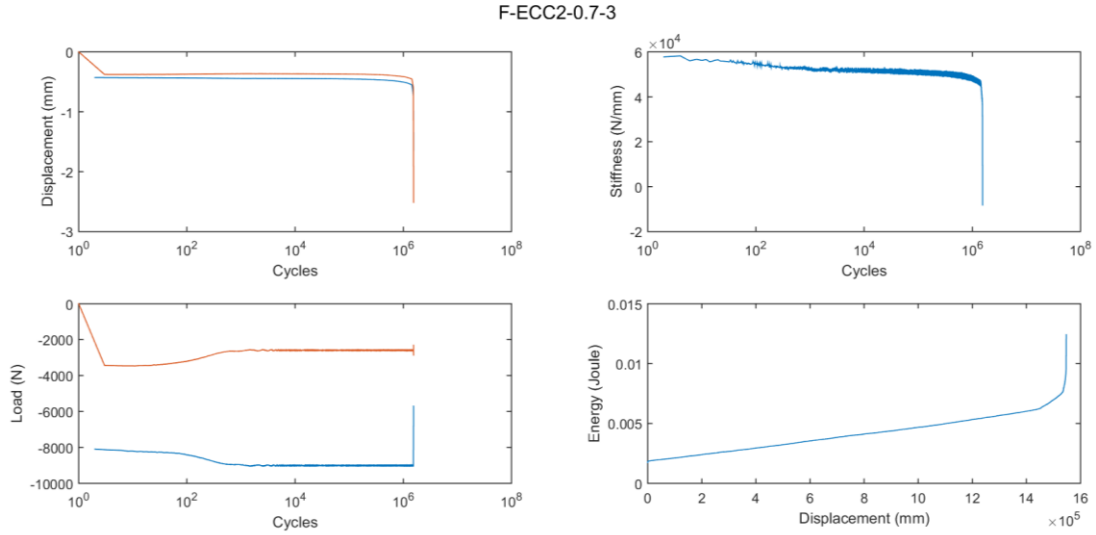

c) F-ECC2 - %70 -3

Figure A.4 (continued)

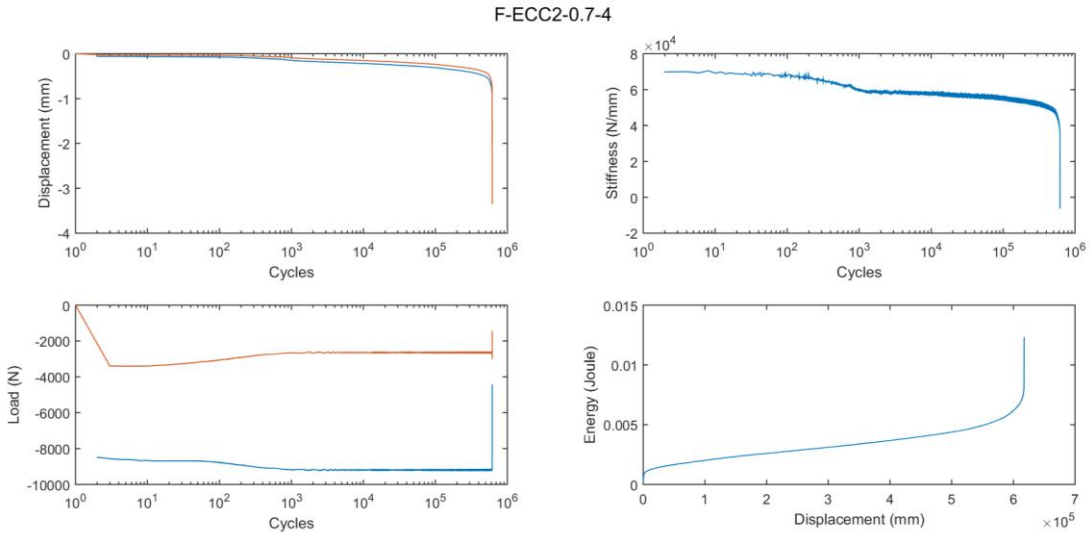

d) F-ECC2 - %70 -4

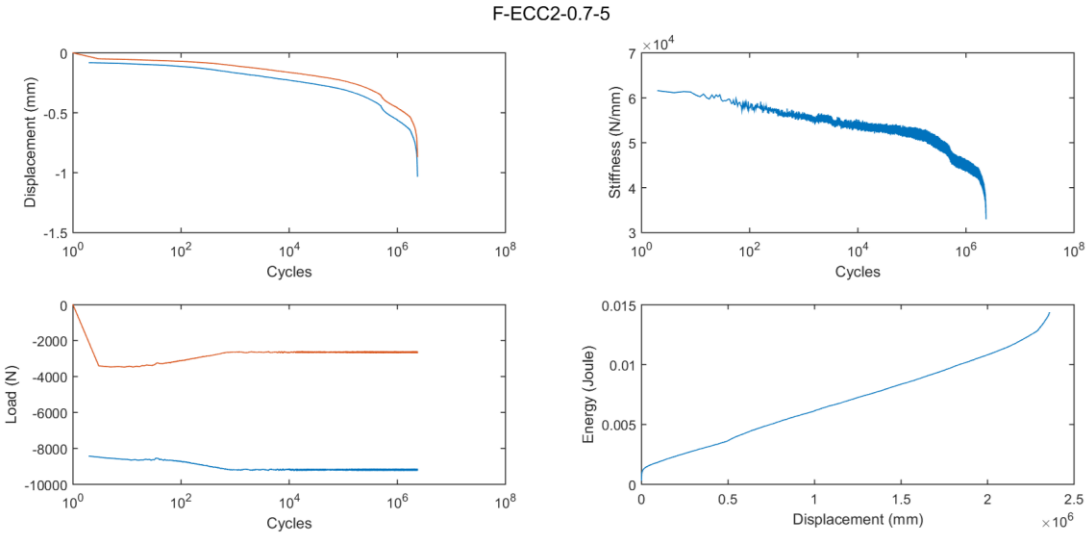

e) F-ECC2 - %70 -5

Figure A.4 (continued)

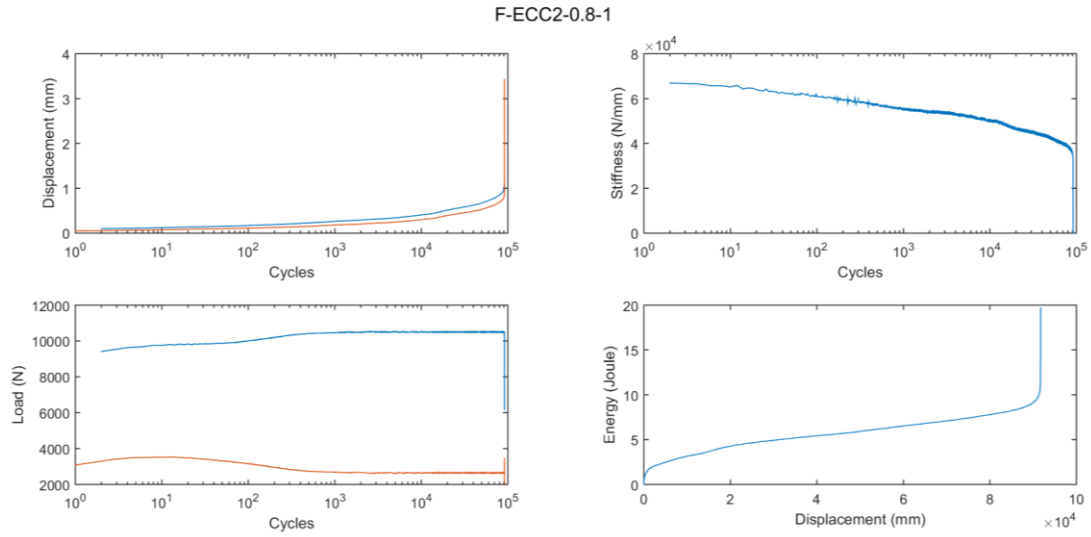

a) F-ECC2 - %80 -1

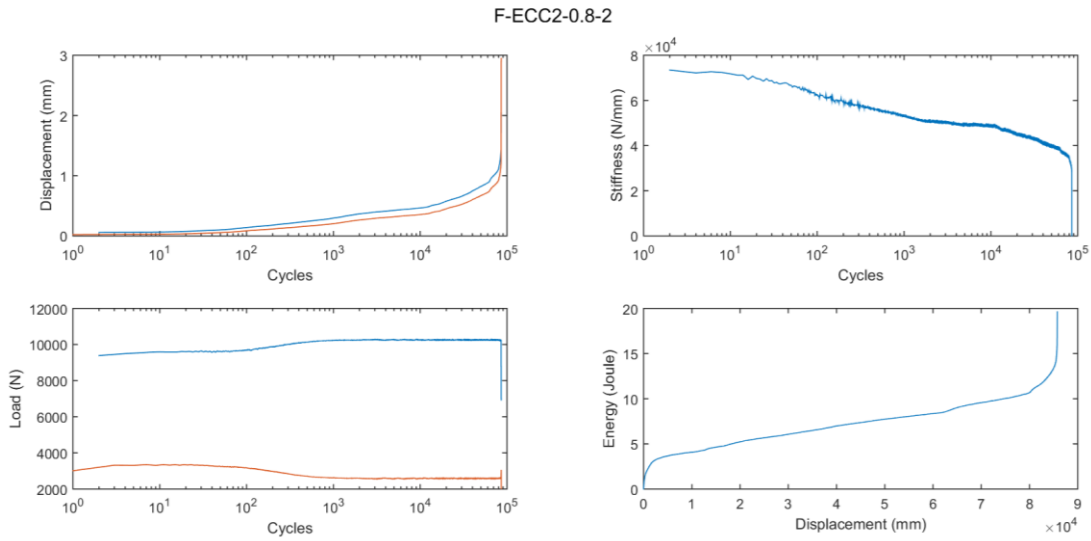

b) F-ECC2 - %80 -2

Figure A.5 Fatigue test results of F-ECC2 specimens at 80% of σ_{max}

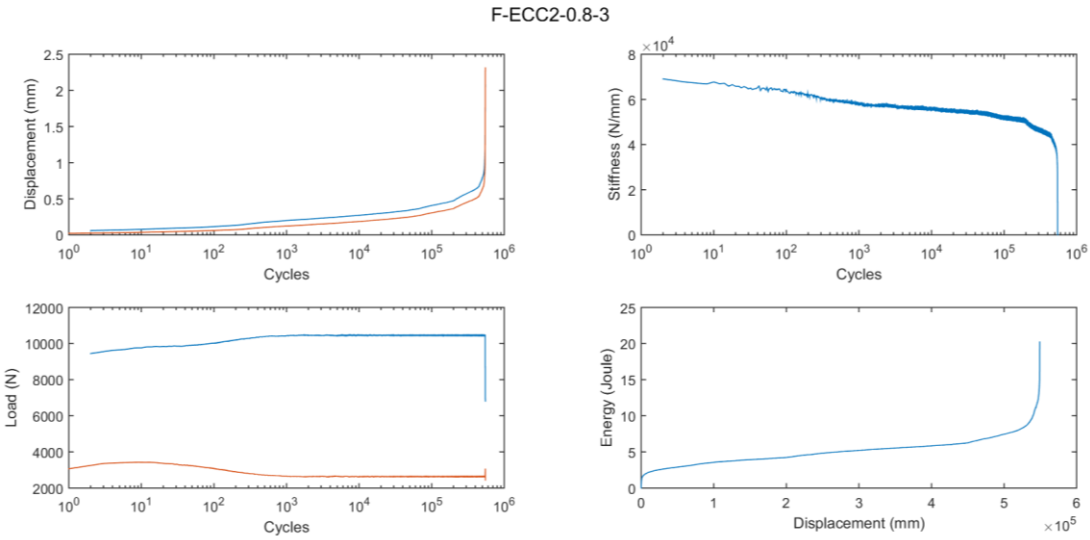

c) F-ECC2 - %80 -3

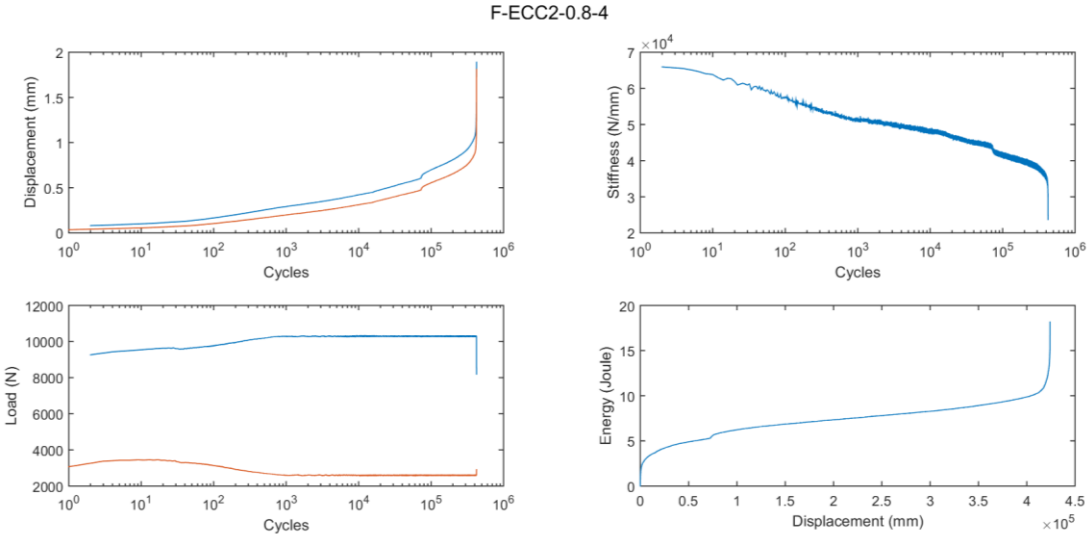

d) F-ECC2 - %80 -4

Figure A.5 (continued)

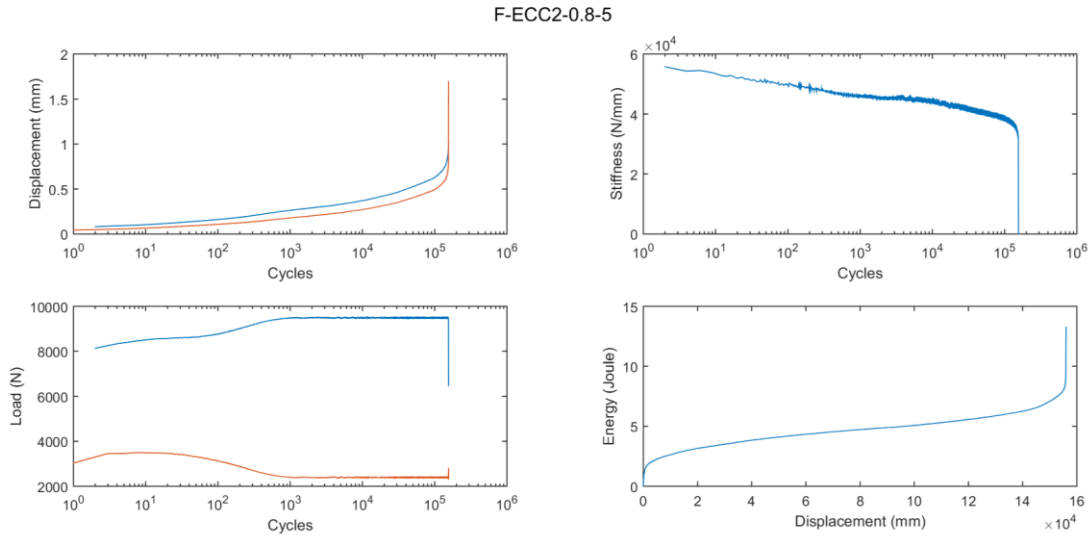

e) F-ECC2 - %80 -5

Figure A.5 (continued)

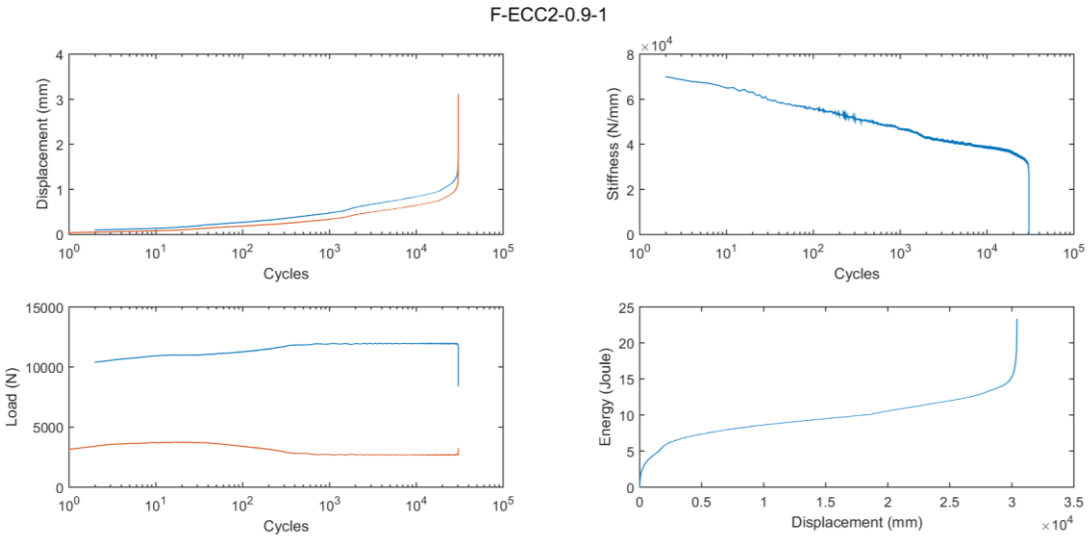

a) F-ECC2 - %90 -1

Figure A.6 Fatigue test results of F-ECC2 specimens at 90% of σ_{max}

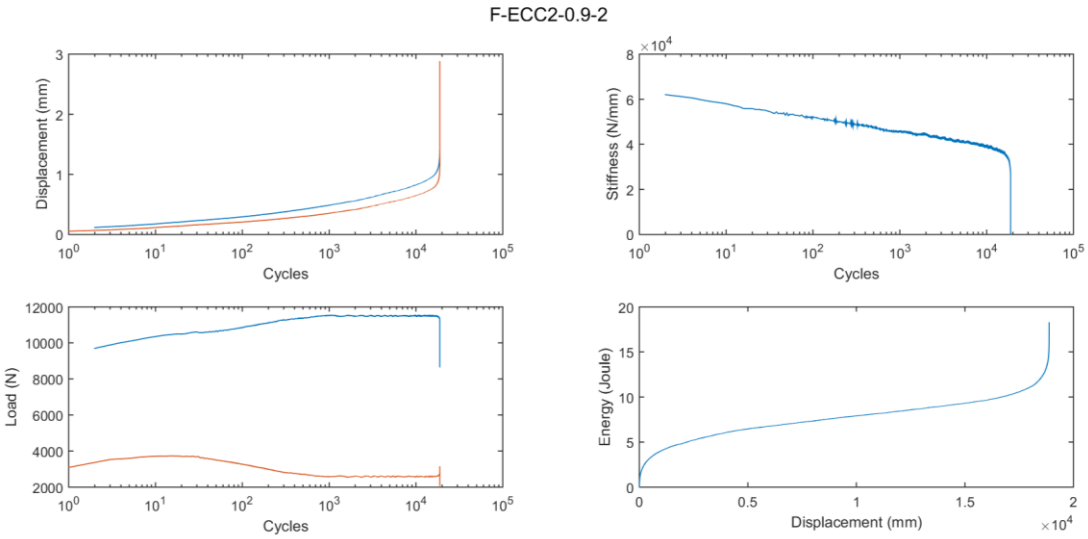

b) F-ECC2 - %90 -2

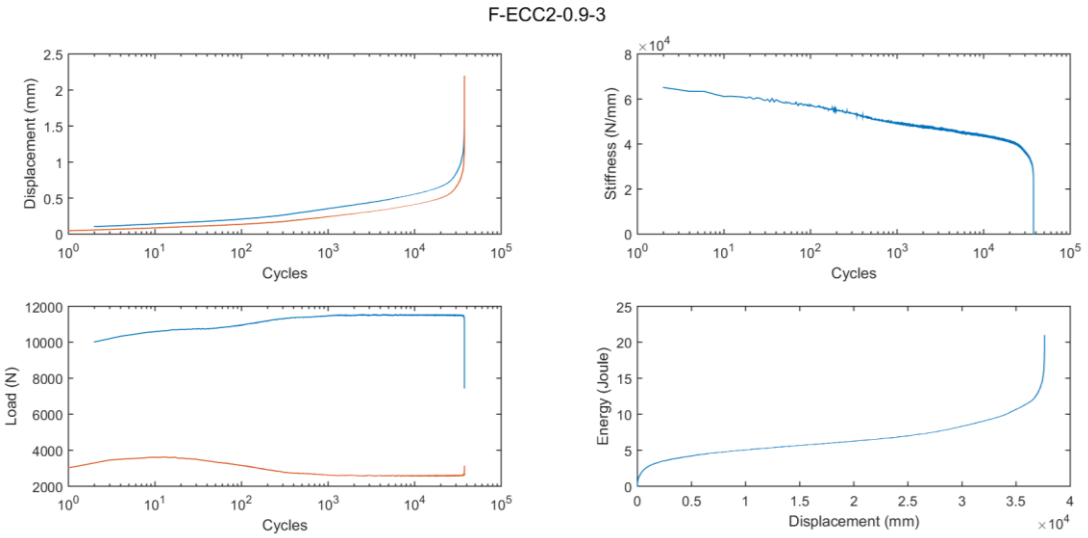

c) F-ECC2 - %90 -3

Figure A.6 (continued)

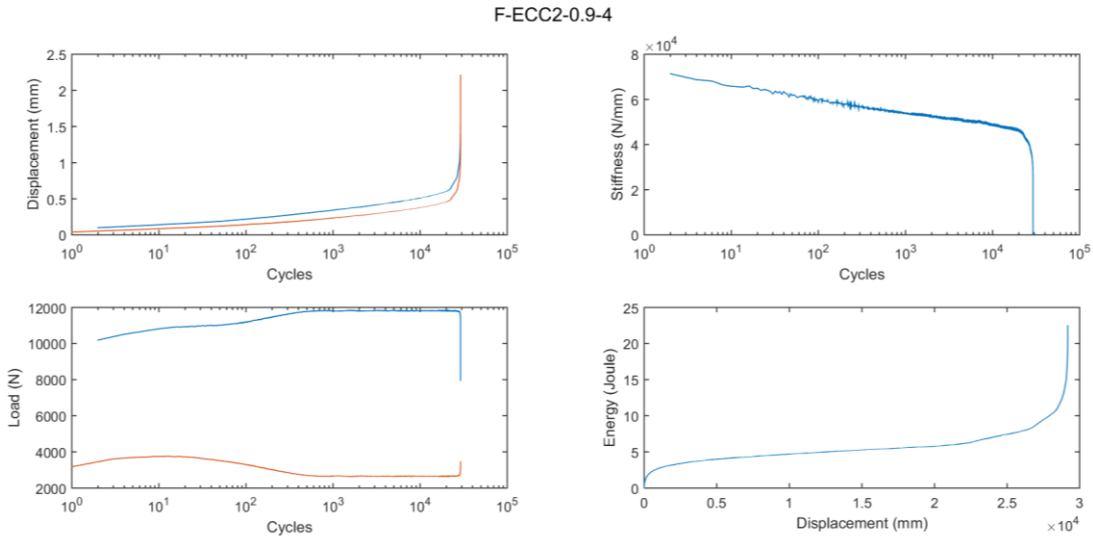

d) F-ECC2 - %90 -4

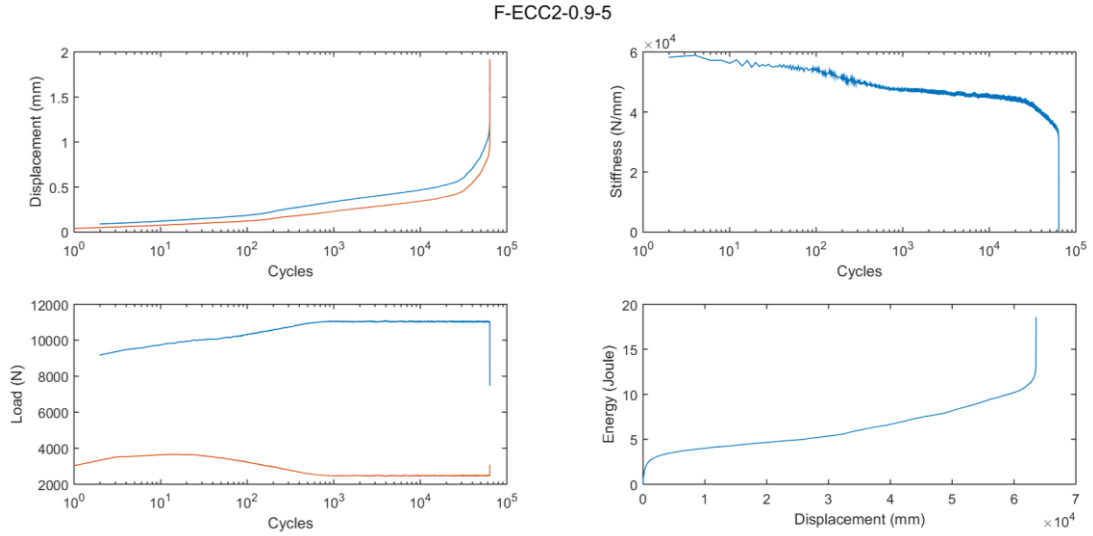

e) F-ECC2 - %90 -5

Figure A.6 (continued)

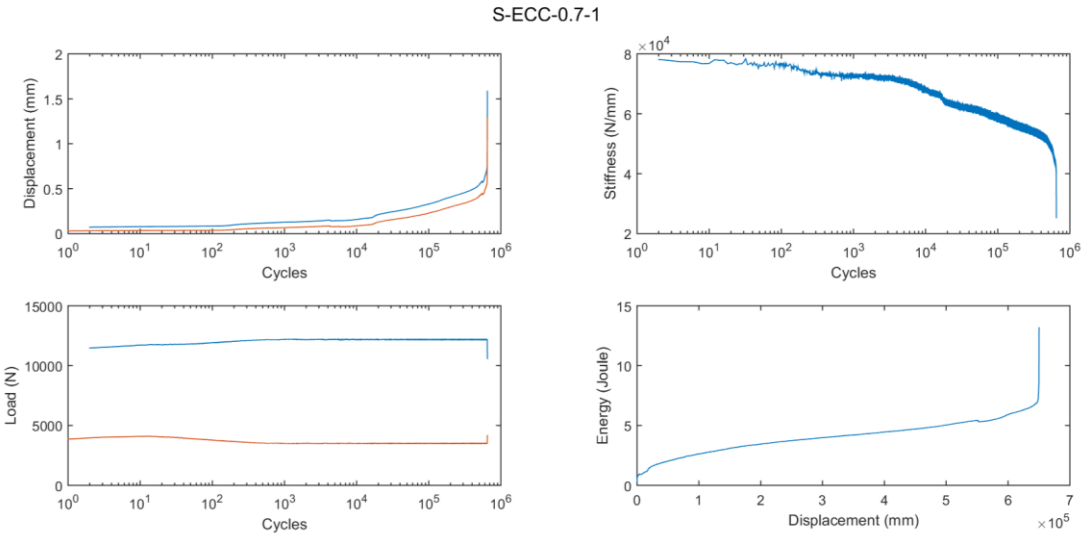

a) S-ECC - %70 -1

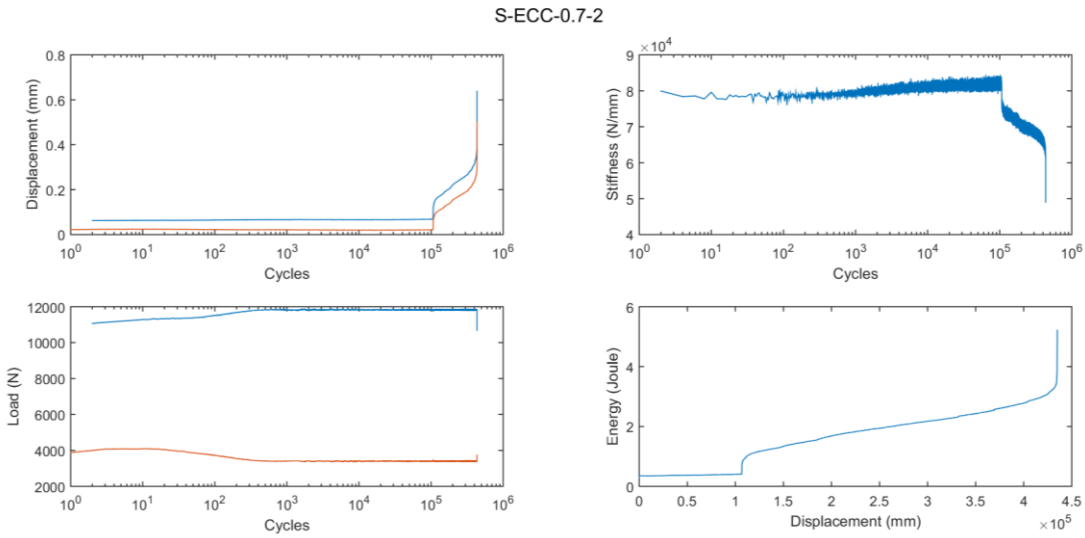

b) S-ECC - %70 -2

Figure A.7 Fatigue test results of S-ECC specimens at 70% of σ_{max}

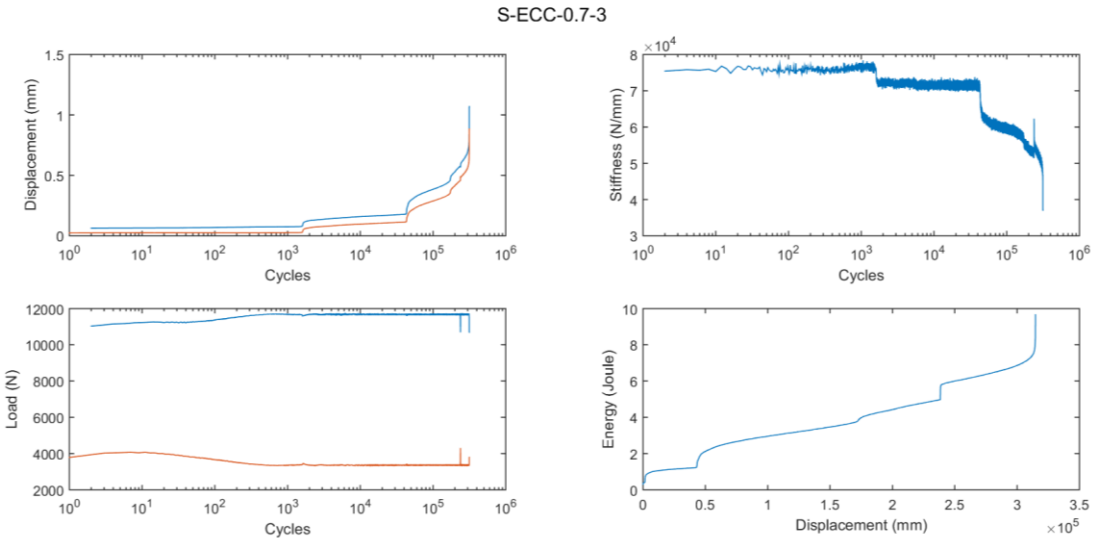

c) S-ECC - %70 -3

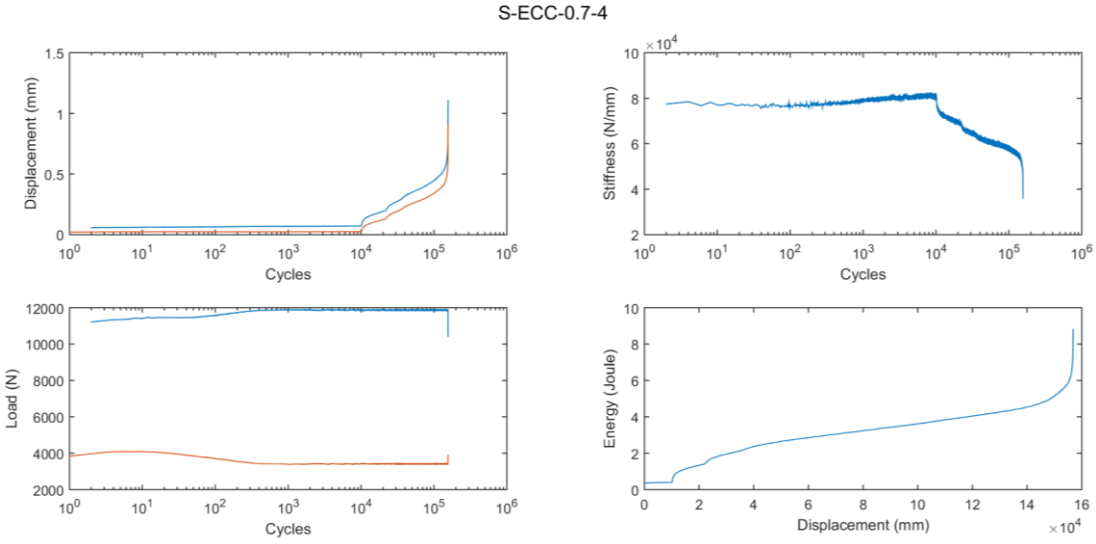

d) S-ECC - %70 -4

Figure A.7 (continued)

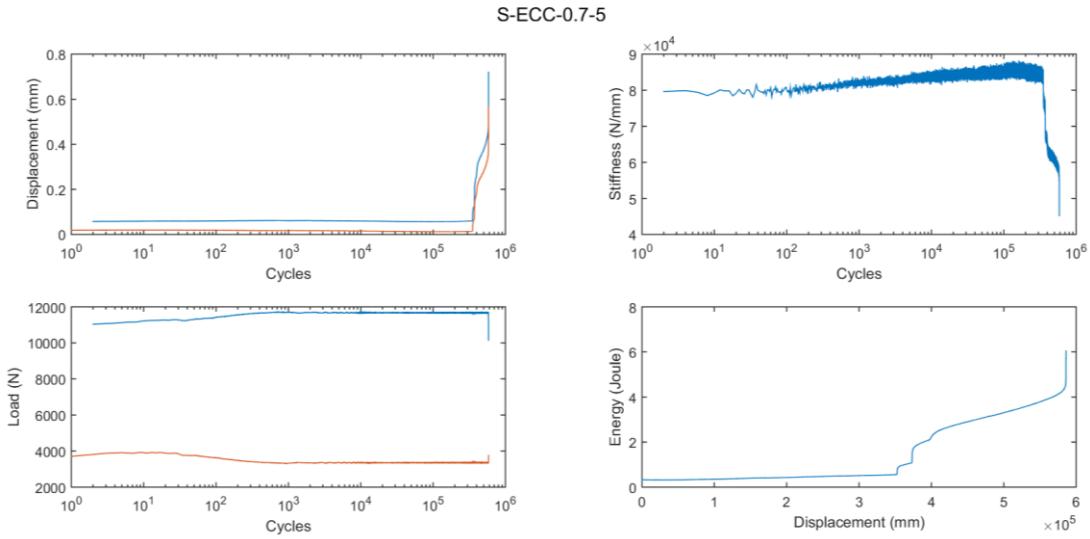

e) S-ECC - %70 -5

Figure A.7 (continued)

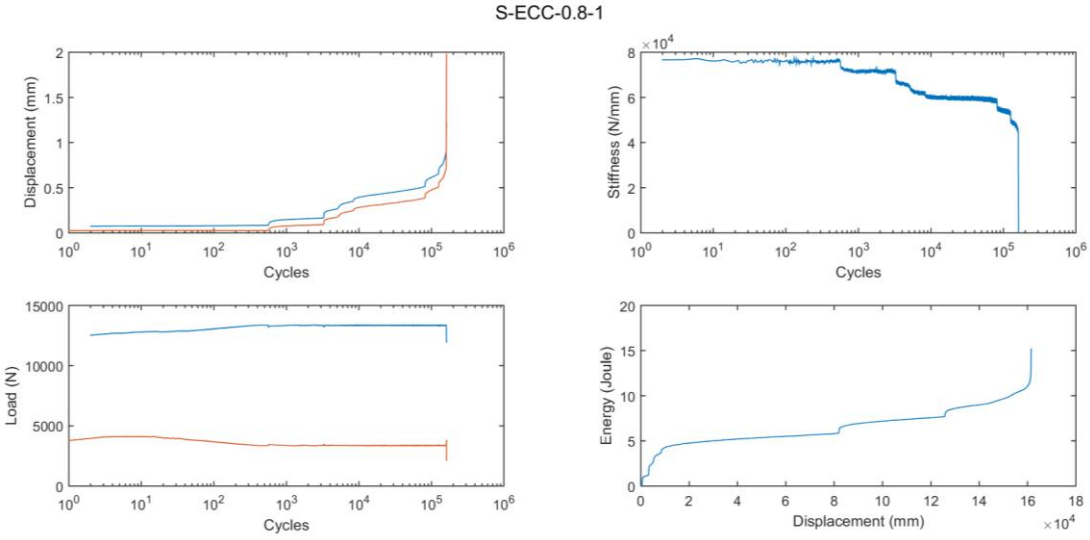

a) S-ECC - %80 -1

Figure A.8 Fatigue test results of S-ECC specimens at 80% of σ_{max}

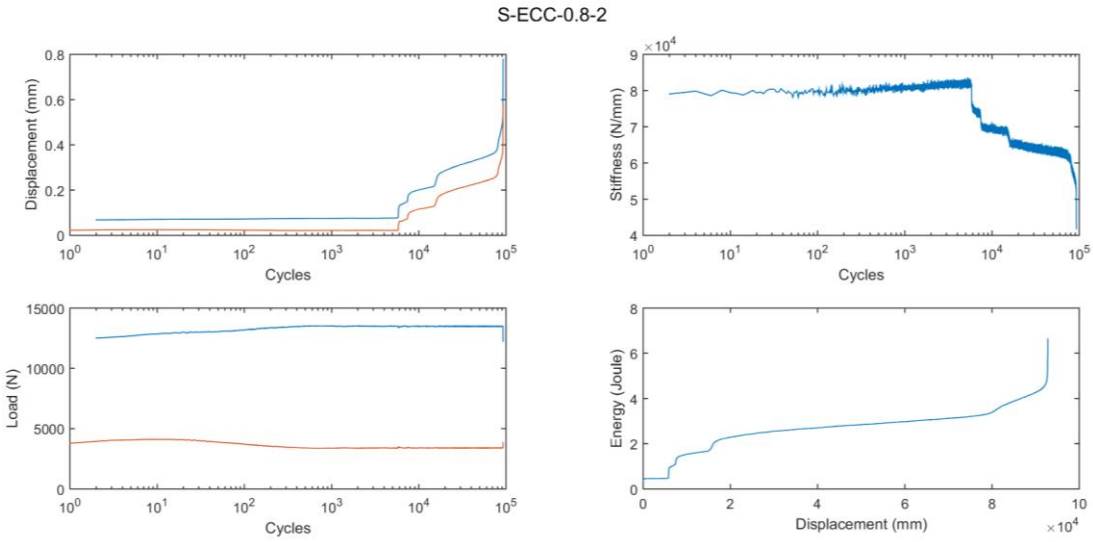

b) S-ECC - %80 -2

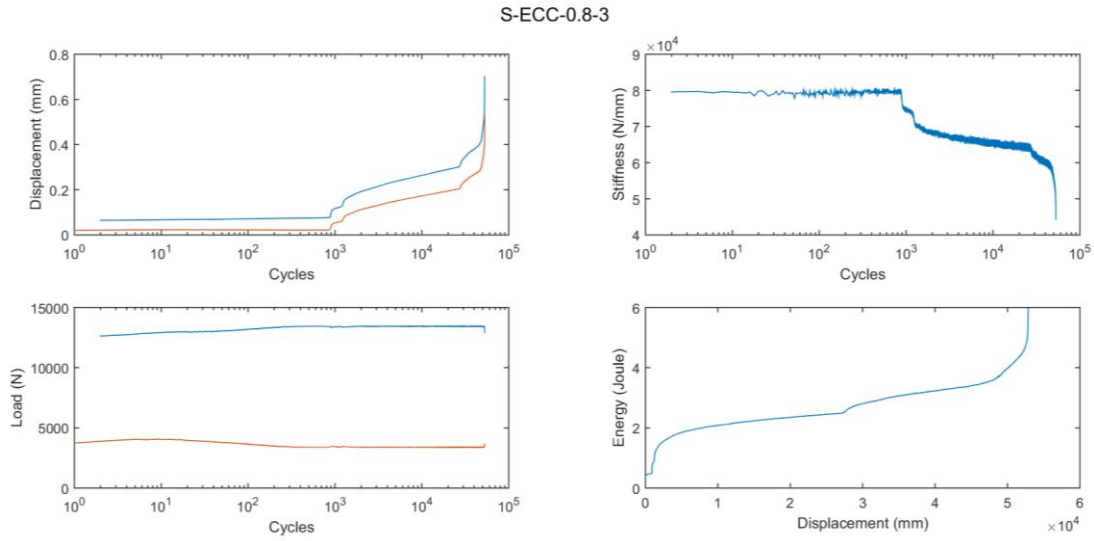

c) S-ECC - %80 -3

Figure A.8 (continued)

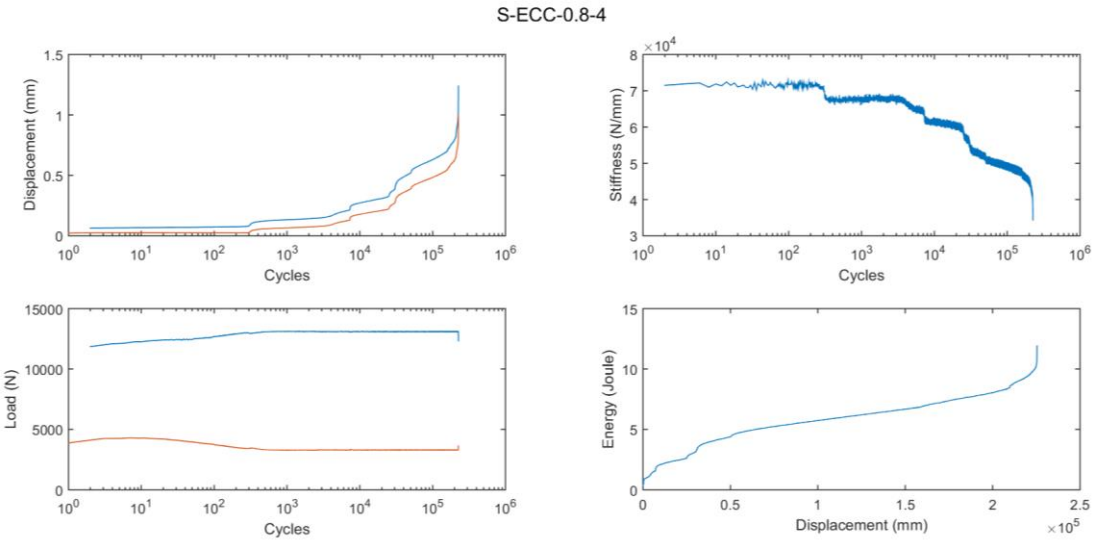

d) S-ECC - %80 -4

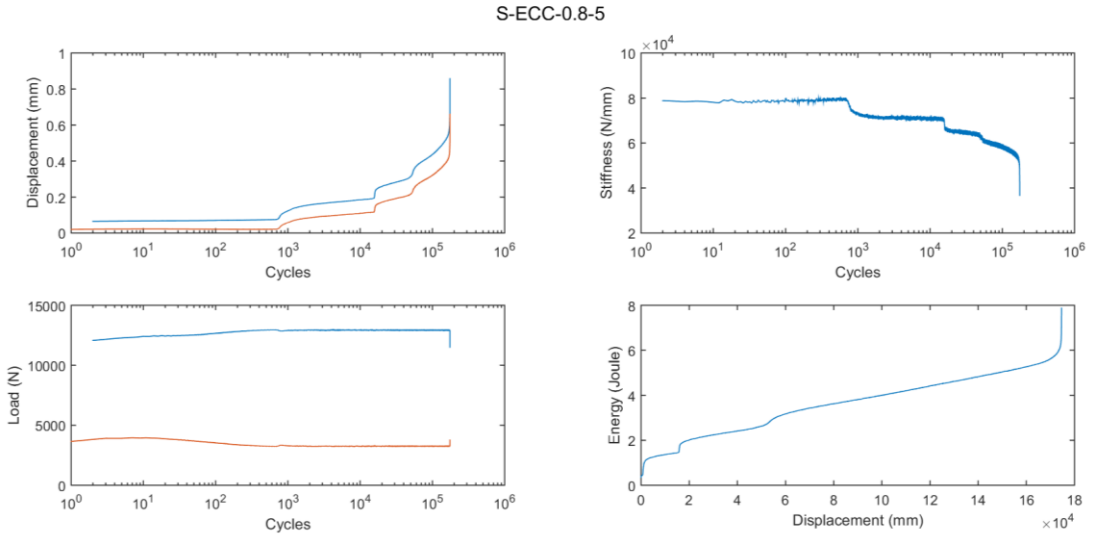

e) S-ECC - %80 -5

Figure A.8 (continued)

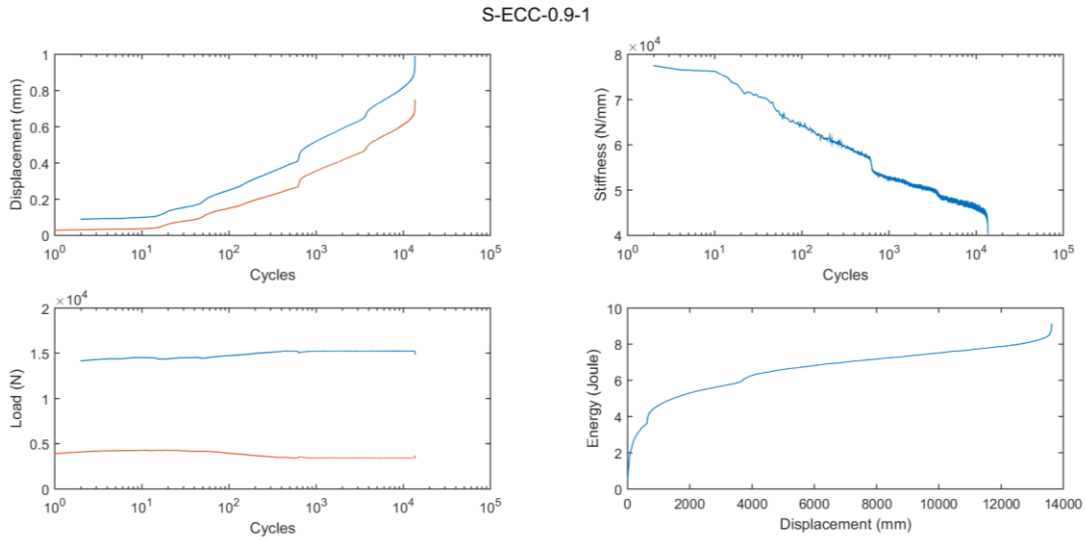

a) S-ECC - %90 -1

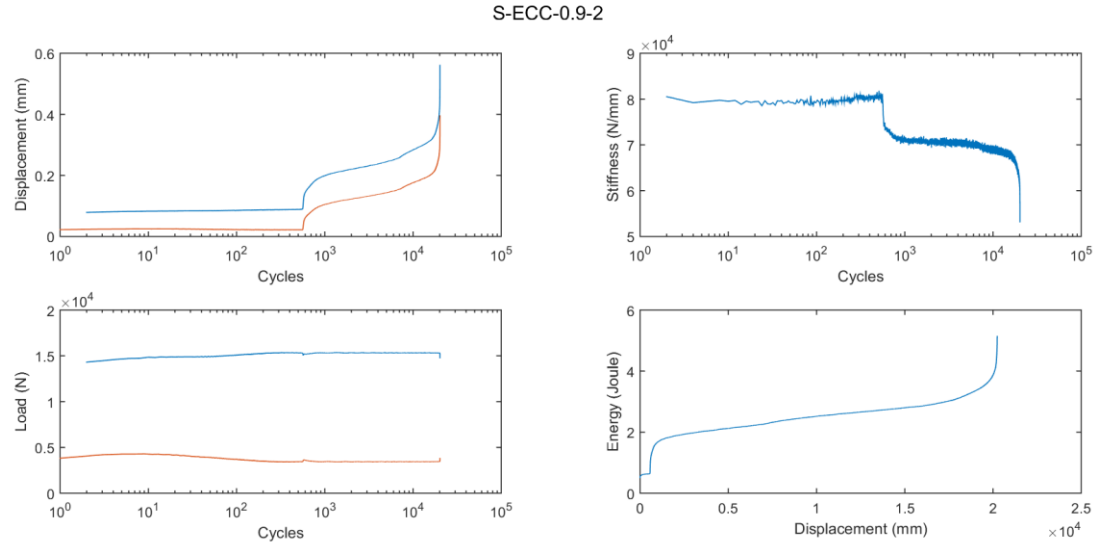

b) S-ECC - %90 -2

Figure A.9 Fatigue test results of S-ECC specimens at 90% of σ_{max}

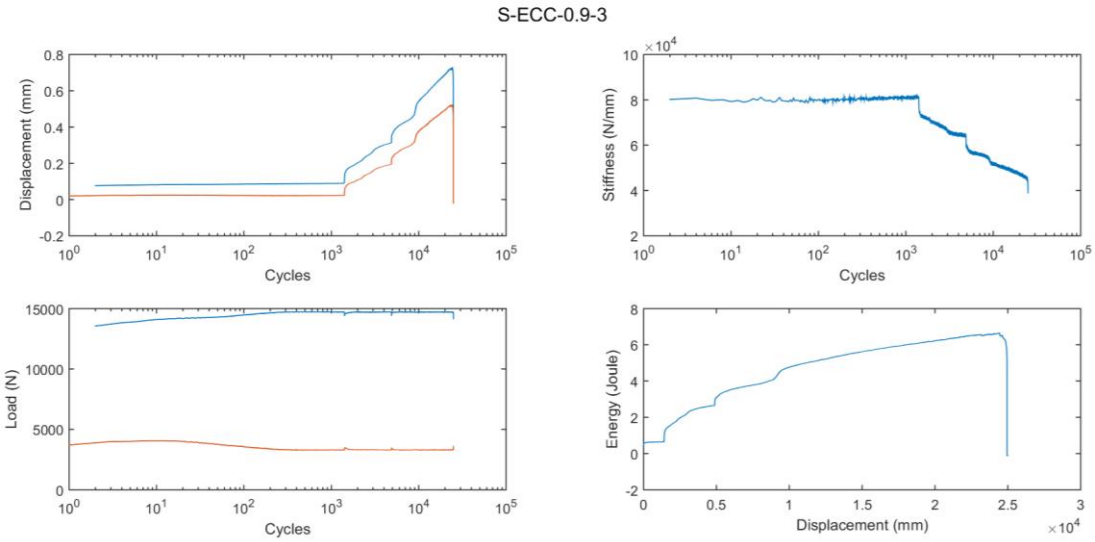

c) S-ECC - %90 -3

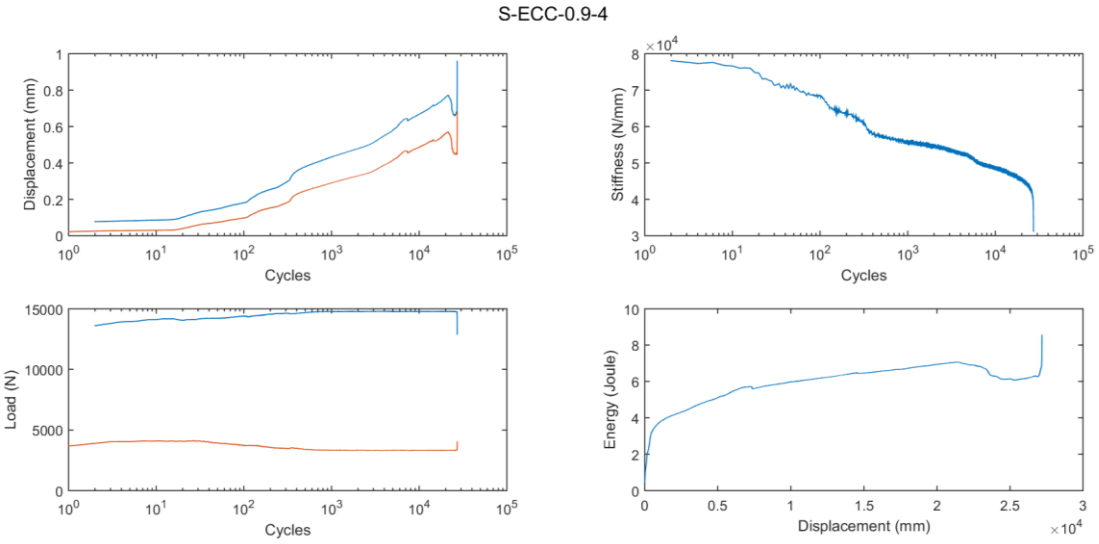

d) S-ECC - %90 -4

Figure A.9 (continued)

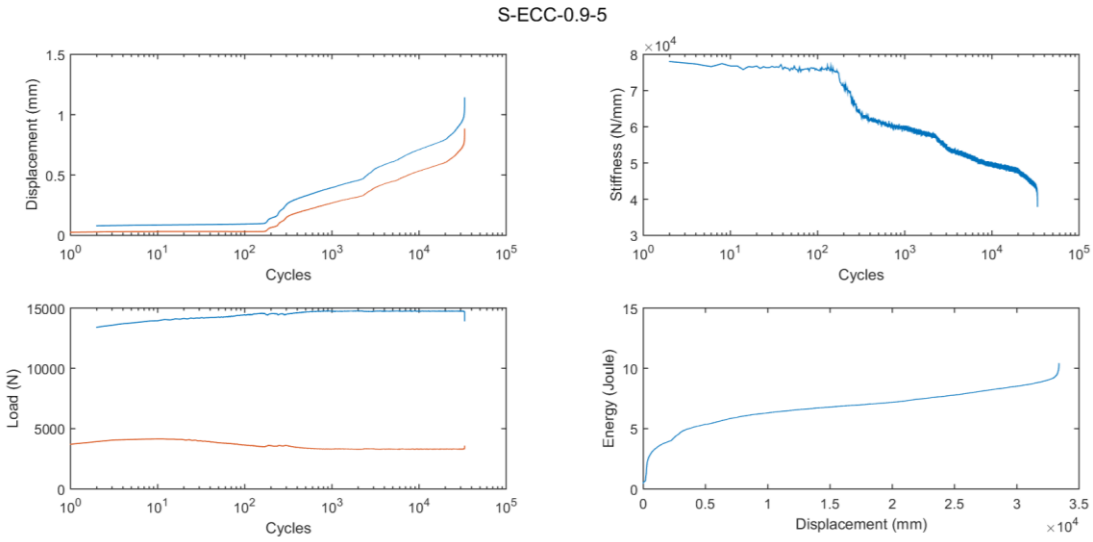

e) S-ECC - %90 -5

Figure A.9 (continued)

APPENDIX B

DETERMINATION OF CRACK PROPAGATION RATE

The crack propagation rate for each fatigue test is calculated from the slope of the crack propagation phase in the energy absorption vs. the number of the cycles curve. The curves corresponding to the fatigue tests examined in this study are presented below. The slopes were calculated from the portions between the markers, ignoring any sudden change in the values.

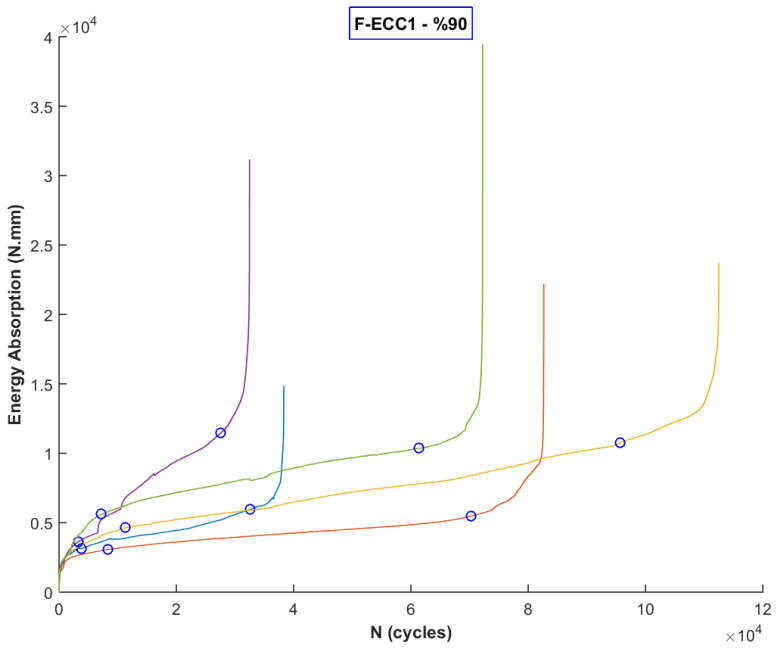

Figure B.1 Energy absorption curves of F-ECC1 – 90%

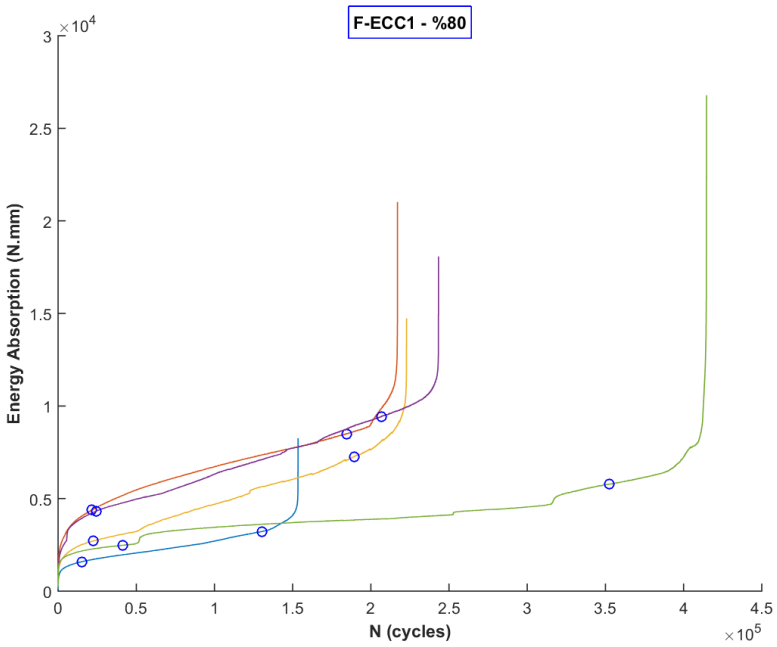

Figure B.2 Energy absorption curves of F-ECC1 – 80%

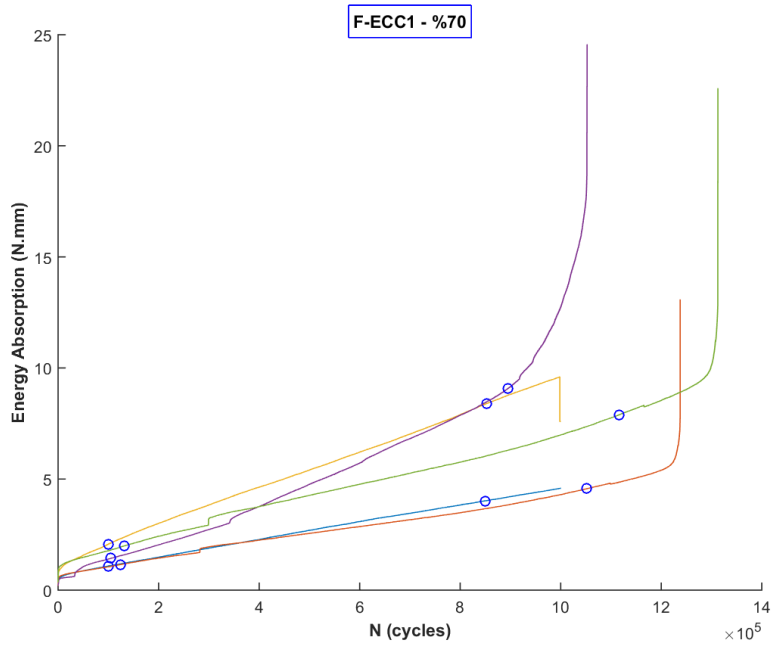

Figure B.3 Energy absorption curves of F-ECC1 – 70%

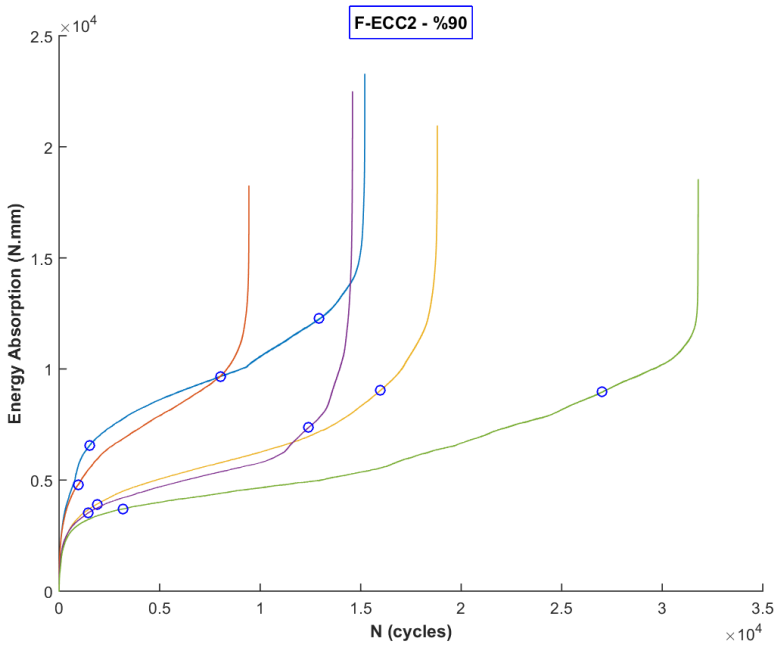

Figure B.4 Energy absorption curves of F-ECC2 – 90%

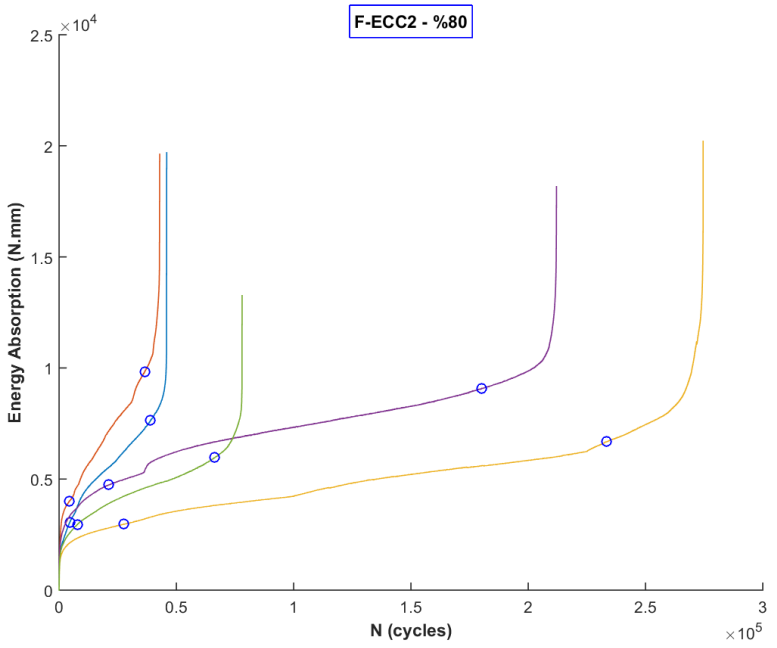

Figure B.5 Energy absorption curves of F-ECC2 – 80%

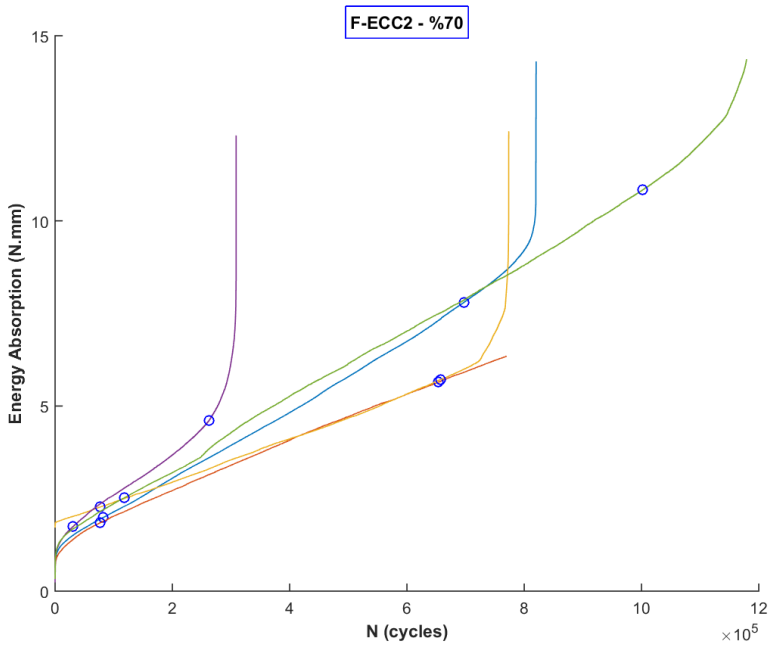

Figure B.6 Energy absorption curves of F-ECC2 – 70%

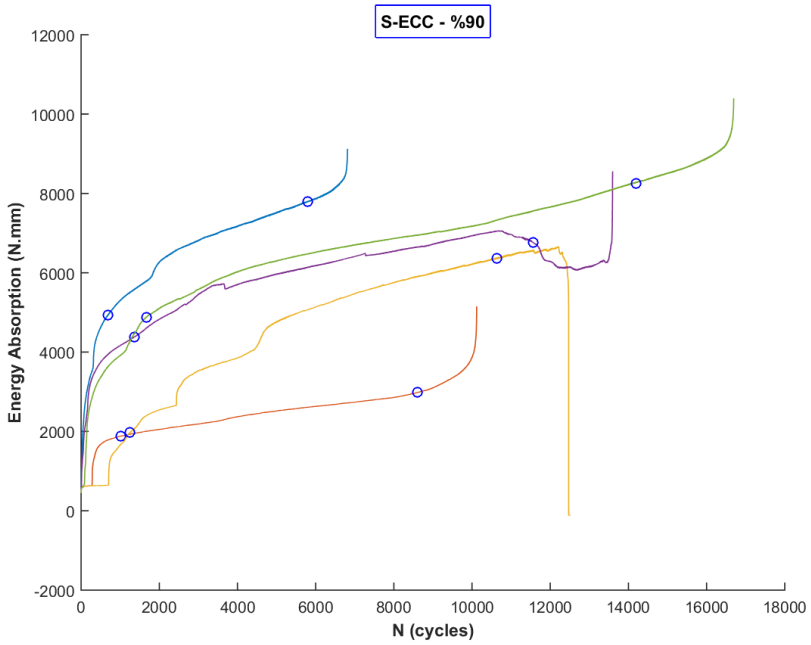

Figure B.7 Energy absorption curves of S-ECC – 90%

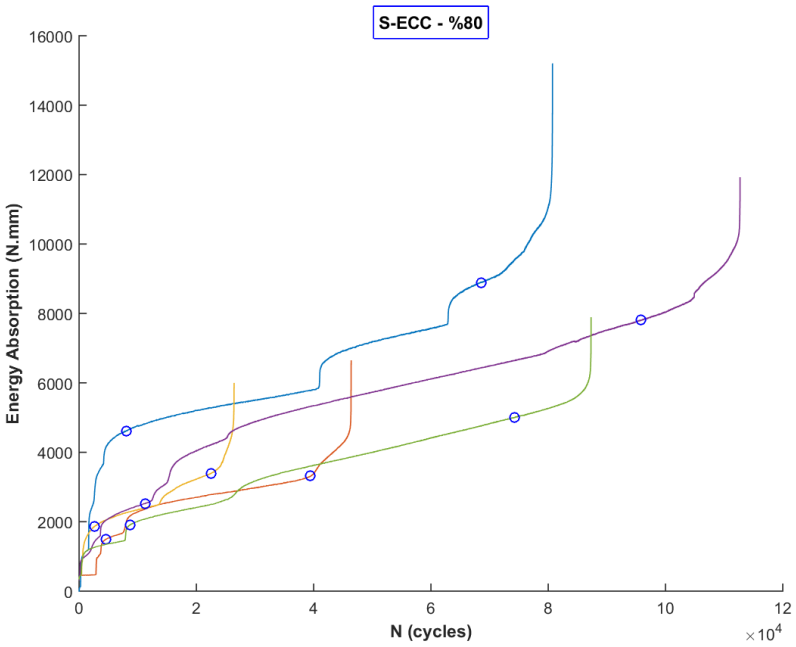

Figure B.8 Energy absorption curves of S-ECC – 80%

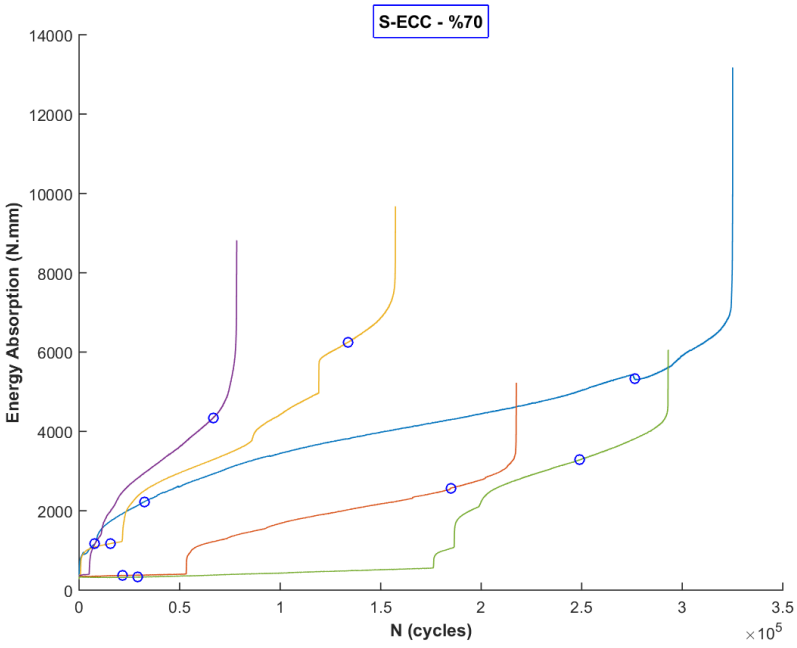

Figure B.9 Energy absorption curves of S-ECC – 70%

The calculated slopes from the curves shown in the figures above are presented in the table below. The crack propagation rates used in the calculation steps in section 5.2 are the averages of these measured slopes.

Table B.1 Calculated slopes of energy absorption curves

Test number		1	2	3	4	5	Average
F-ECC1	90%	0.1321	0.0340	0.1016	0.2015	0.0548	0.1048
	80%	0.0199	0.0258	0.1467	0.0035	0.0280	0.0448
	70%	0.0047	0.0098	0.0110	0.0107	0.0074	0.0087
F-ECC2	90%	0.1950	0.2944	0.1425	0.1375	0.0661	0.1671
	80%	0.0624	0.0783	0.0416	0.0709	0.0281	0.0563
	70%	0.0085	0.0283	0.0125	0.0168	0.0111	0.0154
S-ECC	90%	0.3607	0.1117	0.2053	0.2163	0.2439	0.2276
	80%	0.0385	0.0306	0.0704	0.0531	0.0404	0.0466
	70%	0.0118	0.0088	0.0281	0.0434	0.0317	0.0248

CURRICULUM VITAE

PERSONAL INFORMATION

Surname, Name: ALEESSA ALAM, Burhan
Nationality: Syrian
Date and Place of Birth: December 1981, Damascus
email: baf1tech@hotmail.com

EDUCATION

Degree	Institution	Year of Graduation
MSc	METU Cement Engineering	2009
BS	Damascus University Civil Engineering	2005
High School	Lycée de Laique, Damascus	1998

FOREIGN LANGUAGES

Fluent English, Fluent Arabic, Intermediate French

PUBLICATIONS

Proceedings

1. **Burhan Alam**, İsmail Özgür Yaman, Use of Industrial Wastes in Cement & Concrete production. "III. International Workshop on Earthquake and Sustainable Materials", (2014).

2. Meric, I., Erdil, M., Madani, N., **Alam, B. A**., Tavukcuoglu, A. & Caner Saltik, E. (2014). Material characterization of mudbrick and neighboring plasters in traditional timber frame structures. Monubasin'9 International Conference – Conservation of Monuments in the Mediterranean Basin. Ankara: METU

3. Meltem TANGÜLER, **Burhan ALEESSA ALAM**, İsmail Özgür YAMAN, FARKLI KALIP AYIRICILARININ BETON YÜZEY ÖZELLİKLERİNE ETKİSİ . "Yapılarda Kimyasal Katkılar 4. Sempozyumu", (2013), s.337-348.

4. Meric, I., Erdil, M., Madani, N., **Alam, B. A**., Tavukcuoglu, A. & Caner Saltik, E. (2013). Technological Properties of Earthen Building Materials in Traditional Timber Frame Structures. Kerpic'13 International Conference – New Generation Earthern Architecture: Learning from Heritage (pp.465-473). Istanbul: Istanbul Aydın University.

5. **B. Aleessa Alam**, Süleyman Bahadır Keskin, İsmail Özgür Yaman, Effect of fly ash fineness on the activation of geopolymer concrete. "7th ASIAN SYMPOSIUM on POLYMERS in CONCRETE", (2012).

6. **B. Aleessa Alam**, S. B. Keskin, İ. Ö. Yaman, Drying shrinkage of concrete: A case study in Ankara. "10th International Congress on Advances in Civil Engineering", (2012).

7. S. Bahadır Keskin, Özlem Kasap-Keskin, **B. Aleessa Alam**, İsmail Özgür Yaman, Effect of Fly Ash Fineness on Alkali Aggregate Expansion of Mortars. "10th International Congress on Advances in Civil Engineering", (2012).